International Journal of Basic and Applied Sciences

ISSN: 2277-1921
CIF: 3.658

CRDEEP
CRDEEP International Journals

A Premier Publication of Centre for Rural Development Ecology & Environment Protection

National Conference on «Modern Perspectives In Physical and Chemical Sciences » (MPPCS-2024)
DOI: **10.13140/RG.2.2.13272.40962**

CONTRIBUTED PAPERS

DOI: **10.13140/RG.2.2.13272.40962**

CRDEEP PUBLICATION

National Conference on «Modern Perspectives In Physical and Chemical Sciences » (MPPCS-2024) DOI: **10.13140/RG.2.2.13272.40962**

Content is available at: CRDEEP Journals
Journal homepage: http://www.crdeepjournal.org/category/journals/ijbas/

International Journal of Basic and Applied Sciences
(ISSN: 2277-1921) (Scientific Journal Impact Factor: 6.188)

UGC Approved-A Peer Reviewed Quarterly Journal

A Study of Effect of RO water and Mineral water on Vegetables cooking or Vegetables boiling, TDS check

Dr. Ranjit Ashokrao Gayake and Arun Balasaheb Virkar
Late Nitin College, Pathir Dt. Parbhani – 431 503 (Maharashtra), India.

Abstract:
Due to rapid industrialization and over exploitation of ground water resources, there is a drastic change taking place in environment. Now a day's water pollution is a major problem. This present study deals with the Total Dissolved solids (TDS) of use of RO water and Mineralized water for vegetables boils or vegetable cooking. When RO water used for cooking, RO water was found to cause substantial losses of all essential elements from food . In contrast, when mineralized water is used for cooking, the loss of these elements is much lower, and in some cases, even higher calcium content was reported in food as a result of cooking and TDS of this water decrease.

Keywords:- Total Dissolved solids (*TDS), Mineralized, RO water, vegetable, calcium.*

Introduction :-
Background of study:-
Total dissolved solids (TDS) are generally comprised of inorganic salts (such as chloride, calcium, magnesium, potassium, sodium, bicarbonates, and sulfates) and organicmatters dissolved in water . RO water which doesn't contain enough minerals, when consumed, leaches minerals from the body. [1] This means that the minerals being consumed in food and vitamins are being urinated away. Less minerals consumed plus more minerals being excreted causes serious negative side effects and big health problems[2]. In a scientific study performed to see if minerals consumed in food can make up for the lack of minerals in RO water, scientists concluded that reduced mineral intake from water was not compensated by their diets. Low-mineral water was responsible for an increased elimination of minerals from the body. [3]

Consumption of RO water leads to the dilution of the electrolytes dissolved in the body water. Inadequate body water redistribution between compartments may compromise the function of vital organs. Side effects at the very beginning of this condition include tiredness, weakness and headache; more severe symptoms are muscular cramps and impaired heart rate [4]. Long-term consumption of acidic filtered water devoid of essential elements produced by RO filters is unhealthy[5].

Objectives undertaken:-
Health Advantages of Cooking with Mineral Water
Mineral water has several health benefits thanks to its awesome mineral content, including:
1. Supports Mental Health
2. Controls Blood Pressure
3. Supports Body Fat Regulation
4. Lowers Acidity in the Body
5. Reduces the Risk of Heart Disease
6. Enhances Muscle Performance
7. Promotes Bone Health
8. Restores Fluids and Electrolytes

Materials and Methods:-
Sample collection
A total 24 samples were collected different homes from Pathri city. In which Vegetables were boiled in RO water and Mineralize water with same temperature, quantity.

National Conference on «Modern Perspectives In Physical and Chemical Sciences » (MPPCS-2024) DOI: **10.13140/RG.2.2.13272.40962**

Data Analysis:-
The TDS and electrical conductivity (EC) were measured in situ by using pan type digital EC and TDS meter.
Data collection methods:-
A total of 24 samples (24 bottles) from homes of different area of Pathri. All the samples were retained in their original sealed containers and clearly marked for identification with sample 1 to 24 water samples.

Digital TDS meter:-
- Remove the protective cap of the Digital TDS meter and switch it "ON"
- Dip the Digital TDS meter in the water up to the maximum immersion level (Marking is used to indicating the immersion level in the Digital TDS meter)
- Stir the Digital TDS meter to remove the air bubbles if present in the water. Stirring will remove the air bubble from the water
- Now, wait for 10-15 seconds after placing the Digital TDS meter inside the water to measure the TDS level of the water
- Few brands digital TDS meters bring the reading by multiplying it by 10, but in some TDS meters, you need to multiply the value by 10
- After calculating the TDS level of the water, shake off the excess water from the digital meter and replace the protective cap

Results:-

Vegetables	TDS of RO water	TDS of RO water after boiled with vegetables	TDS of Mineralize water	TDS of Mineralize water after boiled with vegetables
White Cabbage	45	981	850	115
Red Cabbage	53	857	840	165
Cauliflower	43	868	852	177
Potato	55	878	845	186
Spinach	52	935	856	172
Drumstick	54	874	780	96
Radish	52	862	862	186
Spinach	56	845	852	146
Pumpkin	52	943	845	152
Fenugreek	56	768	862	183
Mushroom	47	786	852	174
Bitter Gourd	49	896	864	165

This shows that after washing vegetables with RO water there is loss of mineral in vegetables.

Conclusion:-
It was observed that when RO water used for cooking, RO water was found to cause substantial losses of all essential elements from food (vegetables, meat, cereals). Such losses may reach up to 60 % for magnesium and calcium or even more for some other micro-elements (e.g., copper 66 %, manganese 70 %, cobalt 86 %) and also TDS of RO water increase. In contrast, when mineralized water is used for cooking, the loss of these elements is much lower, and in some cases, even mineral from mineralize water is added in food as a result of cooking and TDS of this water decrease

References:-
[1] Patience, J.F.(2012). The importance of water in pork production. Anim. *Front.*, 2, 28–35.
[2] Anderson, J.S., Anderson, D.M., Murphy, J.M. (1994). The effect of water quality on nutrient availability for grower/finisher pigs. *Can. J.Anim. Sci,.* 74, 141–148.
[3] Lozinski, B.M., Frederick, B. Li, Y, Saqui-Salces, M. Shurson, G.C., Urriola, P.E., Wilson, M.L., Johnston, L.J.(2022). Effects of water quality on growth performance and health of nursery pigs. *Transl. Anim. Sci.* 6, 02-06.
[4] Maenz, D.D., Patience, J.F.,Wolynetz, M.S. (1994). The influence of the mineral level in drinking water and the thermal environment onthe performance and intestinal fluid flux of newly-weaned pigs. *J. Anim. Sci.* 72, 300–308.

[5]Little, S., Woodward, A., Browning, G., Billman-Jacobe, H. (2021), Water Distribution Systems in Pig Farm Buildings: Critical Elementsof Design and Management. *Animals*, 11, 3268-3272.
[6] Vogels, J., Wingender, J., Uphoff, J., Schaule, G., Aumann, K., Hufelschulte, J., Meemken, D., Münster, P., Menrath, A., Nienhaus,F., (2020). Charakterisierung von Belägen in Tränkwasserleitungen in Ferkelaufzuchtställen und mögliche Hygienekonzepte. *Berl.Munch. Tierarztl. Wochenschr.,* 133, 36–48.
[7] Zeamer, K.M., Levesque, C.L., Cortus, E.L., Thaler, R.C, (2021). Findings from a survey of finishing-barn management benchmarks withSouth Dakota pork producers. *Appl. Anim. Sci.,* 37, 320–333.

Content is available at: CRDEEP Journals
Journal homepage: http://www.crdeepjournal.org/category/journals/ijbas/

International Journal of Basic and Applied Sciences
(ISSN: 2277-1921) (Scientific Journal Impact Factor: 6.188)

UGC Approved-A Peer Reviewed Quarterly Journal

Exploring the Role of Zinc Oxide in Modern Optical Sensors using Sol-gel Spin coating method

Neha N Malpure[1], Rajendra S Khadayate[1]*
[1]Research Lab, G. D. M. Arts, K. R. N. Commerce and M. D. Science College, Jamner, Dist.: Jalgaon, Maharashtra, India.

Abstract:
In this work, zinc oxide (ZnO) multilayer nanostructured thin films were deposited on glass substrate using sol-gel spin coating technique and the effect of these multilayer films on optical and structural properties was investigated. It was observed, that these multilayer films have great impact on the properties of ZnO. Numerous methods, including FTIR, IV characterization, UV-visible spectroscopy, FESEM, and X-ray diffraction, were used to characterize all of the deposited films. The obtained multilayer ZnO films are crystalline, according to the XRD measurement. The optical absorption spectra measured using UV–Vis Spectroscopy show the average transmittance in the visible region of all films is 55%. The energy band gap of prepared thin films was found to be 3.25 eV. The film's thickness is determined to be 103.54 nm. It is observed that the multilayer film of ZnO performs better as a transparent conducting material than the single layer film. Hence, as prepared thin films of ZnO can be used in Optical sensors.

Keywords: Multilayer Films, ZnO, Sol-gel, Spin Coating, XRD, SEM, FTIR, Optical Properties

Introduction:

Nanotechnology is a sophisticated technology, which deals with the synthesis of nanoparticles, processing of the nanomaterials and their applications. Nano materials will be defined as those materials, which have size but 100 nm a minimum of in one dimension. Nano materials are of typically tremendous interest. Thanks to their noticeable performance in electronics, optics and photonics. Nanomaterials were classified as zero dimensional, one dimensional, two dimensional, three-dimensional nanostructures. Zero dimensional nano structures are like nano particles or quantum dots, are widely employed in photovoltaic cell. One-dimensional nanostructures like nano wires, nanorods, nano tubes are employed in research also as industrial application. Two-dimensional nano materials like thin films are widely employed in optical coatings. As we know, the skinny film could be a layer of fabric starting from fraction of nanometer to many micrometers in thickness. Thin films are crystalline or amorphous layers, deposited on a substrate. Thin film technology could be a self-organizing structural evolution. The study of thin film phenomena has been accustomed a big extends over the last four decades. Miniaturization criteria made the utilization of thin films practically necessary.

It is a known fact that all the world's human beings strongly depend on natural resources, for example, soil, water, air, etc. Unfortunately, in recent years, contamination of these resources has been very high. Currently, recycling is getting significant attention. Therefore, great attention has to be paid to investigating cost effective and eco-friendly techniques for any research. Semiconducting devices are mostly based on advancement of thin film technology. Thin film is a two-dimensional material deposited by different methods. The thin film technology is deposition of molecules. On the other hand, thick film technology is deposition of particles. Keep this in mind, metal oxides have been actively studied due to its diverse chemical and physical properties [1-3]. During the last years, ZnO thin films have been studied extensively due to their potential applications as piezoelectric transducers, conductive gas sensors, transparent conductive electrodes, solar cell windows, etc. ZnO has attracted much attention as one of the most promising materials for electronic applications. The interest comes from the wide direct band gap and a large binding energy of this material. With such characteristics, it makes ZnO become a potential useful in various optoelectronic applications such as optical sensor and light emitter etc [4-5]. The structural and optical properties of ZnO is indispensable for the design and analysis of various optical and optoelectronic devices. The structural and optical properties of ZnO thin films depend on the preparation methods, substrate temperature, substrate material, and annealing treatment [6].ZnO thin films have been prepared by various techniques such as sputtering, chemical vapour deposition, pulse laser deposition; spray pyrolysis and sol-gel process.

National Conference on «Modern Perspectives In Physical and Chemical Sciences » (MPPCS-2024) DOI: **10.13140/RG.2.2.13272.40962**

Among the different available techniques, the sol-gel technique has been used decades long to deposit thin films. The spin process involves depositing a small material put on the center of a substrate and then to be spin the substrate. Centripetal acceleration causes the material to spread onto the surface of substrate [7]. Spin coating system is a cheap and easy method but specific problems can sometimes be formed such as too thin or too thick film formations [15, 16]. The present study deals with the preparation of ZnO thin films by sol-gel method using spin coater. In addition, this work reports structural, optical and photoluminescence properties of ZnO thin films.

Experimental Details:

Materials

Zinc acetate dihydrate [Zn $(CH_3COO)_2.2H_2O$] (Meark, 98% purity), 2-methoxy ethanol [$CH_3(CH_2)_2OH$] (Rankem, 99% purity) and diethanolamine [$(HOCH_2CH_2)_2NH$] (Rankem, 98% purity) were used for the preparation of ZnO solution. Blue Star Micro glass slides were used as substrate for the deposition of ZnO thin films.

Synthesis of ZnO Thin Films

Zinc Oxide thin films were deposited on glass substrates by spin coating method. As a starting material, 0.4M of Zinc acetate dihydrate was used. The precursor solution was prepared by mixing zinc acetate dihydrate in appropriate proportion with 2-methoxy ethanol and diethanolamine. Here 2-methoxy ethanol and diethanolamine were used as solvent and stabilizer respectively. The glass substrate was cut into equal pieces using a diamond glasscutter. After that washed by labolene, and cleaned in distilled water, acetone, 2-propanol and then dried at 200°C for 3 minutes.

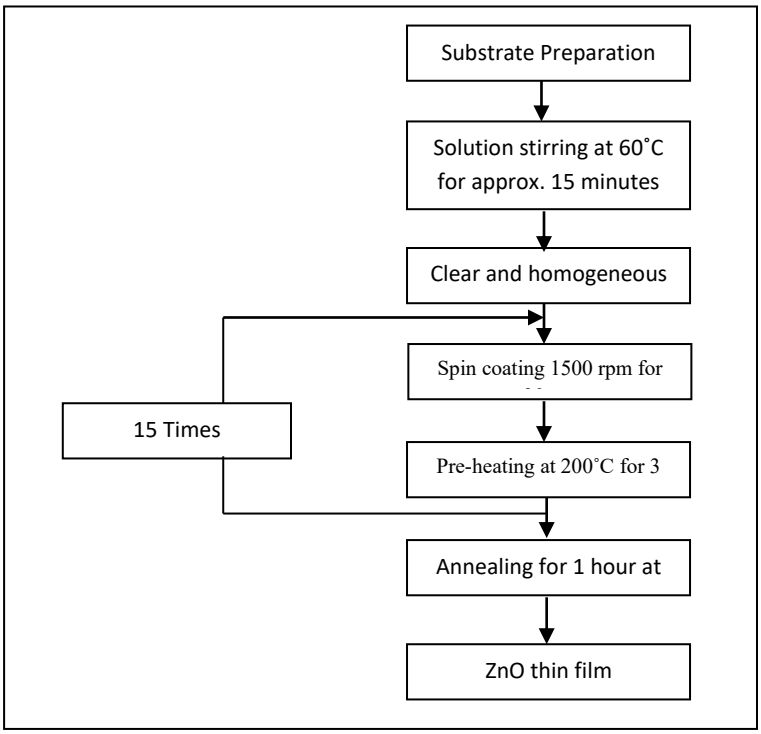

Fig.1. Flowchart for ZnO thin films preparation

The coating solution was dropped using a syringe onto the glass substrate. Then the substrate with solution was rotated at 1500 rpm for 30 seconds by using spin coater. After deposition by spin coater, the film was dried at 200ºC for 3 minutes on a hot plate in order to evaporate the solvent and remove organic residuals. The procedure from coating to drying was repeated 15 times. The film was then annealed in air at 300°C for 1 hour. The procedure of thin film growing could be well understood from the flow chart as shown in fig.1.

Characterization of ZnO Thin Films

XRD and FESEM characterizations were used to analyze the morphology and crystalline size of the prepared ZnO thin film. The energy band gap, optical absorbance, transmittance were measured by UV-Vis spectrometer. The thickness of the films was measured with Stylus Surface Profiler. The initial idea about the surface morphology of solution-processed films was given by optical microscopy. In addition, the study of photoluminescence spectroscopy for prepared ZnO thin films was done by fluoromax-4-spectroflurometer. The optical sensitivity was investigated by controlling light intensity of the lamp.

National Conference on «Modern Perspectives In Physical and Chemical Sciences » (MPPCS-2024) DOI: **10.13140/RG.2.2.13272.40962**

Result and Discussion:

XRD Analysis

The crystal structure of ZnO thin film prepared by sol-gel process was investigated through X-ray diffraction (single crystal x-ray diffractometers, Bruker D8 Venture) [10, 22, 25]. Fig 2 shows XRD pattern of ZnO thin film deposited on glass substrate and annealed at 300°C. The prominent reflection peaks show that the film is polycrystalline in nature. The diffraction peaks corresponding to the crystallographic orientations (100), (002), (101), (102) and (103) at angles 2θ = 28.396°, 29.183°, 32.667°, 49.748° and 61.652° respectively.

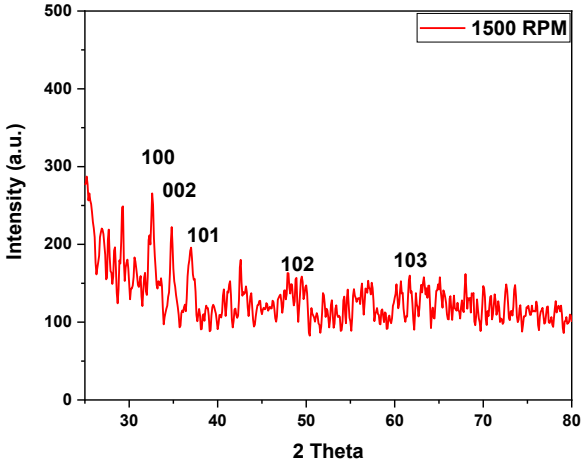

Fig.2. XRD pattern of ZnO thin film

From the XRD spectrum, grain size (D) of the film was calculated using the Debye Scherrer's formula.

$$D_{hkl} = \frac{K\lambda}{\beta cos\theta}$$

Where, K is a constant to be taken 0.94, β is Full Width Half Maximum (FWHM) in radian, λ is wavelength of X ray used and θ is Bragg's angle. The grain size of (100) oriented thin film was calculated to be 43.51nm.

Scanning Electron Microscopy (SEM):

Surface morphology of thin film is very important tool to investigate microstructure of thin films. Fig. 3 shows the surface morphology of the prepared ZnO thin film. It reveals that film is polycrystalline in nature.

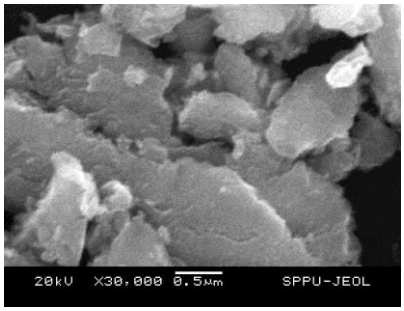

Fig. 3 SEM image of ZnO Thin Film

3.3 UV-Vis Spectroscopy

The optical absorbance and transmittance measurements were recorded by using a double beam UV-Vis spectrophotometer (Shimadzu UV – 1601) in the wavelength range 300 nm to 900 nm [8, 11, 20, 24]. Absorption and transmittance spectra are shown in fig.4 and fig.5 respectively, for prepared ZnO thin films. It is seen that strong absorption is occurs in UV wavelength 353 nm. The transmittance of the film is above 55% in this visible region.

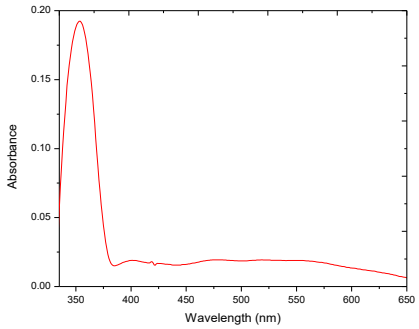

Fig.4. Absorption spectrum of ZnO thin film

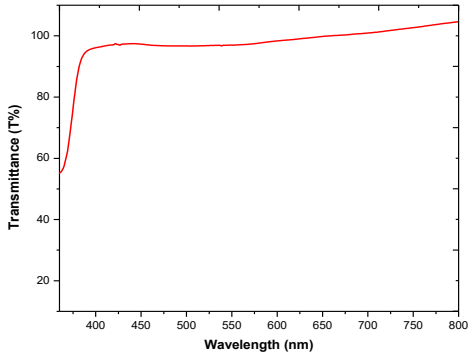

Fig.5. Transmittance spectrum of ZnO thin film

The ZnO is a direct band gap semiconductor. The corresponding optical band gap of ZnO thin film is evaluated from the absorbance spectra of ZnO thin film on glass substrate. Fig.6 describes the Touc's plot curves to estimate energy gap and the band gap value of the sample. The Touc's curves can be obtained by equation

$$(\alpha h\nu)^n = A\,(h\nu - Eg) \quad \text{- (1)}$$

$$\alpha d = \ln (1/T) \quad \text{- (2)}$$

The optical band gap for the ZnO thin film grown at 300°C was estimated to be 3.25eV.

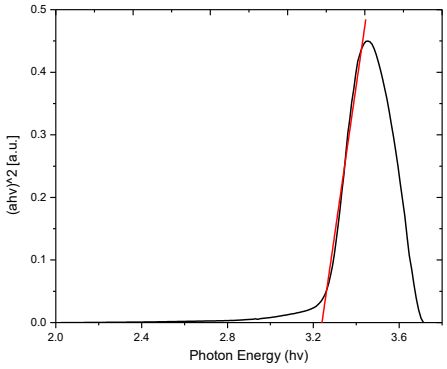

Fig.6. Optical band gap of ZnO thin film

Thickness Measurement

Stylus Surface Profiler (DEKTAK 150) is a measuring instrument used to measure a surface's profile, in order to quantify its roughness and to measure film thickness. Vertical resolution is usually in the nanometer level, though lateral resolution is usually poorer. A profiler can measure small surface variations in vertical stylus displacement as a

National Conference on «Modern Perspectives In Physical and Chemical Sciences » (MPPCS-2024) DOI: **10.13140/RG.2.2.13272.40962**

function of position. A typical profiler can measure small vertical features ranging in height from 10 nanometers to 1 millimeter [17]. The thickness of the films was found to be 103.54 nm.

Photoluminescence

Photoluminescence is a contactless non-destructive method which is widely used to study luminescence properties of thin films using Horiba spectrofluorometer – fluromax4 instrument [12 - 14]. PL spectra of ZnO thin films with 15 cycles are represented in Fig.7. The PL spectrum of ZnO on glass substrate was obtained with an excitation wavelength 353 nm. Spectra represent characteristic intensity peaks in the UV and visible region. From spectra it is clear theta ZnO particles exhibit emission peaks at 387nm in UV region.

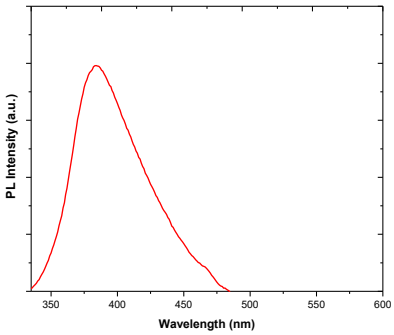

Fig.7. PL spectra of ZnO thin film

I-V characterization

Fig.8 and Fig.9 shows typical current voltage (I-V) characteristic of prepared ZnO thin film with Al as contact electrodes measured under illumination, with 5V bias voltage. Al contact electrode plays important role in rapidly transforming photo electrons in ZnO thin film to the electrode. The linearity of the I-V curves indicted ohmic nature of the contact. As shown in figure there is a significant increase in the photocurrent under illumination. UV light illumination generates electron hole pairs on the film surface [18, 19, 21, 23, 26, and 27]. Dark and photo currents in the undoped ZnO films were recorded as a function of applied voltage, shown in fig. UV light illumination generates electron hole pairs on the film surface. All the IV plots observed from 0V to 5V potential range display a symmetric linear 1V variation. From the IV characteristics, resistance of the film was calculated under dark and under UV illuminated condition. The resistance of the film under dark condition was found to be 2.68 GOhm. The resistance of the film under UV illuminated condition was found to be 1.76 GOhm, It is observed that, resistance of the film decreases under UV illuminated conditions as compared to that under dark conditions. This means the prepared film responds to optical changes in the nearby environment. Hence, as prepared thin films of ZnO can be used in Optical sensors.

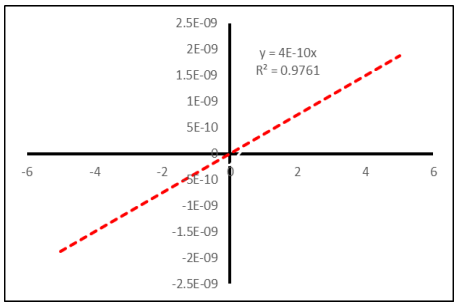

Fig.8. I-V characteristics of ZnO thin film under dark

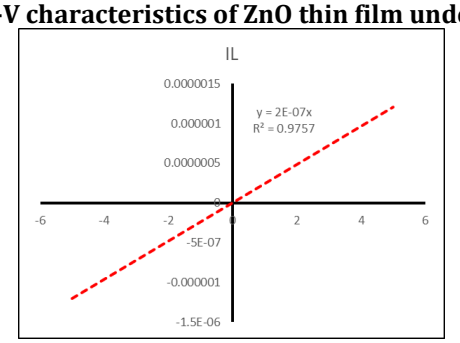

Fig.9. I-V characteristics of ZnO thin film under light

Conclusion:

To summarize, the undoped nanostructured ZnO thin film on glass substrate has been prepared by sol-gel method using spin-coating technique. The structural and optical properties of ZnO thin film are studied. The diffraction peaks corresponding to the crystallographic orientations (100), (002), (101), (102) and (103) at angles 2θ = 28.396˚, 29.183˚, 32.667˚, 49.748˚ and 61.652˚ respectively. The grain size of (100) oriented thin film was calculated to be 43.51nm. The transmittance value of the ZnO films was about 55% and the band gap energy is found to be 3.25eV. Room temperature PL spectra of ZnO thin film show a UV emission band located at 387nm. I-V characteristics of the ZnO thin film on glass substrate can be good, which makes this method promising for fabricating the optical sensor. Future work should be done effect of these properties for doped ZnO thin films.

Acknowledgement:

The authors gratefully acknowledge the support provided by Department of Physics, G. D. M. Arts, K. R. N. Commerce and M. D. Science College, Jamner, Dist. Jalgaon (MH) and Department of physics, School of Physical Sciences, Kavayitri Bahinabai Chaudhari North Maharashtra University, Jalgaon (MH).

References

1) S Ilican, Y Caglar, M Caglar (2008) Preparation and characterization of ZnO thin films deposited by sol-gel spin coating method, *Journal of optoelectronic and advanced material*, 2578-2583

2) Lamia Znaidi, Sol-gel-deposited ZnO thin films: A review, Materials Science and Engineering B, (2010), 18-30

3) Priya Gupta, Savita Maurya, N K Pandey, Vernica Verma (2021), Structural, electrical and humidity sensing properties of nanostructured nickel oxide prepared by sol-gel method, *J material Sci:Mater Electron*

4) Deependra Das Mulmi, Agni Dhakal, Buddha Ram Shah (2014), Effect of Annealing on Optical Properties of Zinc Oxide Thin Films Prepared by Homemade Spin Coater, *Nepal journal of science and technology*, Vol 15, No 2, 111-116

5) Neha N Malpure, Rajendra S Khadayate, Amol P Zerwal, Chetan K Kasar, Dipak M Marathe (2021), A Review: ZnO – From Synthesis to Application, *IJIRT*, Vol 8 Issue 7, 2349-6002

6) K Balachandra Kumar, P Raji (2011), Synthesis and Characterization of Nano Zinc Oxide by Sol Gel Spin Coating, *Recent Research in Science and Technology*, 3(3):48-52

7) Mursal, Irhamni, Bukhari, Zulkarnain Jalil, Structural and optical properties of Zinc oxide (ZnO) based thin films deposited by sol-gel spin coating method

8) David Adegboyega Ajadi, Saint Muyiwa Agboola, Oluwaseun Adedokun (2016), Effect of spin coating speed on some optical properties of ZnO Thin films, *Journal of materials science and chemical engineering*, vol 04, No 05, 66676,6

9) Sandeep Sanjeev, Dhananjaya Kekuda (2015), Effect of annealing temperature on the structural and optical properties of zinc oxide (ZnO) thin films prepared by spin coating process, *IOP conf series* 73, 012149

10) Theopolina Amakali, Likius S Daniel, Veikko Uahengo, Nelson Y Dzade, Nora H de Leeuw (2020), Structural and optical properties of ZnO thin films prepared by molecular precursor and sol-gel methods, *crystals*, 10, 132

11) Jitao Li, Dingyu Yang, Xinghua Zhu (2017), Effects of ageing time and annealing temperature on structural and optical properties of sol-gel ZnO thin films, *AIP advances* 7, 065213

12) C S Prajapati, Ajay Kushwaha, P P Sahay (2013), Optoelectronics and formaldehyde sensing properties of tin-doped ZnO thin films, *Appl. Phys A*

13) C M Firdaus, M S B Shah Rizam, M Rusop, S Rahmatual Hidayah (2012), Characterization of ZnO and ZnO:TiO2 thin films prepared by sol-gel spray spin coating technique, *IRIS procedia engineering* 41, 1367-1373

14) S K Shaikh, V V Ganbavle, S I Inamdar, K Y Rajpure (2016), Multifunctional zinc oxide thin films for high-performance UV photo detectors and nitrogen dioxide gas sensors, *Royal society of chemistry*, 6, 25641

15) R Baranyai, A Deterich, E Volentiru, Z Horvolgyi (2009), Preparation and characterization of ZnO and TiO2 sol-gel thin films deposited by dip coating, *Hungarian Journal of industrial chemistry*, vol 37 (2) pp. 131-137

16) Amol R Nimbalkar, Maruti G Patil (2017), Synthesis of ZnO thin film by sol-gel spin coating technique for H2S gas sensing application, *Elsevier Physica B* 527, 7-15

17) H F Hussein, Ghufran Mohammad Shabeeb, S Sh Hashim (2011), Preparation ZnO thin film by using sol-gel-processed and determination of thickness and study optical properties, *J Mater Envron, Sci.* 2 (4), 423-426

18) Kuo Sheng Kao, Wei Che Shih, Wei Tsuen Ye, Da Long Cheng (2015), Photoluminescence of ZnO thin films deposited at various substrate temperatures, *Thin solid films*, 34643, 7

19) S K Panda, C Jacob (2012), Preparation of transparent ZnO thin films and their application in UV sensor devices, *Solid state electronics* 73, 44-50

20) Khadher AL-Rashedi, Mazahar Farooqui, Gulam Rabbani (2018), Preparation and characterization of ZnO thin films by sol-gel method on glass substrates, *International Journal of current research*, vol 10, issue 09, pp.73689-73692

21) F K Konan, B Hartiti, H J Tchognia Nkuissi, A Boko (2019), Optical - structural characteristics of i-ZnO thin films deposited by chemical route, *J Mater Environ Sci*, vol 10, issue 10, 1003-1010

22) B D Kim, T Pan, J G Kim (2021) Structural investigations of ZnO nanostructure, *Exp. Theo, Nanotechnology 5*, 163-167

23) K L Foo, M Kashif, U Hashim, Wei-Wen Liu (2014) Effect of different solvents on the structural and optical properties of zinc oxide thin films for optoelectronic application, *Ceramics International 40*, 753-761

24) Ziaul Raza Khan, Mohd Shoeb Khan, Mohammad Zulfequar, Mohd Shahid Khan (2011) Optical and structural

properties of ZnO thin films fabricated by sol-gel method, *Materials sciences and applications*, 2, 340-345
25) N Suresh, J Arumugam (2013) Simple preparation and characterization of nano-crystalline zinc oxide thin films by sol-gel method on glass substrate, *IJRRASE*, vol 5, No 2, PP 43-39
26) kathalingam Adaikalam, S Valanarasu, Atif Mossad Ali, M A Sayed, Woochul Yang, Hyun-Seok Kim (2022) Photosensing effect of indium-doped ZnO thin films and its heterostructure with silicon, *J of Asian Ceramic Societies*
27) Bhubesh Chander Joshi, Aadarsh Kumar Chaudhari (2022) Sol-gel-derived Cu-doped ZnO thin films for optoelectronic application, *ACS Omega*, 7, 21877-21881

Content is available at: CRDEEP Journals
Journal homepage: http://www.crdeepjournal.org/category/journals/ijbas/

International Journal of Basic and Applied Sciences
(ISSN: 2277-1921) (Scientific Journal Impact Factor: 6.188)

UGC Approved-A Peer Reviewed Quarterly Journal

Phytochemical screening of aqueous and ethanolic extract of *Azadirachta indica* leaves

Dr. Sharada D. Shirole*[a], Dr. Yogesh Suryawanshi[b]
a- Assistant professor, S. S. M. M. Arts, Science and commerce college, Pachora, Dist. Jalgaon
b- Assistant teacher, D. D. S. P. Arts, Science and commerce college, Erandol, Dist. Jalgaon

Abstract:
Plant-based antimicrobial compounds have emerged as a blessing to medical sciences due to the multitude of bioactive phytochemicals or secondary metabolites, ease of availability and a broad spectrum of action with negligible adverse effects. *Azadirachta indica* (*A. indica*) is reported to possess amultitude of phytochemicals. In the present study, the phytochemical constituents of the aqueous extractof *A. indica* leaves were analysed qualitatively. The chemical nature of the extract and the structurally similar compounds present in it were analysed by Fourier transform infrared (F.T.I.R.) spectroscopy. Preliminary phytochemical analysis by qualitative biochemical tests revealed the presence of alkaloids, flavonoids, terpenoids, glycosides, phenols, steroids, tannins and saponins. Fourier transform infrared spectroscopic analysis revealed the presence of functional groups such as alcohols, carboxylic acid, amine salt, disubstituted alkenes, sulphates and halocompounds.

Keywords: *Azadirachta indica*, aqueous and ethanolic extract, Fourier transform infra-red spectroscopy, Phytochemicals

Introduction

Azadirachta indica plant is a native of India, where it is known as divine tree; "life giving tree". It belongs to maliceae family. Away from India, it is commonly found in Africa and America. It occurs naturally in tropical region and sub-tropical zones. However, it can still be planted or cultivated. *Azadirachta indica* tree is an incredible therapeutic plant [1] that has been declared the tree of the 21st century by the United Nations [2]. The plant kingdom represents a rich store house of organic compounds, many of which have been used for medicinal purposes and could serve as a lead for the development of novel agents having good efficacy in various pathologicaldisorders in the coming years. Neem plant is considered to be the richest sources of drugs for traditional medicine, modern medicine, nutraceuticals, food supplements, folk medicine, pharmaceutical intermediates and chemical entitiesfor synthetic drugs [3]. Some of the phytochemicals contained in *Azadirachta indica* plant have been isolated, quantified and identified through intensive studies. These bioactive chemicals have provided leads in the development of several life-saving drugs, which are in use today [4]. Extract from *Azadirachta indica*, which is referred to neem in some parts of India are mostly recommended in ancient medical texts. The leaves can be used as drug for diabetes, eczema and fever. Thus, the objective of this research was to ascertain the phytochemical constituents of neem plant and relate it to some of its traditional uses. Much of the protective effects of herbal plants have been attributed to their phytochemicals constituents [5], alkaloids,flavonoids, glycosides, saponins for examples exert multiple biological effects like anti-inflammatory, anti-allergic,antioxidant, anti-diabetic, anti-viral and anti-cancer activities, anti-leprosy activities, antimicrobial activity.

Compare to synthetic drugs, use of bio-actives compounds of medicinal plants have several advantages which include fewer side effects, better patient tolerance, relatively less expensive and renewable in nature [6]. Alkaloids acts on diverse metabolic system in humans and animals, with alkaloids such as cocaine, the psychotic psilocin, nicotine, the analgesic morphine used as medications and recreational drugs [7, 8]. Glycosides play numerous important roles in living organisms and are used in medications. Many plants store chemicals in the form of inactive glycosides which can be activated by enzymes breaking off the sugar part and making the glycoside available for use [9]. Terpenoids contribute to the scent of eucalyptus, the flavors of cinnamon, cloves and ginger, the yellow colour in sunflowers and the red colour in tomatoes [10].The steroids and sterols in animals are biologically produced from terpenoid precursors. Through isoprenylation terpenoids are added to proteins to enhance their attachment to the cell membrane. Flavonoids have inhibitory activity against organisms that causes plant diseases such as Fusarisiumoxysporum. In higher plants, flavonoids

are involved in UV filtration, symbiotic nitrogen fixation and floral pigmentation. They may also act as chemical messengers, physiological regulators and cell cycle inhibitors. Steroid and their metabolites are frequently used as signaling molecules. Steroids along with phospholipids function as components of cell membranes with steroids such as cholesterol decrease membrane fluidity [11]. Tannins are widely distributed in many species of plants, where they play a role as pesticides and plant growth regulation [12]. Resins made of tannins have been investigated to remove mercury and methyl mercury from solution [13]. Immobized tannins have been tested to recover uranium from seawater [14]. Phenol derivatives are also used in the preparation of cosmetics including sunscreens [15], hair colorings and skin lightening preparations. In plants, saponins may serve as anti-feed ants and to protect against microbes and fungi [16]. Saponinsare toxic to cold-blooded organisms and insects at particular concentrations [17]. Hence, in the current study the aqueous and ethanol extract of *A. indica* was extracted by ultrasonic cavitation technique and analysed for the presence of its phytochemical constituents.

Experimental

Materials

The *Azadirecta indica* plant leaves were collected from surrounding of hilly region of Khandesh (Maharashtra, India). Other chemicals required for the photochemical analysis were procured from Merk scientific, India.

Preparation of the leaf extracts using ultrasonic cavitation technique

The collected samples were brought to the laboratory and washed using fresh water to remove the contaminants from the leaf surface (Fig. 1), which were shade dried for 15 days under dust free condition. These dried leafs were cut into small pieces and grounded into fine powder on grinder. This powder was sieved using 75 µm mesh size sieve shaker. The extract was prepared using this powder (25 gm) in millipore water (100 ml). This mixture was sonicated for 40 min (B03-Ultrasonic Processor make E-Chrom Tech., Taiwan) at pulse rate of 5 sec on and off with intensity 20KHz. The color of the solution turns to a light yellow (Fig. 2). This leaf extract was allowed to cool at room temperatureand filtered using Whatmann filter paper No.1. This extract was stored in refrigerator to protect it from fungal growth. Same procedure was used for the perperation of ethanolic extract of leafs sample.(Fig.2)

Fig.1 *Azadirachtaindica*l eave sample

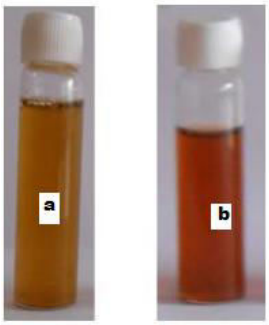

Fig. 2a water and 2b ethanolic extract of *Azadirachtaindica*of leaves samples, respectively

Characterizations

Fourier Transform Infrared (FTIR) Spectroscopy

A Fourier transform infrared (FTIR) spectrum was recorded on FTIR-8400 spectrophotometer (Shimadzu, Tokyo, Japan) within the spectral range of 500 - 4000 cm^{-1} with a resolution of 4 cm^{-1}. The samples were prepared in the pellet form by mixing potassium bromide (KBr) as a binder.

Qualitative tests for analysis of phytochemicals

The aqueous and ethanolic extract from the leaves of *A. indica* was subjected to qualitative analysis for the presence of variousphytochemical components namely steroids, alkaloids, flavonoids, diterpenes, triterpenes and saponins.The presence of steroids and triterpenes was determined by Salkowski's test. Mayer's test, Wagner's test, Hager's test and Dragendroff's tests were used to verify the presence of alkaloids. The sodium hydroxide test was used to confirm the presence of glycosides. The ferric chloride test was used to determine the presence of tannins and flavonoids, while the froth test was performed to determine the presence of saponins.

Results and discussion

Detection of steroids

Salkowski's test was used to detect the presence of steroids in the given sample. For this, fifty milligrams of the extract were dissolved in three millilitres of chloroform. Few drops of concentrated sulphuric acid were added through the sides of the test tube and the solution was allowed to stand. The development of red colour indicates the presence of steroids.

Detection of alkaloids

About 400 ml of the extract was mixed with 5 ml of ammonia and extracted with an equal volume of chloroform. To this extract, 5 ml of dilute HCl was added. The acid layer obtained was used for the following chemical tests for alkaloids.

Mayer's Test

To 1 ml of acid layer, a few drops of Mayer's reagent were added. The development of a creamy white precipitate indicated the presence of alkaloids.

Wagner's Test

A few drops of Wagner's reagent were added to 1 ml of the extract. The development of reddish- brown precipitate indicated the presence of alkaloids.

Hager's Test

To 1 ml acid extract, a few drops of Hager's reagent were mixed. The development of a yellow precipitate by the sample taken indicated the presence of alkaloids.

Dragendroff's Test

A few drops of Dragendroff's reagent were mixed with 1 ml of acid extract. The development of a reddish-brown precipitate indicated the presence of alkaloids.

Detection of Glycosides

The sodium hydroxide test was used for the detection of glycosides. To 50 mg of the extract 1 ml of distilled water and 6 drops of 10 percent sodium hydroxide solution was added and mixed well. The development of yellow colour indicated the presence of glycosides.

Detection of tannins

The ferric chloride test was used for the detection of tannins. For this, treated 2 mgs of the extract was mixed with 3 ml of 1% ferric chloride solution. The development of a brownish green or a blue-black colouration indicated the presence of tannins.

Detection of flavonoids

The presence of flavonoids in the ethanolic extract was assessed by the ferric chloride test. For ferric chloride test, 2 ml of alcoholic solution of the extract was mixed with a few drops of neutral ferric chloride solution. The development of green colour indicated the presence of flavonoids.

Detection of diterpenes

For this, 5 mgs extract was mixed with 3 ml of 5% copper acetate solution. The development of green colour suggested the presence of diterpenes.

Detection of triterpenes

The Salkowski test was used to assess the presence of triterpenes. 3 ml of chloroform were mixed with 3 ml of extract and this was further shaken with 3 ml con sulphuric acid. The development of yellow colour in the lower layer on standing indicated the presence of triterpenes.

Detection of saponins - Froth test

Approximately 200 mg of the extract was shaken with 5 ml of water. The development of foam that persisted for 10 min indicated the presence of saponins.

National Conference on «Modern Perspectives In Physical and Chemical Sciences » (MPPCS-2024) DOI: **10.13140/RG.2.2.13272.40962**

Fourier transform infrared (FTIR) spectroscopic analysis

FT-IR analysis was performed to identify the bio-molecules present in the *Azadirachta indica* leafs samples. Figure 3 shows FT-IR spectra of the shows peaks at 3412.19, 1635.69, 721.19 cm^{-1} and 3412.19, 1631.83, 719.17 cm^{-1} for ethanolic and water extracts, respectively in the region of 700-3500 cm^{-1}. The absorption peak located at 3412.19 cm^{-1} can be attributed to the stretching vibrations of alcohols (-O-H), peaks at 1635.69 and 1631.83 cm^{-1}indicates the presence of H bend bond for 1° proteins, 719 cm^{-1} is forStrong C-Br and Strong C-I stretching.As plant is rich source of carbazole alkaloids, bioactive coumarins, acridine alkaloids and carbazole alkaloids present in both the extracts.

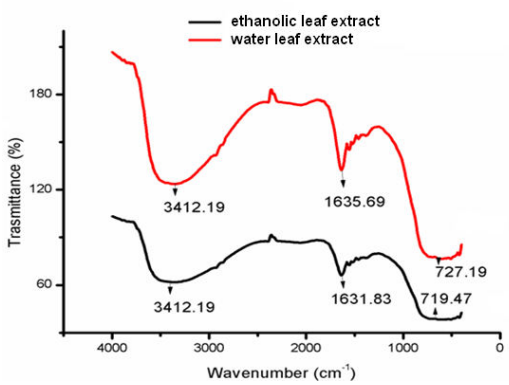

Fig. 3 FT-IR spectra of *Azadirachta indica* leaf samples

Conclusion

The results of the present study have confirmed the presence of numerous medicinally important compounds of *Azadirachta indica* extract that might serve as a good source of drugs for pharmaceutical industries. The identification and characterisation of phytochemicals in the extract could pave way for the development of a wide range of medicinally and industrially beneficial formulations with diverse biomedical applications. The importance of this method is for preparation of extract is efficient due to ultrasound, cheaper, non-toxic, less time consuming.

References

[1] Kumar S, Vandana UK, Agrwal D, Hansa J. Analgesic, Anti-inflammatory and Anti-pyretic Effects of Azadirachtaindica(Neem) Leaf Extract in albino rats. International Journal Scientific Research. 2015;4: 713–721.
[2] Dhama K, Mani S, Chukrubarty S, Tiwari R, Kumar A, Selvaraj P, Rai RB. Herbal Remedies to combat Cancers in Humans and Animals. A Review International Journal of Current Research. 2013; 5: 1908-1919.
[3] Mahima AK, Verma A, Kumar A, Rahal R, Deb SK. Immumomodulatary Therapeutic Potential of Herbal,Traditional and Ethnovertinary Medicine. Pakistan Journal of Biological Science. 2013;15: 754-774.
[4] Padal SB, Sandhya B, Chandrasekhar P, Vijayakumar Y. Folklore treatment of skin diseases by the tribes ofMadugulaMandalam, Visakhapatnam District, Andhra Pradesh, India. Journal of Environmental Science,Toxicology and Food Technology.2013;4: 26-29
[5] Vermani K, Garg S. Herbal medicine for sexually transmitted diseases and AIDS. Journal of Ethnopharmacology.2002; 80: 49-66.
[6] Raymond S, Jonathan S, Jah J, Michael W. Biochemistry of Alkaloids. 2010; 15:83-90
[7] Rhoades DG. Evolution of plants chemical defense against herbivoures in Rosenthal. Their interaction withSecondary Plant Metabolites. 2010; 2:1-45
[8] Lindhorst, TK. Essentials of Carbohydrate Chemistry and Biochemistry. Wiley-VCH. 2007; ISBN 978-3-527-31528-4.
[9] Michael, S. A life of its own. 2009; The New Yorker.
[10] Sadava D, Hillis DM, Heller HC, Berenbaum MR. Life: The Science of Biology 9th Edition. San Francisco:Freeman. 2011; pp. 105–114.
[11] Katie, Jr. EF, Thorington RW. Squirrels: The Animal Answer Guide. Johns Hopkins University Press, Baltimore,London, 2006; 91.
[12] Torres J, Olivares S, De La Rosa D, Lima L, Martínez F, Munita C S, Favaro DIT. "Removal of mercury(II) andmethylmercury from solution by tannin adsorbents". Journal of Radioanalytical and Nuclear Chemistry. 1999; 240(1): 361–365.
[14] Takashi Sakaguchia; Akira Nakajimaa. "Recovery of Uranium from Seawater by Immobilized Tannin". SeparationScience and Technology. 1987;22 (6): 1609–1623
[15] Svobodová A, Psotová J, Walterová D. Natural Phenolics in the Prevention of UV-induced Skin Damage. BiomedPapers, 2003; 147:137–145
[16] Foerster, H. MetaCyc Pathway: Saponin Biosynthesi. 2006.
[17] Liener, IE . Toxic constituents of plant food stuffs. The Proceedings of the Nutrition Society. New York City: AcademicPress. 1980; 29:pp. 56–7

National Conference on «Modern Perspectives In Physical and Chemical Sciences » (MPPCS-2024) DOI: **10.13140/RG.2.2.13272.40962**

Content is available at: CRDEEP Journals
Journal homepage: http://www.crdeepjournal.org/category/journals/ijbas/

International Journal of Basic and Applied Sciences
(ISSN: 2277-1921) (Scientific Journal Impact Factor: 6.188)

UGC Approved-A Peer Reviewed Quarterly Journal

To Investigate the Sintering Influence on Fabrication of Lanthanum oxide nanoparticles via sol-gel tactics

Sangita Shinde[1], Pallavi Nalle[2], N.D. Chaudhari[3], P. Kute[4] , F.B. Quadri[*5]
[1,3,4]Pratishthan Mahavidyalay, Paithan, Chhatarapati Sambhaji Nagar, M.S. India.
[2]Shri Shivaji Science and Arts College, Chikhali, M.S. India.
[5]Department of Physics, Dr. Rafiq Zakaria College for Women, Chhatarapati Sambhaji Nagar, M.S. India.

Abstract
Not Nanotechnology is a cutting-edge field of science, it allows the processing of materials in nanometers. Nanotechnology has numerous applications in different areas such as human health, environment, bio-diagnostics, drug delivery etc. In this paper a facile sol-gel tactics was used to fabricate Lanthanum Oxide nanoparticles (La_2O_3 NPs). For this La_2O_3 powder, nitric acid and polyethylene glycol (PEG) was used as an initial materials. After fabrication of La_2O_3 nano particles, their characteristics were studied through various characterization techniques, like X-Ray diffraction (XRD), SEM, etc. To interrogate the influence of sintering temperatures on the particle size and other properties, the fabricated La_2O_3 La_2O_3 nanopowder was sintered at various temperatures which includes 600 ^{0}C, 700 ^{0}C and 800 ^{0}C. The obtained results shows the calcination effect on particles size. Here XRD confirms hexagonal phase of La_2O_3 NPs of which lattice constant values are a = 0.3963 nm, b = 0.3963 nm and c = 0.6118 nm. In this investigation we observe that the average particle size of the La_2O_3 NPs calculated were in good agreement with the average crystal size obtained from the XRD data.

Keywords: La_2O_3 NPs, Sol-Gel tactics, Sintering, XRD, SEM

Introduction

The Rare earth elements are discriminated by their high melting point, high density, high thermal conductance and high conductivity. They possess specific physical as well as chemical properties because of their 4f orbital electron. The Rare earth elements have extensive applications in medical, electronics, biomedical and agronomical fields [1, 2]. The metal oxides retain extraordinary remarkable contributions in a lot of areas of material science, physics and Chemistry [3]. As they can take huge number of structural geometries with a specific electronic structure, it shows the semiconductor, insulator or metallic character. They have huge applications like sensors, fuel cell, as a catalysts….etc. The Metal oxides has used as a catalysts for the preparation of various product in petrochemical and chemical industries [4, 5]. The huge section of semiconductor industry uses of metal oxide to make electronic components, like microchips used in computers [6]. If once the metal oxide particle size is demolished to nanometer range, due to surface chemistry a huge number of properties depending on particle size was initially developed [7-9] and on ratifying size of nanoparticles they reveal particular physical and chemical properties. There has an impact of particle size on three fundamental properties of a material which have structural characteristics, lattice symmetry and unit cell parameters [10]. Lanthanum ((III) oxide), is a rare earth metal oxide. Lanthanum (III) oxide, (La_2O_3), is called as lanthania which is an odorless, white solid, insoluble in water and soluble in dilute acid. La_2O_3 has the significant optical band gap which was 4.3 eV, high dielectric constant, 27 and the minimum lattice energy [11]. Due to these special properties lanthania has a huge applications in drastic areas like ceramics, optics, gas sensors, dielectric layers in devices, magnetic data storage, for preparing high refraction optical fibers, biosensors, automobiles, water treatment, biomedicine and other alloys materials etc. [12-14].

The various methods have developed for the fabrication of La_2O_3 ultrafine powders, nanowires, nano-sheets, nano-needles, and nanoparticles, incorporate with sol–gel [15, 16], hydrothermal [17, 18], sonochemical [19, 20], microwave , thermal decomposition [21], chemical precipitation , green carbonation [22], starch template [23] and other chemical and physical techniques. All these sintering methods have their own advantages and disadvantages. Among these fabrication methods, the sol-gel is a superficial, economical and ecofriendly. The simplest sol– gel method have been carried out by Wang et al. [24] to fabricate La_2O_3 nanoparticles They were reported that particle size was affected by sintering temperature as well as concentration of PEG in the solution [25]. In this study we have reported the fabrication of rare

earth metal oxide lanthania nano particles via sol-gel tactics using PEG as precursors. The fabricated rare earth metal oxide lanthania La_2O_3 NPs were characterized by XRD, SEM … etc.

Materials and Methods

In this fabrication process the chemicals were used of analytical grade and all chemicals were used as it is purchased from market. Here, the sol-gel technique was used to prepare La_2O_3 NPs. In order to prepare sol solution, 2.50 g of La_2O_3 powder was kept in glass beaker then 25% aqueous solution of HNO_3 was added drop wise in beaker with continuous fast magnetic stirring until an aqueous solution of lanthanum nitrate ($La(NO_3)_3$ was produced. $6H_2O$). By adding different amount of PEG solutions of different concentrations were prepared. The solution was then further stirred for 15 minutes using a magnetic stirrer. The solution was then kept in a water bath at 90 °C with continuous stirring for 2.5 hours until maximum amount of water was evaporated and a clear gel was formed. The obtained product was allowed to cool down to room temperature. Finally, the product is heated in Oven at 95 °C for 70 h to obtain a dry gel. The dry gel was then grounded using an agate mortar and pestle to produce a white powder. The powder was heat treated in a furnace at 300 °C. Then afterward, the product powder was sintered at the various temperatures including 600 °C, 700 °C, and 800 °C. The final product was La_2O_3 NPs. To interrogate the influence of sintering temperatures on the particle size and other properties, the fabricated La_2O_3 nanopowder was sintered at various temperatures which includes 600 ^{0}C, 700 ^{0}C and 800 ^{0}C.

Characterization of Samples

An 3000 X-ray powder diffractometer was used to do the structural characterization of the fabricated La_2O_3 NPs in the 2θ range (λ = 0.154 18 nm). The SEM (surface morphology) of all NPs samples was probed using a Philips XL 30 ESEM electron microscope (20 kV).

Results and **Discussion**

XRD Characterization

Fig. 1 shows the X-ray diffraction patterns of La2O3 NPs fabricated with PEG concentration sintered at 600 0C, 700 0C and 800 0C, and these XRD patterns were divulge phase purity and also crystal structure of the La2O3 NPs. The diffraction peaks of all samples were pointed to (100), (002), (101), (102), (110), (200), (112), and (201) reflections corresponding to the pure hexagonal phase with lattice constant, a =0.3963, b = 0.3963 nm and c = 0.6118 nm. The sharp diffraction peaks of all samples confirm the best crystallization of the La2O3 NPs. The broader peaks advise that La2O3 NPs have the nanometer-size structures. It was notice that with increasing sintering temperature from 600 0C to 800 0C the height of peak was increases and full width at half maximum was decreases, which indicates that crystallization of the samples improve and the size of particles acquire larger [24, 25].

The width of peak varies with the crystallite size of the material. The crystallite size, D of sample material can be estimated by using the Scherrer's formula [26]:

$$D = \frac{M\lambda}{\beta cos\theta_B}$$

Where, D= diameter of the crystallite, β = FWHM of the selected diffraction peak, θB = Bragg angle, λ is the wavelength of the X-ray used, and M is a constant. The average crystal size calculated by the Debye Scherrer's equation was found to be in the range of 19.10-30.31 nm.

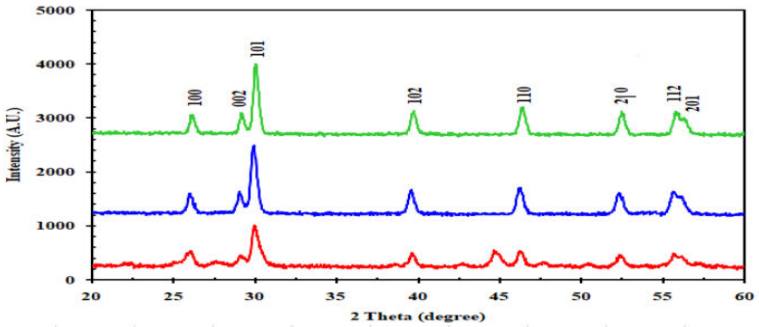

Fig. 1. XRD patterns of La_2O_3 NPs samples sintered at 600 ^{0}C, 700 ^{0}C and 800 ^{0}C

SEM Characterization

As shown in Fig. 2, Fig. 3 and Fig. 4, SEM micrographs of dispersed La2O3 NPs prepared with PEG sintered at 600 0C, 700 0C and 800 0C, respectively. The SEM characterization shows that there was change of the average particle size with sintering temperature. It can be clearly deduced that the mastery of particle size on the sinteration temperature. It can be also shows that the particle size is moderately increased with the increase in sintering temperatures. This is can be take

place as the particles increases gently at low temperature while particles grow very vigorously at higher temperature to form agglomeration. This result was in good agreement of previous work [24].

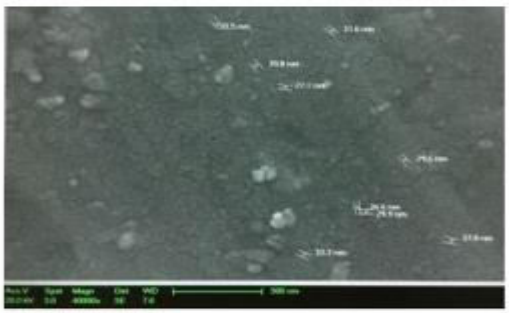

Fig. 2: SEM micrographs of dispersed La_2O_3 NPs sample sintered at 600 ^{0}C

Fig. 3: SEM micrographs of dispersed La_2O_3 NPs sample sintered at 700 ^{0}C

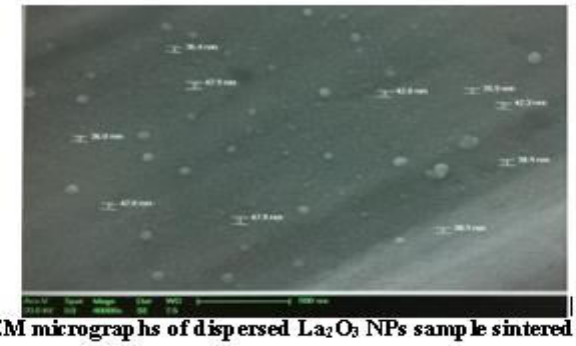

Fig.4: SEM micrographs of dispersed La_2O_3 NPs sample sintered at 800 ^{0}C

Conclusion

La2O3 nanoparticles were successfully fabricated via sol-gel tactics and the influence of sintering temperature on the size of nanoparticles was investigated. All of the diffraction peaks of La2O3 NPs obtained from XRD data were confirm the pure hexagonal phase. The average crystal size calculated by the Debye Scherrer's equation was found to be in the range of 19.10-30.31 nm. The particle size was found to be increased with increasing sinteration temperature

References

[1] P. Huang, J. Li, S. Zhang, C. Chen, Y. Han, N. Liu, Y. Xiao, H. Wang, M. Zhang, Q. Yu, Y. Liu, and W. Wang, Effects of lanthanum, cerium, and neodymium on the nuclei and mitochondria of hepatocytes: Accumulation and oxidative damage, Environ. Toxicol. Pharmacol. 31 (2011) 25–32.

[2] Z. K. Bolaghi, S. M. Masoudpanah, M. Hasheminiasari, Photocatalytic properties of ZnO powders synthesized by conventional and microwave-assisted solution combustion method, J. Sol-Gel Sci Technol. 86 (2018) 711-718.

[3] M. H. Oghaz, R. S. Razavi, M. Barekat, M. Naderi, S. Malekzadeh, M. Rezazadeh, Synthesis and characterization of Y2O3 nanoparticles by sol–gel process for transparent ceramics applications, J. Sol-Gel Sci. Technol. 78 (2016) 682–691.

[4] Y. Xin, Y. Qi, X. Ma, Z. Wang, Z. Zhang, and S. Zhang, Rare-earth (Nd, Sm, Eu, Gd and Y) enhanced CeO2 solid solution nanorods prepared by co-precipitation without surfactants, Mater. Lett. 64 (2010) 2659–2662.

[5] G. Oskam, Metal oxide nanoparticles: synthesis, characterization and application, J. Sol-Gel Sci Techn. 37 (2006) 161-164.

[6] A. H. Lu, E. L. Salabas, and F. Schüth, "Magnetic nanoparticles: Synthesis, protection, functionalization, and application, Angew. Chemie - Int. Ed. 46 (2007) 1222–1244.

[7] J. Das, V. S. Moholkar, S. Chakma, Structural, magnetic and optical properties of sonochemically synthesized Zr-ferrite nanoparticles, Powder Technol. 328 (2018) 1-6.

[8] C. Aubery, C. Solans, S. Prevost, M. Gradzielski, and M. Sanchez-Dominguez, Microemulsions as reaction media for the synthesis of mixed oxide nanoparticles: Relationships between microemulsion structure, reactivity, and nanoparticle characteristics, Langmuir 29 (2013) 1779–1789.

[9] N. C. Zheng, Z. Wang, J. Y. Long, L. J. Kong, D. Y. Chen, Z. Q. Liu, Shape-Dependent Adsorption of CeO2 Nanostructures for Superior Organic Dye Removal, J. Colloid Interface Sci. 525 (2018) 225–233.

[10] H. Abdulhamid, E. Fridell, and M. Skoglundh, Influence of the type of reducing agent (H2, CO, C3 H6 and C3 H8) on the reduction of stored NOX in a Pt / BaO / Al2O3 model catalyst, 2004 (2010) 161–168.

[11] Y. Gao, Y. Masuda, and K. Koumoto, Micropatterning of lanthanum-based oxide thin film on self-assembled monolayers, J. Colloid Interface Sci. 274 (2004) 392–397.

[12] L. Zhang, L. Zhou, Q. X. Li, H. Liang, H. Qin, S. Masutani, B. Yoza, Toxicity of lanthanum oxide nanoparticles to the fungus Moniliella wahieum Y12T isolated from biodiesel, Chemosphere 199 (2018) 495-501.

[13] J. Kang, Y. Kim, D. W. Cho, Y. Sohn, Synthesis and physicochemical properties of La(OH)3 and La2O3 nanostructures, Mater. Sci. Semicon. Proces. 40 (2015) 737–743.
[14] S. Khanjani and A. Morsali, Synthesis and characterization of lanthanum oxide nanoparticles from thermolysis of nanostructured supramolecular compound, J. Mol. Liq. 153 (2010) 129–132.
[15] A. V. Murugan, S. C. Navale, V. Ravi, Synthesis of nanocrystalline La2O3 powder at 100 °C, Mater. Lett. 60 (2006) 848–849.
[16] A. Bahari, A. Anasari and Z. Rahmani, Low temperature synthesis of La2O3 and CrO2 by Sol – Gel process, J. Engi. Technol. Res. 3(2011) 203-208.
[17] S. Jafari Nejad, H. Abolghasemi, M. a. Moosavian, A. Golzary, and M. G. Maragheh, Fractional factorial design for the optimization of hydrothermal synthesis of lanthanum oxide nanoparticles under supercritical water condition, J. Supercrit. Fluids 52 (2010) 292– 297.
[18] J. Sheng, S. Zhang, S. Lv, W. Sun, Surfactant-assisted synthesis and characterization of lanthanum oxide nanostructures, J. Mater. Sci. 42 (2007) 9565–9571.
[19] M. Salavati-Niasari, G. Hosseinzadeh, and F. Davar, Synthesis of lanthanum hydroxide and lanthanum oxide nanoparticles by sonochemical method, J. Alloys Compd. 509 (2011) 4098–4103.
[20] M. Ranjbar and M. Yousefi, Synthesis and Characterization of Lanthanum Oxide Nanoparticles from Thermolysis of Nano-sized Lanthanum(III) Supramolecule as a Novel Precursor, J. Inorg. Organomet. Polym. Mater. 24 (2014) 652–655.
[21] M. Ghiasi, A. Malekzadeh, Synthesis, characterization and photocatalytic properties of lanthanum oxy-carbonate, lanthanum oxide and lanthanum hydroxide nanoparticles, Superlattices and Microstructures 77 (2015) 295–304.
[22] Y. Xiao, Z. Feng, X. Huang, L. Huang, Z. Long, Q. Wang,Y. Hou, Synthesis of lanthanum oxide nanosheets by a green carbonation process, Chin. Sci. Bull. 59 (2014)1864–1867.
[23] M. Moothedan, K.B. Sherly, Synthesis, characterization and sorption studies of nano lanthanum oxide, J. Water Process Engi. 9 (2016) 29–37.
[24] X. Wang, M. Wang, H. Song, and B. Ding, A simple sol-gel technique for preparing lanthanum oxide nanopowders, Mater. Lett. 60 (2006) 2261–2265.
[25] M. S. Niasaria, G. Hosseinzadeh, F. Davar, Synthesis of lanthanum carbonate nanoparticles via sonochemical method for preparation of lanthanum hydroxide and lanthanum oxide nanoparticles, J. Alloys Compd. 509 (2011) 134–140.
[26] B. D. Cullity, Elements of X-ray Diffraction, Second Ed., Addison-Wesley Company, USA, 1978.

National Conference on «Modern Perspectives In Physical and Chemical Sciences » (MPPCS-2024) DOI: **10.13140/RG.2.2.13272.40962**

Content is available at: CRDEEP Journals
Journal homepage: http://www.crdeepjournal.org/category/journals/ijbas/

International Journal of Basic and Applied Sciences
(ISSN: 2277-1921) (Scientific Journal Impact Factor: 6.188)

UGC Approved-A Peer Reviewed Quarterly Journal

Development and Validation of Area under Curve Method for the Estimation of Sitagliptin and Dapagliflozin in Bulk and Dosage Form

Ashwini D. Nikam, Dr. Sachin S. Rane
Honorable Lok sevak Madhukar Rao Chaudhari College of Pharmacy, Faizpur Dist.: Jalgaon.

Abstract
A simple, accurate and precise Area Under Curve (AUC) spectrophotometric method was been developed for simultaneous estimation of sitagliptin and dapagliflozin in bulk and pharmaceutical dosage form. It involves measurement of area under curve in the range of 260- 270 nm for sitagliptin 275-285 nm for dapagliflozin respectively. Calibration curves were plotted for the method by using instrumental response at selected wavelengths and concentrations of analyte in the solution. In both the methods linearity was found in the concentration range of 10-50 µg/ml for sitagliptin and 5-25 µg/ml for dapagliflozin. The percentage estimation of the drugs was found to be 99.74 % and 99.69 % for sitagliptin and dapagliflozin representing the accuracy of the method. The method showed good reproducibility and recovery with % RSD less than 2. The method found to be rapid, specific, precise and accurate, and can be applied for routine analysis in combined dosage form without any interference by the excipients. The above method was validated according to ICH guidelines.

Keywords*:* Sitagliptin and Dapagliflozin Area Under Curve method, ICH, Validation etc.

Introduction

Sitagliptin is an oral dipeptidyl peptidase-4 (DPP-4) inhibitor used in conjunction with diet and exercise to improve glycemic control in patients with type 2 diabetes mellitus [1,2] The effect of this medication leads to glucose dependent increases in insulin and decreases in glucagon to improve control of blood sugar Chemically sitagliptin is(2R)-4-oxo-4-[3-(trifluoromethyl)-5,6-dihydro(1,2,4)triazolo(4,3-a)pyrazin-7(8H)-yl]-1-[2,4,5-trifluorophenyl]butan-2-amine.(2R)-4-oxo-4-[3-(trifluoromethyl)-5,6-dihydro(1,2,4)triazolo(4,3-a)pyrazin-7(8H)-yl]-1-[2,4,5-trifluorophenyl]butan-2-amine [3,4,5,6].Sitagliptin is an oral dipeptidyl peptidase-4 (DPP-4) inhibitor used for the management of type 2 diabetes mellitus Sitagliptin is an oral dipeptidyl peptidase-4 (DPP-4) inhibitor used in conjunction with diet and exercise to improve glycemic control in patients with type 2 diabetes mellitus [7,8,9]. The effect of this medication leads to glucose dependent increases in insulin and decreases in glucagon to improve control of blood sugar. it consequently inhibits the degradation of incretin hormones, like glucagon-like peptide-1 (GLP-1) and glucose-dependent insulinotropic peptide (GIP), resulting in increased insulin secretion and inhibited glucagon release by the beta and alpha cells of the pancreas, improving glycemic control [10,11,12]. It is one of the most effective dipeptidyl-peptidase-4 inhibitors involved in reducing glycosylated hemoglobin (HbA1c) [13]

The chemical name for dapagliflozin is (2S,3R,4R,5S,6R)-2-(4-chloro-3-(4-ethoxybenzyl) phenyl)-6-(hydroxymethyltetrahydro-2H-pyran-3,4,5-triol [14]. Dapagliflozin is in a class of medications called sodium-glucose co-transporter 2 (SGLT2) inhibitors [15]. Dapagliflozin is inhibiting renal glucose reabsorption through the solid-glucose cotransporter offer insulin independent alternative to controlling blood glucose concentration in patient with type 2 diabetes [16]. It lowers blood sugar by causing the kidneys to get rid of more glucose in the urine. Its mechanism of action is independent of pancreatic β cell function and modulation of insulin sensitivity. Its mechanism of action is independent of pancreatic β cell function and modulation of insulin sensitivity. Glycemic control in patient with type 2 diabetes mellitus by inhibiting the sodium glucose Co-Transporter 2, intern by reducing glucose reabsorption [17].

The reason behind the combination of sitagliptin and dapagliflozin is used to treat type-2 diabetes mellitus. Type-2 diabetes mellitus (also known as non-insulin-dependent diabetes or adult-onset diabetes) is a medical condition in which blood glucose levels are above normal due to insulin deficiency, insulin resistance, or both. Sitagliptin is an oral dipeptidyl peptidase-4 (DPP-4) inhibitor used in conjunction with diet and exercise to improve glycemic control in patients with type 2 diabetes mellitus..Sitagliptin works to competitively inhibit the enzyme dipeptidyl peptidase 4 (DPP-4) [18] . By increasing

insulin levels and lowering glucagon levels (the hormone that raises blood glucose levels), sitagliptin decreases the amount of glucose the liver produces [19]. Thus, sitagliptin and dapagliflozin helps control blood sugar levels sitagliptin and dapagliflozin is used to treat type-2 diabetes mellitus. Type-2 diabetes mellitus (also known as non-insulin-dependent diabetes or adult-onset diabetes) is a medical condition in which blood glucose levels are above normal due to insulin deficiency, insulin resistance, or both [20].

Sitagliptin and Dapagliflozin is a new drug combination. There are various published papers on this drug single or in combination with other drug by UV 9,10,11, HPLC12,13,14,15,16,17,18 but there are very few published papers on this drug combination and not a single paper on AUC method on same. The method is easy, simple and gives reproducible results as compared to other UV methods. Therefore, this is a humble attempt to develop simple, robust, reproducible method for the determination of efficacy and safety of sitagliptin and dapagliflozin combination. This method was fully validated according to International Conference on Harmonization (ICH) and ready for the application in routine analysis without interference of an excipients.

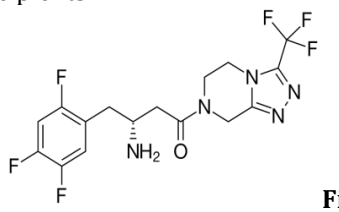

Fig. No. 1. Structure of Sitagliptin

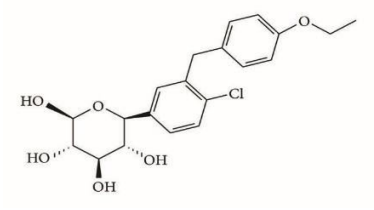

Fig. No. 2. Structure of Dapagliflozin

Materials and Methods

Instruments

Shimadzu UV-1800 double beam spectrophotometer was used to record the spectra of sample and reference solutions using pair of quartz cells of 10 mm path length. All weighing was carried out on Sansui Vibra DJ-150S-S weighing balance. Sonicator of Fast Clean is used for the purpose of sonication, Filter papers of Sartorius Stedim Biotech of grade 292 are used for the filtration purpose.

Chemicals

Sitagliptin (100 mg) and dapagliflozin (10 mg) API were obtained as a gift sample from Cadila Healthcare, Sanand. The combined formulation Dapanorm® (100 mg/10 mg) of the two drugs purchased from Pramod Medicals, Faizpur. Analytical grade methanol purchased from Merck Chemicals Pvt. Ltd. Mumbai.

Preparation of stock solution and selection of wavelength

Sitagliptin stock solution

An accurately weighed quantity of Sitagliptin (10 mg) was taken in 10 mL volumetric flask and dissolved in methanol (8 mL) with the help of ultrasonication for about 10 min. Then the volume was made up to the mark using methanol to get Sitagliptin standard stock solution (1 mg / mL).

Sitagliptin working solution

Sitagliptin standard stock solution (5 mL) was diluted to 50 mL using 80 % v/v methanol to get working standard solution (100 µg/mL)

Dapagliflozin stock solution

An accurately weighed quantity of Dapagliflozin (10 mg) was taken in 10 mL volumetric flask and dissolved in methanol (8 mL) with the help of ultrasonication for about 10 min. Then the volume was made up to the mark using methanol to get Dapagliflozin standard stock solution (1 mg / mL).

Dapagliflozin working solution

Dapagliflozin standard stock solution (5 mL) was diluted to 50 mL using 80% v/v methanol to get working standard solution (100 µg / mL)

Determination of λ Max of Individual Component

National Conference on «Modern Perspectives In Physical and Chemical Sciences » (MPPCS-2024) DOI: **10.13140/RG.2.2.13272.40962**

The overlay spectra of both drugs were recorded and two wavelengths 265 nm (λ of sitagliptin) and 275 nm (λ of dapagliflozin) were selected for further study.

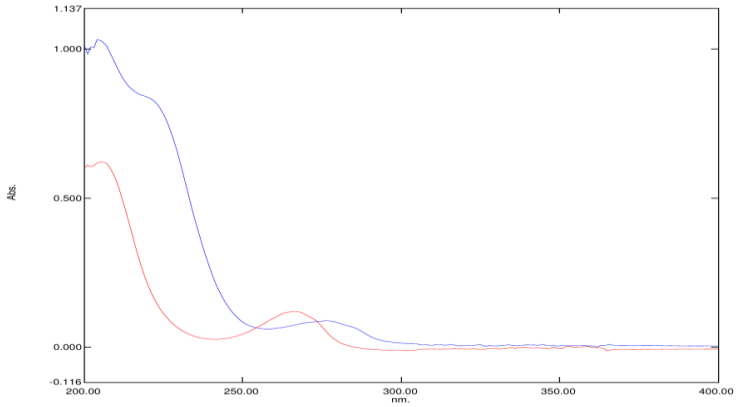

Graph No. 1 Overlay spectra of sitagliptin and dapagliflozin

Linearity study for Sitagliptin

An accurately measured aliquot portion of working standard solution of Sitagliptin was transferred to five separate 10 mL volumetric flasks. The volume was made up to the mark using 80 % v/v methanol to obtain concentrations of Sitagliptin (10µg/ml, 20µg/ml, 30µg/ml,40µg/ml,50 µg/ml). Absorbance of these solutions was measured at 265 nm, Calibration curve was plotted, absorbance Vs concentration.

Linearity study for Dapagliflozin

Accurately measured aliquot portions of working standard solution of Dapagliflozin were transferred to five separate 10 mL volumetric flasks. The volume was made up to the mark using 80% v/v methanol to obtain concentrations (5µg/ml, 10µg/ml, 15µg/ml, 20µg/ml, 25µg/ml) Absorbance of these solutions was measured at 275 nm. Calibration curve was plotted, absorbance Vs concentration. The results are shown in the Table No.1

Table No. 1 Regression and Optical characteristics of SITA and DAPA

Parameters	Value for Sitagliptin	Value for Dapagliflozin
Beer's law limit (µg/ml)	10-50 µg/ml	5-25 µg/ml
Regression Coefficient(R^2)	0.998	0.999
Regression equation	y= 0.0066x + 0.0456	y= 0.0092x + 0.0197
Slope	0.00660	0.0092
Intercept	0.0456	0.0197

The study of regression and optical characteristics of SITA and DAPA are carried out in which Regression Coefficient (R^2) of SITA is 0.998and of DAPA is 0.999. The slope of SITA 0.0066 and slope of DAPA is 0.0092 with Intercept of SITA 0.0456 and for DAPA 0.0197Therefore, Concentration vs Absorbance are fairly linear between both co-ordinates by statistical manner and obey ICH guidelines.

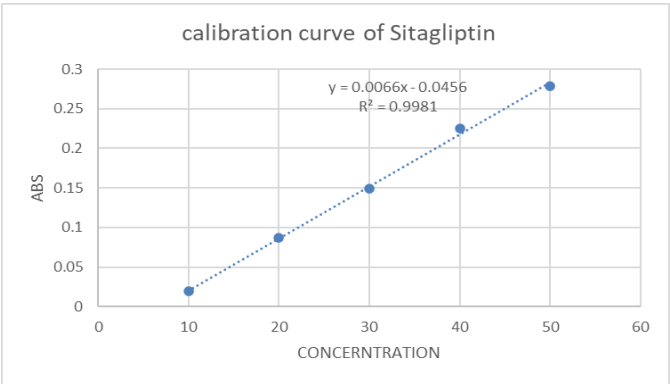

Graph No.2 Calibration curve of Sitagliptin at 265 nm

National Conference on «Modern Perspectives In Physical and Chemical Sciences » (MPPCS-2024) DOI: **10.13140/RG.2.2.13272.40962**

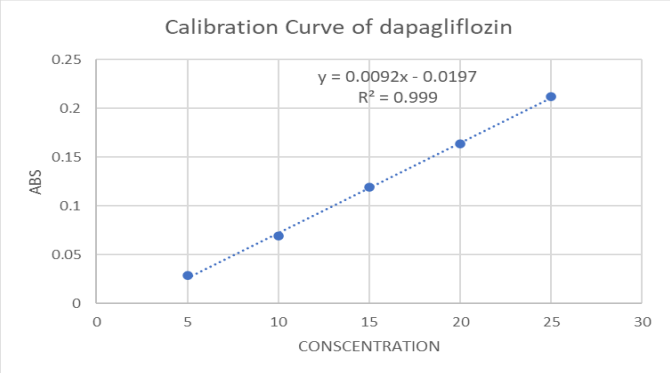

Graph No.3 Calibration curve of Dapagliflozin at 275 nm

Area Under Curve Method

It involves the calculation of integrated value of absorbance with respect to the wavelength between two selected wavelengths λ1 and λ2. Area calculation processing item calculates the area bound by the curve and the horizontal axis. The horizontal axis is selected by entering the wavelength range over which the area has to be calculated. This wavelength range is selected on the basis of repeated observations so as to get the linearity between area under curve and concentration. For the selection of analytical wavelength suitable. dilutions of Sitagliptin (10-50µg/ml) and Dapagliflozin(5-25µg/ml) of the standard stock solutions of both the drugs were prepared separately and scanned in the range of 400-200 nm. Maximum absorbance was observed at 265 nm and 275 nm for Sitagliptin and Dapagliflozin respectively. The wavelength ranges selected for the estimation of sitagliptin and dapagliflozin are 260-270 nm (λ1 and λ2) and 275-285 (λ3 and λ4) respectively. Aliquots were prepared for the sample solution in the concentration range of 10-50µg/ml and 5-25µg/ml for Sitagliptin and Dapagliflozin and their area under curve was measured at above selected wavelengths.

Graphical reports for sitagliptin

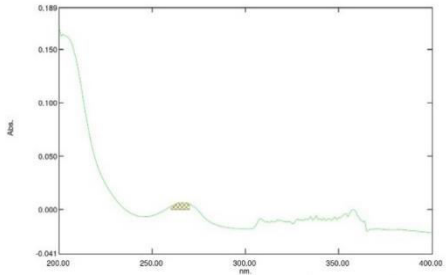

Fig. No3. AUC of SITA for concentration of 30µg/ml

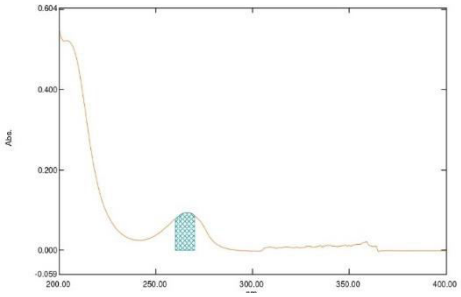

Fig. No4. AUC of SITA for concentration of 30µg/ml

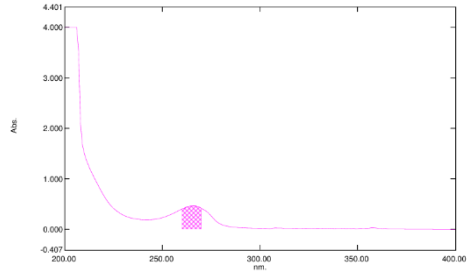

Fig. No5. AUC of SITA for concentration of 30µg/ml

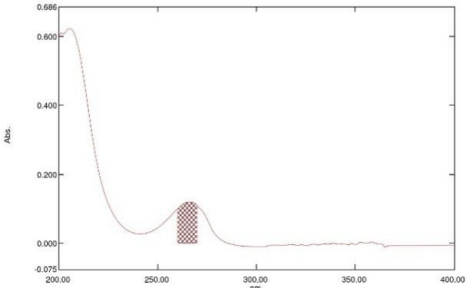

Fig. No7. AUC of SITA for concentration of 50µg/ml

Graphical Reports For Dapagliflozine

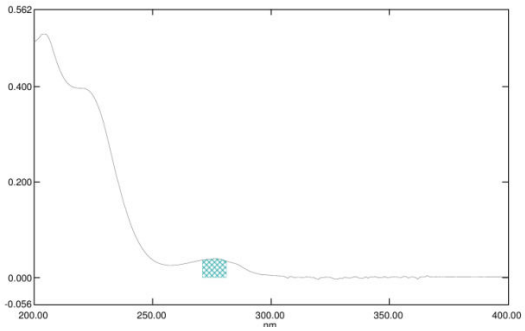

Fig. No.8 AUC of dapa for concentration of 5µg/ml

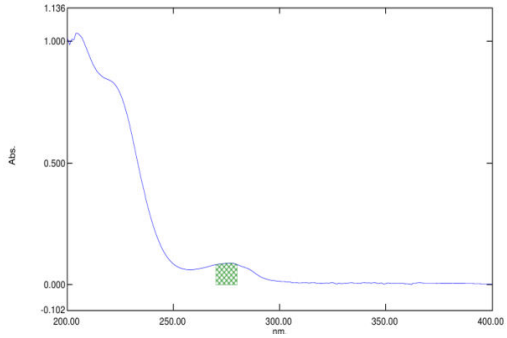

Fig. No. 9 AUC of dapa for concentration of 10µg/ml

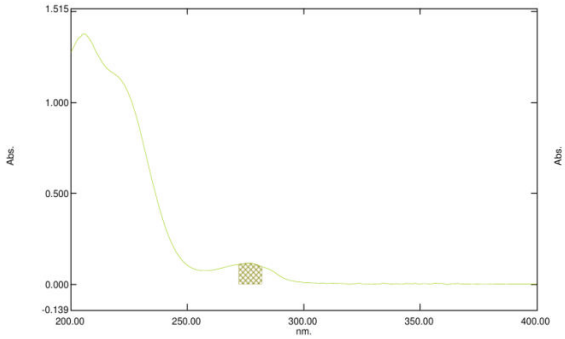

Fig. No.10 AUC of dapa for concentration of 15µg/ml

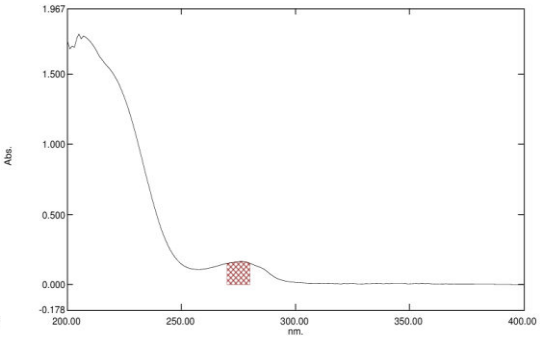

Fig No.11 AUC of dapa for concentration of 20µg/ml

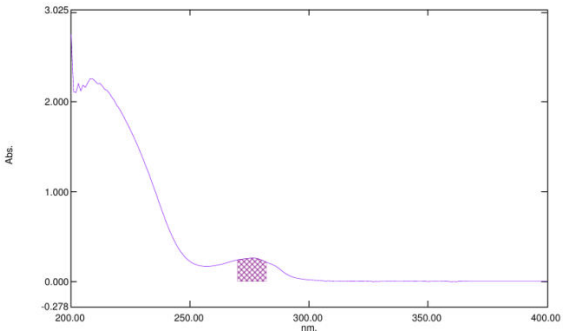

Fig No.12 AUC of dapa for concentration of 25µg/ml

Estimation of Laboratory mixture by proposed method
Method: Area Under Curve Method

The Area Under Curve range of sitagliptin and dapagliflozin was taken as 260-270 nm and 271-281nm respectively. The absorptivity values calculated. The calibration curve was plotted with concentration v/s area under curve and regression equation was calculated.

Determination of absorptivity values:
Absorptivity = Absorbance / Concentration of the component in gm/l
Csita = A2ay1 – A1ay2 / ax2ay1 – ax1ay2 ----------(1)
Cdapa = A1ax2- A2ax1 / ax2ay1- ax1ay2----------(2)
Were,
Csita = Concentrations Sitagliptin
Cdapa = Concentrations of Dapagliflozin
A1 = Area of Sitagliptin at 260 nm to 270 nm
A2 = Area of Dapagliflozin at 275 nm to 285 nm

Table No. 2. Results of Estimation of SITA and DAPA in standard laboratory mixture

Analyte	% Concentration estimated (Mean ± S.D)	% R.S.D
Sitagliptin	99.86 ± 0.011	0.115
Dapagliflozin	99.58 ± 0.063	0.063

The estimation of SITA and DAPA in Standard Laboratory Mixture are carried out in which % concentration of SITA and DAPA were found to be 99.86 and 99.58 respectively. Those values are fairly accurate by statistical manner and are as per ICH guidelines.

Application of proposed method for Estimation of drugs in tablets

Twenty 'Dapanorm' tablets containing Sitagliptin (100 mg) and Dapagliflozin (10 mg) were weighed and ground to fine powder. A quantity of sample equivalent to Sitagliptin (100 mg) and Dapagliflozin (10 mg) was transferred into 100 mL volumetric flask containing methanol (60 mL), sonicated for 15 min and the volume was made up to the mark and filtered through Whatman filter paper (No. 45). This solution was (1 mL) transferred to 10 mL volumetric flaks, dissolved and volume was adjusted to the mark. The absorbances of the solutions were measured at 265 nm and 275 nm against blank. The concentrations of two drugs in sample were determined by using simultaneous equations. The results are shown in the Table No.3

Table No. 3 Results of Estimation of SITA and DAPA in tablets dosage form.

Analyte	Label claim(mg/tab)	% Label claim estimated (Mean±S.D)	% R.S.D
Sitagliptin	100	99.74 ± 0.158	0.159
Dapagliflozin	10	99.59 ± 0.152	0.153

The results of Estimation of SITA and in tablets dosage shows the % purity 99.74 & 99.59 with SD and RSD bellow 2 which is fairly accurate by statistical manner and are as per ICH guidelines.

Validation of proposed method

The proposed method was validated as per ICH guidelines [21]

Accuracy (Recovery study)

Accuracy of proposed method was ascertained on the basis of recovery study performed by standard addition method. A known amount of standard drug solutions were added to the tablet powder to make final concentrations in the range of 80%, 100% and 120% and re-analyzed it by the proposed method. The absorbance recorded and the % recoveries were calculated using formula.

% Recovery = [A - B/ C] X 100

Where, A = Total amount of drug estimated; B = Amount of drug found on preanalysed basis; C = Amount of Pure drug added

The results are shown in the Table No.4

Table No. 4 Recovery study

Drug in mixture solution (µg/ml)		% Recovery ± S.D.	
Sitagliptin	Dapagliflozin	Sitagliptin	Dapagliflozin
10	5	99.74 ± 0.159	99.82 ± 0.025
20	10	99.75 ± 0.165	99.79 ± 0.378
30	15	99.78 ± 0.168	98.85 ± 0.050

The results of Recovery study of SITA and DAPA are found to be fairly by statistical way and are obey ICH guidelines

Precision

Precision was determined as intra-day and inter-day variations. Intra-day precision was determined by analyzing Sitagliptin (10, 20, and 30 µg/mL) and Dapagliflozin (5,10 and 15 µg/mL) for three times on the same day. Inter-day precision was determined by analyzing the same concentration of solutions for three different days over a period of week. The results are shown in the Table No. 5

Table No.5 Precision Study

Drug	Conc. [µg/mL]	Intra-day Amount Found		Inter-day Amount Found	
		Mean ±S.D [*n* = 5]	% R.S.D.	Mean ± S.D. [*n* =5]	% R.S.D.
SITA	10	9.81 ± 0.2887	0.2928	9.87 ± 0.1546	0.1546
	20	19.84 ± 0.1501	0.0504	19.85 ± 0.0257	0.1267

	30	29.80 ± 0.692	0.5048	29.68 ± 0.173	0.5836
DAPA	5	4.93± 0.0360	0.7313	4.86 ± 0.0602	1.2385
	10	9.94± 0.0416	0.4195	9.88 ± 0.0305	0.3091
	15	14.95 ± 0.0355	0.2043	14.95 ± 0.0351	0.2348

n=3

The Precision Study of SITA and DAPA were carried out and Results are found to be fairly accurate by statistical manner and obeys ICH guidelines.

Ruggedness

Ruggedness of the proposed method was determined by analysis of aliquots from homogenous slot by two different analyst using same operational and environmental conditions. The results are shown in Table No. 6.

Table No. 6 Ruggedness study

	Sitagliptin 50 µg/ml		Dapagliflozin 10 µg/ml	
	Amount found in µg/ml Mean ± S.D. (n=3)	% R.S.D	Amount found in µg/ml Mean ± S.D. (n=3)	% R.S.D
Analyst I	49.96 ± 0.2066	0.2584	9.95 ± 0.0404	0.4060
Analyst II	49.75 ± 0.4686	0.5876	9.94 ± 0.0264	0.2661
Day I	49.97 ± 0.2254	0.2819	9.93 ± 0.0360	0.3631
Day II	49.81 ± 0.5412	0.6780	9.96 ± 0.0288	0.2887
Instrument I	49.85 ± 0.1184	0.1483	9.95 ± 0.0264	0.2656
Instrument II	49.86 ± 0.1228	0.1538	9.96 ± 0.02082	0.2090

n=3

LOD: Limit of detection of Sitagliptin and Dapagliflozin were found to be 06519 µg/ml and 0.4676 µg/ml respectively.
LOQ: Limit of Quantitation of Sitagliptin and Dapagliflozin were found to be 0.9755µg/ml and 1.4172 µg/ml respectively.

Results and Discussion

Area under curve UV Spectrophotometric Estimation method was developed for Sitagliptin and Dapagliflozin. The method employs 265 nm as λ1 and 275 nm as λ2 for formation of equations. Sitagliptin and Dapagliflozin obeys Beer's law in the concentration range 10-50 µg/ml (R^2=0.981) and 5-25 µg/ml (R^2=0.999) respectively. The mean recovery for Sitagliptin and Dapagliflozin was found to be 99.76and 99.82 % respectively. The developed method were validated according to ICH guidelines and values of accuracy, precision and other statistical analysis were found to be in good accordance with the prescribed values

Conclusion

The proposed area under curve UV Spectrophotometric Estimation method presented in this paper has advantages of simplicity, accuracy, precision and convenience for quantitation of Sitagliptin and Dapagliflozin. The proposed method can be used for the quality control of Sitagliptin and Dapagliflozin in typical laboratories.

Acknowledgement

Dr. Vijay R. Patil, Dr. Rajesh Y. Chaudhari, Dr. Sachin S. Rane.
Thank You for their valuable guidance providing the necessary resources and facilities to carried out this research and I am very Grateful to Everyone.

References

1. Pinak Patel, Yesha Patel, Shivani Jani1 and Krunal Detholia. Quantitative Computation of Synthetic Mixture Comprising Sitagliptin and Dapagliflozin from Synthetic Mixture by Verdot's Method.Journal of Pharmaceuticals Sciences and Drug Discovery.J Pharm Sci Drug Discov, 1(2): 2022

2. Mayank Yadav, Rekha Chauhan, Ranjit Singh. UV-Spectrophotometric Approach for Concurrent Assessment of Sitagliptin and Dapagliflozin. https://doi.org/

3.Shilpi Pathak, Development and Validation of UV-Spectroscopy Method for the Determination of Dapagliflozin, Bulletin of Environment, Pharmacology and Life Sciences Vol 9[12] November 2020.

4. https://go.drugbank.com/drugs/DB01261

5. A P Ravinandan G M Basavanagowda O D Jimmy Review on Sitagliptin J Pharm Res Scholars20143257781

6. https://pubchem.ncbi.nlm.nih.gov/compound/Sitagliptin
7. Jalkote RN, Kalshetti MS (2019) UV Spectrophotometric method development and validation for determination of Sitagliptin in API and in pharmaceutical dosage form. World J Pharm Pharm Sci 8(5): 916-925
8.Retrospective Observational Study on Assessing Sitagliptin and Dapagliflozin as a Fixed-Dose Combination in the Indian Population with Type 2 Diabetes Mellitus: The SIDAXA Study
Manoj Chawla [1], Dharmarajan Panneerselvam
9. https://pmc.ncbi.nlm.nih.gov/articles/PMC11191412
10. Berger, J.P.; Sinharoy, R.; Pocai, A.; Kelly, T.M.; Scapin, G.; Kelly, Y.G.; Pryor, A.D.; Wu, J.K.; Eiermann, G.J.; Xu, S.S.; et al. A comparative study of the binding properties, dipeptidyl peptidase-4 (DPP-4) inhibitory activity and glucose-lowering efficacy of the DPP-4 inhibitors alogliptin, linagliptin, saxagliptin, sitagliptin and vildagliptin in mice. Endocrinol. Diabetes Metab. 2018, 1, 1–8. [CrossRef] [PubMed]
11. Green, J.B.; Bethel, M.A.; Armstrong, P.W.; Buse, J.B.; Engel, S.S.; Garg, J.; Josse, R.; Kaufman, K.D.; Koglin, J.; Korn, S.; et al. Effect of Sitagliptin on Cardiovascular Outcomes in Type 2 Diabetes. N. Engl. J. Med. 2015, 373, 232–242. [CrossRef] [PubMed]
12**.** Nayana C.F.S., Andressa V., Laiane J.O. (2019). Solid-State Characterization of Different Crystalline Forms of Sitagliptin. Materials. 12, 2351
13. A P Ravinandan G M Basavanagowda O D Jimmy Review on Sitagliptin J Pharm Res Scholars20143257781
14. https://go.drugbank.com/drugs/DB06292
15. https://pubchem.ncbi.nlm.nih.gov/compound/Dapagliflozin
16. Bodade BJ, Kande DA, Chaudhari SS (2019) Quantitative Estimation of Dapagliflozin in blood plasma by using UV Spectroscopy. Pharmaceutica Analytica Acta 10(2): 2153-2435.
17. Mante GV, Gupta RK, Hemke AT (2017) Estimation of Dapagliflozin from its Tablet Formulation by UV spectroscopy. Pharma Methods 8(2): 102-107
18. Bodade BJ, Kande DA, Chaudhari SS (2019) Quantitative Estimation of Dapagliflozin in blood plasma by using UV Spectroscopy. Pharmaceutica Analytica Acta 10(2): 2153-2435.
19. Mante G.V., Hemke A.T., Umekar M.J. (2018). RP-HPLC Method for Estimation of Dapagliflozin from its Tablet. International Journal of Chemtech Research. 11(1), 242- 248.
20. Chaudhury A., Chittaranjan D., Vijaya S.R.D. (2017). Clinical Review of Antidiabetic Drugs: implications for Type 2 Diabetes Mellitus Management. Frontier in Endocrinology. 8, 6.
21. ICH Harmonized Tripartite Guideline. (1996). Validation of Analytical Procedure: Methodology[Q2B].

Books
1.A. H. Beckett, J. B. Sten Lake, Book of Practical Pharmaceutical Chemistry Fourth Edition Part Two CBS Publication and Distributors, New Delhi 2005 ISBN: 8123905149 (284-286).

Content is available at: CRDEEP Journals
Journal homepage: http://www.crdeepjournal.org/category/journals/ijbas/

International Journal of Basic and Applied Sciences
(ISSN: 2277-1921) (Scientific Journal Impact Factor: 6.188)

UGC Approved-A Peer Reviewed Quarterly Journal

Development And Validation Of Uv Spectrophotometric Method For The Simultaneous Estimation Of Dapagliflozin And Gliclazide In Bulk Drugs And Tablet Dosage Form.

Ms. Hemangi V. Changare*, Ms. Ashwini D. Patil, Dr. Sachin S. Rane, Dr. Rajesh Y. Chaudhari, Dr. Vijay R. Patil
TVES's Hon'ble Loksevek Madhukarrao Chaudhari College of Pharmacy, Faizpur

Abstract
A simple, robust, precise, UV spectroscopic method has been developed for the simultaneous estimation of Dapagliflozin and Gliclazide in bulk and tablet dosage form. In this paper the estimation of those drugs was carried out by Q-Absorption ratio method. In this method absorption is showed an iso-absorptive point at 274 nm and second wavelength use was 284nm i.e, λmax of Dapagliflozin. The linearity observed for Dapagliflozin is in the range of 5-25µg/ml and for Gliclazide is in the range of 15-75µg/ml. The accuracy of methods was assessed by recovery studies and was found to be within the range of 99%-101% for both Dapagliflozin and Gliclazide. The developed methods were validated with respect to linearity, accuracy (recovery), and precision. The method can be employed for estimation of pharmaceutical formulations with no interference from any other excipients and diluents. The results were validated as per ICH guidelines.

Keywords: Dapagliaflozin, Gliclazide, ICH, Validation, UV, HPLC etc.

Introduction

Diabetes mellitus belongs to a category of metabolic disorder, characterized by chronic hyperglycemia due to deficiency in insulin secretion or action or both people with type 2 diabetes mellitus are susceptible to various short-term complications including premature death and coma.[1]

Dapagliflozin is a highly selective, orally active and reversible inhibitor of the human Sodium-Glucose Co-Transporter 2 (SGLT2), the major transporter responsible for the renal glucose reabsorption. It improves glyceamic control in patients with Type 2 Diabetes Mellitus by inhibiting the Sodium-Glucose Co-Transporter 2, intern by reducing glucose reabsorption. Dapagliflozin is a first generation selective SGLT inhibitor that blocks for SGLT 2 over SGLT1.[2] Chemically Dapagliflozin is called as (2S,3R,4R,5S,6R)-2-{4-chloro-3-[(4-ethoxyphenyl)methyl]phenyl}-6-(hydroxymethyl)oxane-3,4,5-triol. Fig. 1.[3] Dapagliflozin retard the sodium glucose co-transporter 2 (SGLT2) which is essentially present in the primary part of the nephron. Since SGLT2 aides in 92% of the kidneys' ability to uptake glucose , it's blockage enables glucose to be released in urine. Patient with type 2 diabetes may experience better glucose control and possible weight loss due to this excretion.[4]

Gliclazide is a second generation sulphonylurea that is widely used in the treatment of patients with type 2 diabetes because it has similar efficacy to other sulphonylureas but a lower risk of hypoglycaemia.[5,6] Chemically Gliclazide is (1-(1-azabicyclo [3, 3, 0] oct-3-yl)-3-(p-to-ly sulphonyl) urea). Fig. 2 Gliclazide acts by stimulating the Ca++ transport across the pancreatic beta cells membrane by reducing conductance of ATP sensitive K+ channel and hence stimulates insulin secretion from pancreas.[7] It reduces blood glucose levels by correcting both defective insulin secretion and peripheral insulin resistance, increasing the sensitivity of ß-cells to glucose, decreasing hepatic glucose production, and increasing glucose clearance. It also has anti-platelet adhesive activity and reduces levels of free radicals, thereby preventing vascular complications. It also has been reported to reduce plasma cholesterol and triglyceride levels after repeated administration.[20, 21]

In case monotherapy fails, a Fixed-Dose Combination of Dapagliflozin and Gliclazide is used. This combination is approved by the CDSCO (Central Drugs Standard Control Organization) to grant permission for manufacturing and marketing in November 2023. The literature survey disclose that analytical methods in UV spectrophotometric methods, RP - HPLC

methods, and HPTLC methods were reported for Dapagliflozin and Gliclazide individually and in combination with others. But Literature survey did not disclose a spectrophotometric method for fix-dose combination of Dapagliflozin and Gliclazide. In current investigation, an efforts has been made to create a simple reliable and affordable approach.

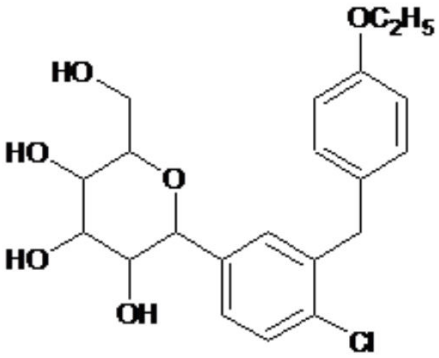

Figure 1: Structure of Dapagliflozin

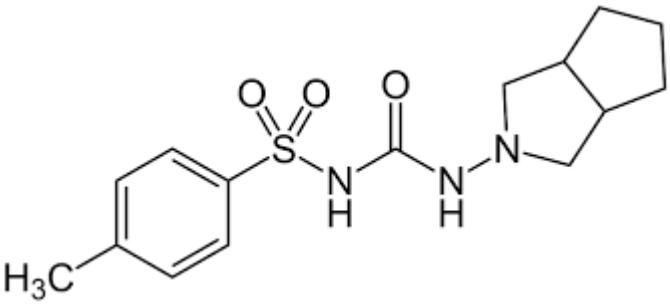

Figure 2: Structure of Gliclazide

Materials and Methods

Instruments

Shimadzu UV-1800 double beam spectrophotometer was used to record the spectra of sample and reference solutions using pair of quartz cells of 10 mm path length. All weighing was carried out on Sansui Vibra DJ-150S-S weighing balance. Sonicator of Fast Clean is used for the purpose of sonication, Filter papers of Sartorius Stedim Biotech of grade 292 are used for the filtration purpose.

Chemicals

Dapagliflozin (20 mg) and Gliclazide (20 mg) pure drugs were obtained as a gift sample from Pons Laboratories, Tamil Nadu, India, and Atlas Life Sciences Private Limited, Gujarat, India. The combined formulation Cyblex D 60 (10 mg/60 mg) manufacture by Eris Lifesciences Limited, purchased from Vikram Pharmacy Jalgaon. Analytical grade methanol purchased from Merck Chemicals Pvt. Ltd. Mumbai.

Preparation of stock solution and selection of wavelength

Dapagliflozin stock solution

An accurately weighed quantity of Dapagliflozin (10 mg) was taken in 10 mL volumetric flask and dissolved in methanol (8 mL) with the help of ultrasonication for about 10 min. Then the volume was made up to the mark using methanol to get Dapagliflozin standard stock solution (1 mg / mL).

Dapagliflozin working solution

Dapagliflozin standard stock solution (0.1 mL) was diluted to 10 mL using methanol and water in the ratio 30:70 to get working standard solution (10 µg/mL).

Gliclazide stock solution

An accurately weighed quantity of Gliclazide (10 mg) was taken in 10 mL volumetric flask and dissolved in methanol (8 mL) with the help of ultra sonication for about 10 min. Then the volume was made up to the mark using methanol to get Gliclazide standard stock solution (1 mg / mL).

Gliclazide working solution

Gliclazide standard stock solution (0.6 mL) was diluted to 10 mL using methanol and water in the ratio 30:70 to get working standard solution (60 µg / mL).

Determination of λ_{max} of Individual Component

An appropriate aliquot portion of Dapagliflozin(0.1 mL) and Gliclazide(0.6 mL) were transferred to two separate 10 ml volumetric flasks, the volume was made up to the mark using methanol and water in ratio 30:70 to obtain Dapagliflozin (10 µg/mL) and Gliclazide(60µg/mL). Drug solutions were scanned separately between 200 nm to 400 nm. Through this method absorption is showed an iso-absorptive point at 274 nm and second wavelength use was 284nm i.e., λ_{max} of Dapagliflozin.

Overlay spectra of Dapagliflozin and Gliclazide

National Conference on «Modern Perspectives In Physical and Chemical Sciences » (MPPCS-2024) DOI: **10.13140/RG.2.2.13272.40962**

The overlay spectra of both drugs were recorded and two wavelengths first is iso-absorptive point at 274nm and second wavelength was found to be 284nm i.e. λ_{max} of Dapagliflozin were selected for further study.

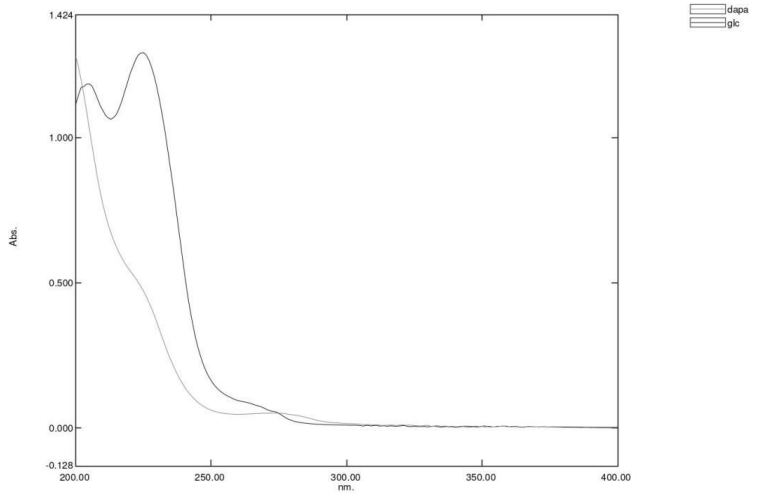

Graph No. 1 Overlay spectra of Dapagliflozin and Gliclazide

Linearity study for Dapagliflozin

An accurately measured aliquot portion of working standard solution of Dapagliflozin was transferred to five separate 10 mL volumetric flasks. The volume was made up to the mark using methanol and water in ratio 30:70 to obtain concentrations of (5µg/ml, 10µg/ml, 15µg/ml, 20µg/ml, 25µg/ml). Absorbance of these solutions was measured at 284nm, Calibration curve was plotted, absorbance Vs concentration.

Linearity study for Glicazide

Accurately measured aliquot portions of working standard solution of Gliclazide were transferred to five separate 10 mL volumetric flasks. The volume was made up to the mark using methanol and water in ratio 30:70 to obtain concentrations (15µg/ml, 30µg/ml, 45µg/ml, 60µg/ml, 75µg/ml) Absorbance of these solutions was measured at 274 nm. Calibration curve was plotted, absorbance Vs concentration. The results are shown in the Table No.1.

Table No. 1 Regression and Optical characteristics of Dapagliflozin and Gliclazide

Parameters	Value for Dapagliflozin	Value for Gliclazide
Beer's law limit (µg/ml)	5-25µg/ml	15-75µg/ml
Regression Coefficient(R^2)	0.997	0.996
Regression equation	y = 0.0051x + 0.1042	y =0.0008x+0.0993
Slope	0.0051x	0.0008x
Intercept	0.1042	0.0993

The study of regression and optical characteristics of Dapagliflozin and Gliclazide are carried out in which Regression Coefficient (R^2) of Dapagliflozin is 0.997 and of Gliclazide is 0.996. The slope of Dapagliflozin is 0.0051 and slope of Gliclazide is 0.0008 with Intercept of Dapagliflozin is 0.1042 and of Gliclazide is 0.0993. Therefore, Concentration vs Absorbance are fairly linear between both coordinates and are well mannered and obeys ICH guidelines.

Estimation of Laboratory mixture by proposed method

Method: Q-Absorption ratio method

If a drug sample contains two absorbing drugs (X and Y) each of which absorbs at the λ_{max} of the other. Then, it may possible to estimate both drugs by this method. The scanning spectra of 10µg/ml solution of Dapagliflozin and 60µg/ml solution of Gliclazide show clear peaks at 284nm and 274nm respectively.

Amount of each drug was estimated using following equations,

$$C_X = \frac{Qm-Qy}{Qx-Qy} \times \frac{A1}{ax1} \qquad C_Y = \frac{Qm-Qx}{Qy-Qx} \times \frac{A2}{ay1}$$

Where, ax1 and ax2 are absorptivity's of Dapagliflozin.

ay1 and ay2 are absorptivity's of Gliclazide.

A1 and A2 are the absorbances of sample solution.

Cx and Cy are the concentrations of Dapagliflozin and Gliclazide respectively in sample solution.

National Conference on «Modern Perspectives In Physical and Chemical Sciences » (MPPCS-2024) DOI: **10.13140/RG.2.2.13272.40962**

$Qm = \frac{A2}{A1}$; $Qx = \frac{ax2}{ax1}$; $Qy = \frac{ay2}{ay1}$

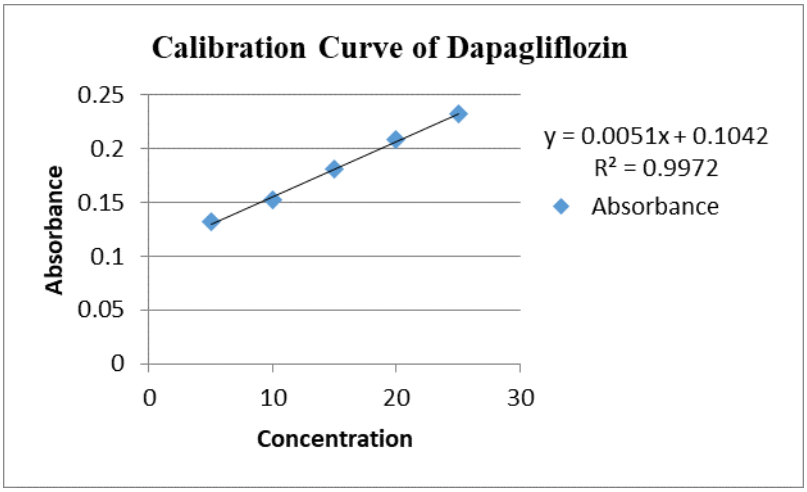

Graph No.2 Calibration curve of Dapagliflozin

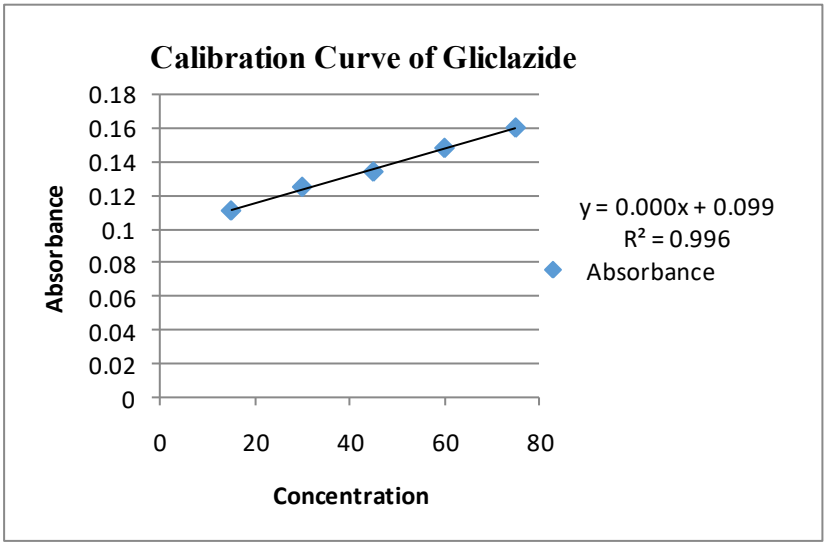

Graph No.3 Calibration curve of Gliclazide

The results are determined in the Table No. 2

Table No. 2. Results of Estimation of Dapagliflozin and Gliclazide in standard laboratory mixture

Analyte	% Concentration estimated (Mean ± S.D)	% R.S.D.
Dapagliflozin	99.74 ± 0.1113	0.1116
Gliclazide	99.69± 0.1789	0.1792

The estimation of Dapagliflozin and Gliclazide in Standard Laboratory Mixture are carried out in which % concentration of Dapagliflozin and Gliclazide were found to be 99.74 and 99.69 respectively. Those values are fairly accurate by statistical manner and are as per ICH guidelines.

Application of proposed method for Estimation of drugs in tablets

Twenty 'Cyblex D 60' Tablets containing Dapagliflozin (10mg) and Gliclazide (60 mg) were weighed and ground to fine powder. A quantity of sample equivalent to Dapagliflozin (10 mg) and Gliclazide (60 mg) was transferred into 100 mL volumetric flask containing methanol (60 mL), sonicated for 15 min and the volume was made up to the mark and filtered through Whatman filter paper (No. 45). This solution was (1 mL) transferred to 10 mL volumetric flaks, dissolved and volume was adjusted to the mark with methanol and water in the ratio 30:70. The absorbances of the solutions were measured at 274nm and 284nm against blank. The concentrations of two drugs in sample were determined by using Q-Absorption ratio method. The results are shown in the Table No.3

Table No. 3 Results of Estimation of Dapagliflozin and Gliclazide in tablets dosage form.

Analyte	Label claim(mg/tab)	% Label Claim estimated (Mean ± S.D)	% R.S.D.
Dapagliflozin	10	99.35±0.0953	0.0956
Gliclazide	60	99.53±0.1101	0.1106

The results of Estimation of Dapagliflozin and Gliclazide in tablets dosage shows the % purity 99.35 & 99.53 with SD and RSD below 2 which is fairly accurate by statistical manner and are as per ICH guidelines.

Validation of proposed method

The proposed method was validated as per ICH guidelines

Accuracy (Recovery study)

Accuracy of proposed method was ascertained on the basis of recovery study performed by standard addition method. A known amount of standard drug solutions were added to the tablet powder to make final concentrations in the range of 80%, 100% and 120% and re-analyzed it by the proposed method. The absorbance recorded and the % recoveries were calculated using formula.

% Recovery = [A - B/ C] X 100

Where,

A = Total amount of drug estimated

B = Amount of drug found on preanalysed basis

C = Amount of Pure drug added

The results are shown in the Table No.4

Table No. 4 Recovery study

Drug in mixture solution (µg/ml)		% Recovery ± S.D.	
Dapagliflozin	**Gliclazide**	**Dapagliflozin**	**Gliclazide**
5	15	99.83 ± 0.051	99.78± 0.1234
10	30	99.91 ± 0.0321	99.56± 0.547
15	45	99.7±0.05	99.80 ±0.1193

The results of Recovery study of Dapagliflozin and Gliclazide are found to be fairly accurate between 99.7 to 99.91 for Dapagliflozin 99.56 to 99.80 % for Gliclazide between various concentrations under observation by statistical way and are obey ICH guidelines.

Precision

Precision was determined as intra-day and inter-day variations. Intra-day precision was determined by analyzing Dapagliflozin (5µg/mL, 10µg/mL 15µg/mL 20µg/mL 25µg/mL) and Gliclazide (15µg/mL 30µg/mL 45µg/mL 60µg/mL 75µg/mL) for three times on the same day. Inter-day precision was determined by analyzing the same concentration of solutions for three different days over a period of week. The results are shown in the Table No. 5.

(Table No.5 Precision Study

Drug	Conc. [µg/mL]	Intra-day Amount Found		Inter-day Amount Found	
		Mean ±S. D. [*n* = 3]	**% R.S.D.**	**Mean ± S.D. [*n* =3]**	**% R.S.D.**
Dapagliflozin	5	4.92 ±0.0301	0.6201	4.93 ±0.0264	0.5355
	10	9.93 ±0.043	0.4389	9.92 ± 0.0251	0.2535
	15	14.96 ±0.03	0.0200	14.94± 0.037	0.2533
Gliclazide	15	14.91 ± 0.5196	0.3485	14.93 ± 0.4163	0.2787
	30	29.91± 0.0305	0.1021	29.91 ± 0.0251	0.0841
	45	44.94 ± 0.0288	0.0642	44.94 ± 0.0416	0.0926

The Precision Study of Dapagliflozin and Gliclazide were carried out and results are found to be fairly accurate by statistical manner and obeys ICH guidelines.

National Conference on «Modern Perspectives In Physical and Chemical Sciences » (MPPCS-2024) DOI: **10.13140/RG.2.2.13272.40962**

Ruggedness

Ruggedness of the proposed method was determined by analysis of aliquots from homogenous slot by two different analyst using same operational and environmental conditions. The results are shown in Table No. 6.

Table No. 6 Ruggedness study

	Dapagliflozin 10µg/ml		Gliclazide 60 µg/ml	
	Amount found in µg/ml Mean ± S.D. (n=3)	**% R.S.D**	**Amount found in µg/ml Mean ± S.D. (n=3)**	**% R.S.D**
Analyst I	9.90± 0.0624	0.6301	59.92 ±0.0378	0.0631
Analyst II	9.74± 0.0501	0.5164	59.87 ±0.0152	0.0255
Day I	9.89± 0.0356	0.3547	59.93±0.0321	0.0536
Day II	9.87 ±0.0665	0.6744	59.88±0.010	0.0167
Instrument I	9.94 ± 0.0630	0.6332	59.96 ±0.0251	0.0419
Instrument II	9.93± 0.0743	0.7488	59.93 ± 0.0351	0.0585

Ruggedness study of Dapagliflozin and Gliclazide are carried out and result are found to be fairly accurate by statistical manner and obeys ICH guidelines.

LOD: Limit of Detection of Dapagliflozin and Gliclazide were found to be 0.89 µg/ml and 0.62 µg/ml respectively

LOQ: Limit of Quantification of Dapagliflozin and Gliclazide were found to be 1.72 µg/ml and 2.32 µg/ml respectively.

Results And Discussion

A UV Spectrophotometric Estimation method was developed for Dapagliflozin and Gliclazide. The method employs 274nm as iso-absorptive point and 284 nm as λmax for formation of equations. Dapagliflozin and Gliclazide obeys Beer's law in the concentration range 5-25µg/ml (R^2=0.997) and 15-75µg/ml (R^2=0.996) respectively. The mean recovery for Dapagliflozin and Gliclazide was found to be **99.81 and 99.71 %** respectively. The developed method was validated according to ICH guidelines and values of accuracy, precision and other statistical analysis were found to be in good accordance with the prescribed values.

Conclusion

The proposed UV Spectrophotometric Estimation method presented in this paper has advantages of simplicity, accuracy, precision and convenience for quantitation of Dapagliflozin and Gliclazide. The proposed method can be used for the quality control of Dapagliflozin and Gliclazide in typical laboratories.

Acknowledgement

I sincerely thank our Guide Dr. Vijay R. Patil, Dr. Rajesh Y. Chaudhari, Dr. Sachin S. Rane, for their valuable guidance, resource and support during this research. We extend our gratitude to the faculty and staff for their assistance and constructive feedback. Special thanks to our peers and families for their unwavering encouragement. Lastly, we acknowledge the contributions of previous researchers, whose work provided the foundation for this study.

.

References

Journal

1. Patel D. K., etal Diabetes Mellitus: An overview on its pharmacological aspects & reported medicinal plants having Antidiabetic activity, Asian Pacific Journal of topical Biomedicine, 2012, 2(5), 411-420.
2. Mante G. V., etal. ,Estimation of Dapagliflozin from its Tablet formulation by U.V. Spectroscopy, Pharmaceutical Method 2017, 8(2), 102-107.
3. Gunasekar Monoharan, etal., Stability indicating RP-HPLC Method Development for Simultaneous determination &estimation of Dapagliflozin in Raw and tablet Formulation, Chemistry Research Journal, 2018, 3(2), 159-164.
4. L.B. Borse, etal, RP- HPLC Method Development and Validation for Estimation of Dapagliflozin in Tablet Formulation, Journal of Pharmaceutical Negative Result, 2022, 13(5) 364-372.
5. Garber A. J. 200. Using dose Response Characteristic of Therapeutic agent for treatment decision in type 2 diabetes. Diabetes obes. Metab., 2, 139-147.
6. Lindblad U & Melander A. 200, Sulphonylurea dose esponse relationships: relation to clinical practice, Diabetes obes. Metab. 2, 25-31.
7. Bhaskar et al. UV-Spectrophotometric-Assisted Chemometric Methods for the Simultaneous Determination of Metformin Hydrochloride and Gliclazide in Pharmaceutical Formulations. Pharmaceutica Analytica Acta, 2012, 3(4).
8. Ameeduzzafar et al. Quality by Design (QbD) based development and validation of bioanalytical RP-HPLC method for dapagliflozin: forced degradation and preclinical pharmacokinetic study. Journal of Liquid Chromatography & Related Technologies; 2014.

9. Hemke et al. RP-HPLC Method for Estimation of Dapagliflozin from its Tablet. International Journal of ChemTech Research, 2018,11(01): 242-248.
10. Dass CR et al. Development and validation of a new analytical HPLC method for simultaneous determination of the antidiabetic drugs, metformin and gliclazide. Food and Drug Administration, Taiwan; 27 (2019) 315-322.
11. Karmankar et al. A Validated Stability Indicating High Performance Thin Layered Chromatographic Method for the Analysis of Dapagliflozin in Bulk Drug and Marketed Tablet Formulation. Asian Journal of Chemistry; Vol. 31, No. 7 (2019), 1457-1460.
12. Mounika G et al. Estimate gliclazide simultaneously in tablet dosage form by RP-HPLC. International Journal of Advanced Research. In Medical & Pharmaceutical Sciences; Volume.5, Issue.2, February; 2020.
13. Prasad N et al. Ultraviolet-visible Spectrophotometric Method for Estimation of Gliclazide in Presence of Excipients Interacting in UV-visible Region. Indian Journal of Pharmaceutical Education and Research; Vol 54, Issue 2; Apr-Jun, 2020.
14. Ahmad et al. Development and Validation of UV Spectrophotometric method for estimation of Saxagliptin and Dapagliflozin in bulk and dosage form. International Journal of Pharmaceutical Sciences and Research (2021), Volume 12, Issue 4: 2185-2192.
15. Abdel Gawad et al. Spectrodensitometric and ultra-performance liquid chromatographic quantification of dapagliflozin and saxagliptin in their dosage form and human plasma. Tropical Journal of Pharmaceutical Research June 2021; 20 (6): 1223-1231.
16. Sathya Sowmya and Siva Krishna. Analytical method Development and Validation of Dapagliflozin and Linagliptin Tablets by RP-HPLC. YMER, 22(04), April 2023.
17. Cornelia Locher et al. Development and validation of an assay for the quantification of glycosides using high-performance thin-layer chromatography (HPTLC). Journal of Planar Chromatography – Modern TLC 2023, 179–190.
18. Suganthi A, Syed Iffran I, Ravi T.K Development of a Validated Highly Sensitive and Eco-Friendly Approach for the Simultaneous Determination of Dapagliflozin and Gliclazide in Bulk and Tablet Formulation by RP-HPLC Method, YMER 23(5), May 2024, 560-570.
19. ICH Guildlines: Validation of Analytical Procedure Text & methodology Q2 (B) 2005.

20. Brunton L.L., et al. Goodman & Gillman's The pharmacological Basis of Therapeutics Mc graw- Hill Medical Piblishing Division, edition 11. 2006, 1634-1639.
21. Tripathi K. D. : Essential of medical pharmacology, Jaypee Brothers Medical Publishers Pvt. Ltd. Edition 5, 2004, 245-253.
22. A. H. Beckett, J. B. Sten Lake, Book of Practical Pharmaceutical Chemistry Fourth Edition Part Two CBS Publication and Distributors, New Delhi 2005 ISBN: 8123905149 (286-288).

Content is available at: CRDEEP Journals
Journal homepage: http://www.crdeepjournal.org/category/journals/ijbas/

International Journal of Basic and Applied Sciences
(ISSN: 2277-1921) (Scientific Journal Impact Factor: 6.188)

UGC Approved-A Peer Reviewed Quarterly Journal

Development and Validation of UV Spectrophotometric Method for the Simultaneous Estimation of Myo-Inositol and Metformin Hydrochloride Bulk Drugs and Pharmaceutical Dosage Form.

Miss. Pathan Mahek Firoz Khan; Prof. (Dr.)Rajesh Y. Chaudhari and Prof. (Dr.) Sachin S. Rane
TVES's Honorable Loksevak Madhukarrao Chaudhari College of Pharmacy, Faizpur Dist.: Jalgaon.

Abstract
Developed a simple, rapid, accurate, economic and precise UV-VIS spectrophotometric method for myo-Inositol and Metformin Hydrochloride in bulk and tablets formulation. In current research the estimation of those drugs was carried out by simultaneous equation method. This method is based on measurement of absorption maxima at 278nm and 231nm i.e., λ_{max} of myo-Inositol and Metformin Hydrochloride respectively. The linearity observed for myo-Inositol was in the range of 15-75µg/ml and for Metformin Hydrochloride is in the range of 10-50µg/ml. The accuracy of methods was assessed by recovery studies and was found to be 99.16 and 99.15% for both myo-Inositol and Metformin Hydrochloride in tablet dosage form. LODof Myo-inositol and Metformin HCl was found to be 1.8025µg/ml and 1.9412µg/ml respectively. LOQ of Myo-inositol and Metformin HCl was found to be 5.4622µg/ml and 6.4707µg/ml respectively. This method is quantitively evaluated in terms of linearity, accuracy, precision, ruggedness, robustness and recovery as per ICH guidelines. The method can be employed for estimation of pharmaceutical formulations with no interfere from any other excipients and diluents.

Introduction

Myo-inositol is a 6-carbon cyclic polyalcohol (Figure 1) that occurs as anhydrous, hydroscopic crystals. Myo-inositol has a sweet taste, is soluble in water, and is slightly soluble in alcohol. It is insoluble in ether and other organic solvents. [1] Inositols are pseudovitamin compounds that are falsely said to belong to the B-complex family. Inositol or its phosphates and associated lipids are found in many foods, in particular fruit, especially cantaloupe and oranges. PCOS is one of the most common endocrine disorders, affecting up to 20% of women of reproductive age.[2] The diagnostic criteria for PCOS include chronic oligomenorrhea or anovulation, hyperandrogenism, and polycystic ovarian morphology. [3] PCOS is associated with an increased risk of developing hypertension, dyslipidemia, type 2 diabetes, and heart disease. [4-6] Insulin resistance is another common feature of PCOS in both overweight and lean women,[7]and it is often treated with insulin sensitizers like metformin. [8-9] Over the last decade, myo-inositol, an isomerized and dephosphorylated precursor of glucose-6-phosphate, has been used more and more as a natural insulin sensitizer. High doses (usually in the 12-18g range) are required for any neurological effects while lower doses (2-4g) are sufficient for fertility and insulin sensitizing effects.[10] Literature survey revealed The HPLC methods for estimation of Myo-inositol in Bulk, human plasma and pharmaceutical dosage forms. LC-MS-MS method was reported for the determination of Myo-inositol in human plasma. Literature survey reveals several Analytical and Bioanalytical methods for the analysis of Myo-inositol. These methods reported with Myo-inositol alone or in combination with other drug. These include, HPLC and spectrophotometric analysis of Myo-inositol in tablets. Metformin HCl [figure 2] is an oral antidiabetic drug in the biguanide class. It is most widely prescribed antidiabetic drug in the world used to treat type 2 diabetes. Metformin HCl helps to control the amount of glucose (sugar) in blood. It decreases the amount of glucose and also increases body's response to insulin, a natural substance that controls the amount of glucose in the blood. It is not used to treat type 1 diabetes. It is also used for treatment of gestational diabetes, polycystic ovary syndrome (PCOS). [11] It works by decreasing hyperglycemia primarily by suppressing glucose production by the liver (hepatic gluconeogenesis). It helps to reduce LDL cholesterol and triglyceride levels, and is not associated with weight gain. Metformin HCl comes as a liquid, as a tablet, and as an extended-release (long-acting) tablet taken orally. It is used alone or with other medications. Very rare but serious side effect with Metformin HCl is lactic acidosis. Other than that common side effect are gastrointestinal irritations, including diarrhea, cramps, nausea, vomiting and increased flatulence. Literature survey revealed the HPLC methods for estimation of Metformin HCl in Bulk, human plasma and pharmaceutical dosage forms. [12-17] LC-MS-MS method was reported for the determination of Metformin in human plasma. [18]

National Conference on «Modern Perspectives In Physical and Chemical Sciences » (MPPCS-2024) DOI: **10.13140/RG.2.2.13272.40962**

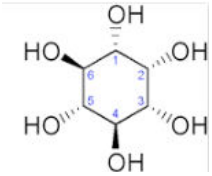

Figure 1: Structure of Myo-Inositol.

Literature survey reveals several Analytical and Bioanalytical methods for the analysis of Metformin. These methods reported with Metformin alone or in combination with other drug. These include HPLC [19-21] and spectrophotometric analysis of Metformin in tablets. [22-25]

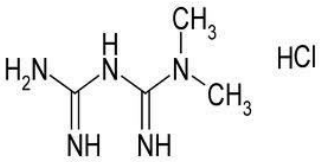

Figure 2: Structure of Metformin HCl.

PCOS is one of the most common endocrine disorders of reproductive age group women with rising prevalence of obesity, gestational and type 2 diabetes mellitus globally. Due to its progressive nature, untreated PCOS results in long-term metabolic and fertility consequences as well as distressing symptoms to affected women, lead to an important public health issue.

The combination of myo-inositol and metformin HCl is often used to manage Polycystic Ovary Syndrome (PCOS). Here's a brief overview of their pharmacology:

Myo-Inositol

- **Function**: Myo-inositol is a vitamin-like substance that plays a crucial role in cellular signaling and insulin sensitivity.
- **Mechanism**: It helps improve insulin sensitivity, which can lead to better ovulation and menstrual cycle regulation in women with PCOS.

Metformin HCl

- **Function**: Metformin is an antidiabetic medication belonging to the biguanide class.
- **Mechanism**: It works by reducing glucose production in the liver, improving insulin sensitivity, and enhancing peripheral glucose uptake.

Combination Therapy

- **Benefits**: Combining myo-inositol with metformin can enhance the body's response to insulin and improve hormonal balance. This combination is particularly effective in regulating menstrual cycles and improving ovulation in women with PCOS.
- **Clinical Evidence**: Studies have shown that this combination can be more effective than either agent alone in improving metabolic and hormonal parameters

Materials and Methods

Instruments

Shimadzu UV-1800 single beam spectrophotometer was used to record the spectra of sample and reference solutions using pair of quartz cells of 10 mm path length. All weighing was carried out on Sansui vibra DJ-150S-S weighing balance. Sonicator of fast clean is used for the purpose of sonication, Filter papers of Sartorius Stedim Biotech of grade 292 are used for the filtration purpose.

Chemicals

Myo-inositol (10 mg) and Metformin HCL (10 mg) pure drugs were obtained as a gift sample from Eris Lifesciences Limited Amingaon, North Guwahati.

METHOD

Preparation of stock solution and selection of wavelength

Myo-inositol stock solution

An accurately weighed quantity of Myo-inositol (10 mg) was taken in 10 mL volumetric flask and dissolved in methanol (8 mL) with the help of ultrasonication for about 10 min. Then the volume was made up to the mark using methanol to get Myo-inositol standard stock solution (1mg / mL).

Myo-inositol working solution

National Conference on «Modern Perspectives In Physical and Chemical Sciences » (MPPCS-2024) DOI: **10.13140/RG.2.2.13272.40962**

Myo-inositol standard stock solution (5 mL) was diluted to 50 mL using 85 % v/v methanol to get working standard solution (100 µg/mL).

Metformin HCl stock solution

An accurately weighed quantity of Metformin HCL (10 mg) was taken in 10 mL volumetric flask and dissolved in methanol (8 mL) with the help of ultrasonication for about 10 min. Then the volume was made up to the mark using methanol to get Metformin
HClstandard stock solution (1 mg / mL).

Metformin HCl working solution

Metformin HCL standard stock solution (5 mL) was diluted to 50 mL using 85 % v/v methanol to get working standard solution (100 µg / mL)

Determination of λ Max of Individual Component

An appropriate aliquot portion of Myo-inositol (0.6mL) and Metformin HCl (0.5 mL) were transferred to two separate 10 ml volumetric flasks, the volume was made up to the mark using 85 %v/v methanol to obtain Myo-inositol (60 µg/mL) and Metformin HCl (50 µg/mL). Drug solutions were scanned separately between 200 nm to 400 nm. Myo-inositol shows the λ_{max} at 278 nm while Metformin HCl shows λ_{max} at 231 nm.

Overlay spectra of Myo-inositol and Metformin HCl

The overlay spectra of both drugs were recorded and two wavelengths 278 nm (λ_{max} of Myo-inositol) and 231nm(λ_{max} of Metformin HCL) were selected for further study.

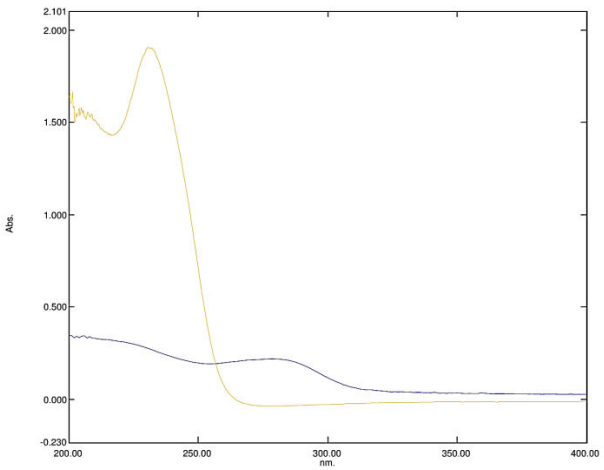

Graph No. 1 Overlay spectra of Myo-inositol and Metformin HCl

Linearity study for Myo-inositol

An accurately measured aliquot portion of working standard solution of Myo-inositol was transferred to five separate 10 mL volumetric flasks. The volume was made up to the mark using 85 % v/v methanol to obtain concentrations of Myo-inositol (15µg/ml, 30µg/ml, 45µg/ml, 60µg/ml, 75µg/ml). Absorbance of these solutions was measured at 278 nm, Calibration curve was plotted, absorbance Vs concentration.

Linearity study for Metformin HCl

Accurately measured aliquot portions of working standard solution of Montelukast were transferred to five separate 10 mL volumetric flasks. The volume was made up to the mark using 85% v/v methanol to obtain concentrations (10µg/ml, 20µg/ml, 30µg/ml, 40µg/ml, 50µg/ml) Absorbance of these solutions was measured at 231 nm. Calibration curve was plotted, absorbance Vs concentration. The results are shown in the Table No.1.

Table No. 1 Regression and Optical characteristics of MIL and MET

Parameters	Value for Myo-inositol	Value for Metformin HCl
Beer's law limit (µg/ml)	15-75µg/ml	10-50µg/ml
Regression Coefficient(R^2)	0.9996	0.9987
Regression equation	y = 0.0332x + 9E-05	y = 0.0308x + 0.0309
Slope	0.00319	0.03084
Intercept	9E-05	0.03092

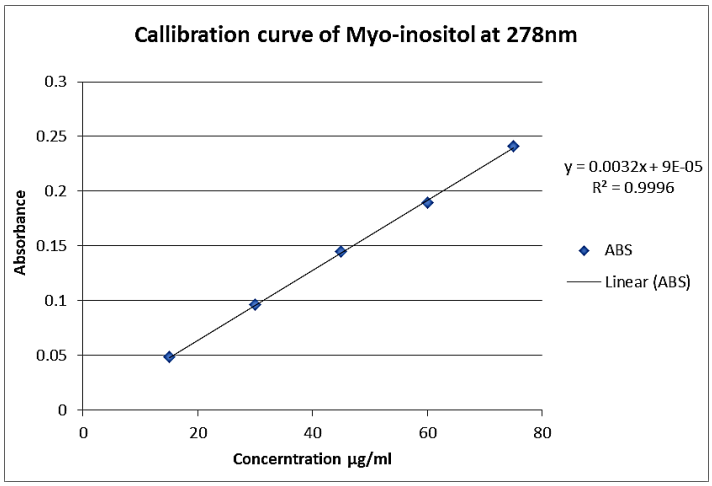

Graph No.2 Calibration curve of Myo-inositol at 278 nm

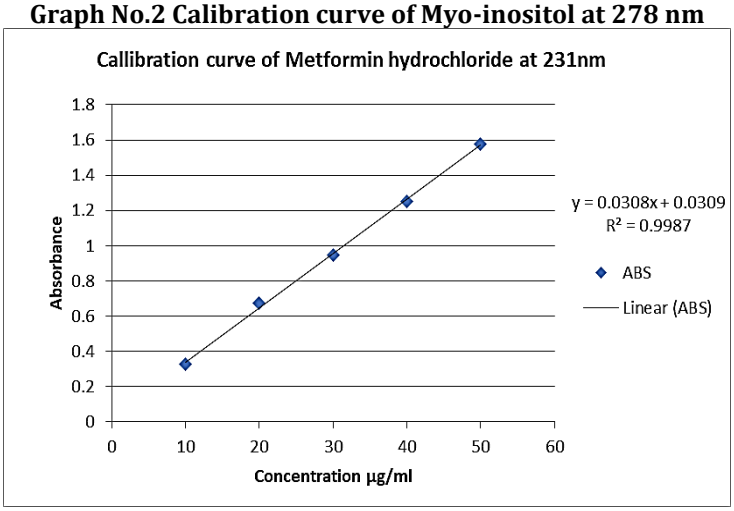

Graph No.3 Calibration curve of Metformin HCl at 231nm

Method:

Simultaneous Estimation Method

If a drug sample contains two absorbing drugs (X and Y) each of which absorbs at the λ_{max} of the other. Then, it may possible to estimate both drugs by this method. The scanning spectra of 60µg/ml solution of Myo-inositol and 50µg/ml solution of Metformin HCl show clear peaks at 278 nm and 231nm respectively.

Amount of each drug was estimated using following equations,

$$C_x = \frac{A_2 \times ay_1 - A_1 \times ay_2}{ax_2\, ay_1 - ax_1\, ay_2}$$

$$C_y = \frac{A_1 \times ax_2 - A2 \times ax_1}{ax_2\, ay_1 - ax_1\, ay_2}$$

Where;

A1 and A2 are the absorbance of diluted mixture at λ_1 and λ_2

Cx and Cy are the concentration of X and Y respectively

ax1 and ax2 are absorptivity's of X at λ_1 and λ_2 respectively

ay1 and ay2 are absorptivity's of Y at λ_1 and λ_2 respectively.

The results are determined in the Table No. 2

Table No. 2. Results of Estimation of MIL and MET in standard laboratory mixture

Analyte	% Concentration estimated (Mean ± S.D)	% R.S.D.
Myo-inositol	99.91 ± 0.1000	0.1000
Metformin HCl	99.67 ± 0.1095	0.1098

n=3

National Conference on «Modern Perspectives In Physical and Chemical Sciences » (MPPCS-2024) DOI: **10.13140/RG.2.2.13272.40962**

The estimation of MIL and MET in Standard Laboratory Mixture are carried out in which % concentration of MIL and MET were found to be 99.91 and 99.67respectively. Those values are fairly accurate by statistical manner and are as per ICH guidelines.

Application of proposed method for Estimation of drugs in tablets

Twenty 'Metital'Tablets containing Myo-inositol (600 mg) and Metformin HCl (500 mg) were weighed and ground to fine powder. A quantity of sample equivalent to Myo-inositol (600 mg) and Metformin HCl (500 mg) was transferred into 100 mL volumetric flask containing methanol (60 mL), sonicated for 15 min and the volume was made up to the mark and filtered through Whatman filter paper (No. 45). This solution was (1 mL) transferred to 10 mL volumetric flaks, dissolved and volume was adjusted to the mark. The absorbances of the solutions were measured at 278nm and 231nm against blank. The concentrations of two drugs in sample were determined by using simultaneous equations. The results are shown in the Table No.3

Table No. 3 Results of Estimation of MIL and MET HCL in tablets dosage form.

Analyte	Label claim(mg/tab)	% Label Claim estimated (Mean±S.D)	% R.S.D.
Myo-inositol	600	99.16 ± 0.1140	0.9261
Metformin HCL	500	99.15 ± 0.1675	0.9343

n=3

The results of Estimation of MIL and MET in tablets dosage shows the % purity 99.16 & 99.15 with SD and RSD bellow 2 which is fairly accurate by statistical manner and are as per ICH guidelines.

Validation of proposed method

The proposed method was validated as per ICH guidelines

Accuracy (Recovery study)

Accuracy of proposed method was ascertained on the basis of recovery study performed by standard addition method. A known amount of standard drug solutions were added to the tablet powder to make final concentrations in the range of 80%, 100% and 120% and re-analyzed it by the proposed method. The absorbance recorded and the % recoveries were calculated using formula.

% Recovery = [A - B/ C] X 100

Where,

A = Total amount of drug estimated

B = Amount of drug found on preanalysed basis

C = Amount of Pure drug added

The results are shown in the Table No.4

Table No. 4 Recovery study

Drug in mixture solution (µg/ml)		% Recovery ± S.D.	
Myo-inositol	Metformin HCl	Myo-inositol	Metformin HCl
15	10	98.88 ± 1.817	99.75 ± 0.360
30	20	100 ± 1.855	99.90 ± 0.120
45	30	99.88 ± 1.301	98.91 ± 0.170

The results of Recovery study of MIL and MET are found to be fairly accurate between 99.88 to 101.5% for MIL 99.75 to 100 % for MET between various concentrations under observation by statistical way and are obey ICH guidelines.

Precision

Precision was determined as intra-day and inter-day variations. Intra-day precision was determined by analyzing Myo-inositol (15,30,45,60, and 75 µg/mL) and Metformin HCl (10,20,30,40 and 50 µg/mL) for three times on the same day. Inter-day precision was determined by analyzing the same concentration of solutions for three different days over a period of week. The results are shown in the Table No. 5.

Drug	Conc. [µg/mL]	Intra-day Amount Found		Inter-day Amount Found	
		Mean ±S. D. [*n* = 3]	% R.S.D.	Mean ± S.D. [*n* =3]	% R.S.D.

MIL	15	14.91 ± 0.519	0.348	14.93 ± 0.416	0.278
	30	29.91 ± 0.305	0.121	29.95 ± 0.250	0.840
	45	44.94 ± 0.288	0.642	44.95 ± 0.251	0.559
MET	10	9.89 ± 0.3055	0.387	9.92 ± 0.20	0.2012
	20	19.90 ± 0.104	0.502	19.93 ± 0.3519	0.1761
	30	29.89 ± 0.208	0.696	29.92 ± 0.208	0.695

n=3

(Table No.5) Precision Study

The Precision Study of MIL and MET HCL were carried out and Results are found to be fairly accurate by statistical manner and obeys ICH guidelines.

Ruggedness

Ruggedness of the proposed method was determined by analysis of aliquots from homogenous slot by two different analyst using same operational and environmental conditions. The results are shown in Table No. 6.

Table No. 6 Ruggedness study

	Myo-inositol 60 µg/ml		Metformin HCl 50 µg/ml	
	Amount found in µg/ml Mean ± S.D. (n=3)	% R.S.D	Amount found in µg/ml Mean ± S.D. (n=3)	% R.S.D
Analyst I	59.92 ± 0.378	0.631	49.92 ± 0.264	0.153
Analyst II	59.87 ± 0.152	0.255	49.87 ± 0.154	0.306
Day I	59.93 ± 0.321	0.536	49.93 ± 0.321	0.643
Day II	59.88 ± 0.105	0.167	49.87 ± 0.30	0.601
Instrument I	59.96 ± 0.251	0.419	49.94 ± 0.152	0.305
Instrument II	59.93 ± 0.351	0.585	49.89 ± 0.104	0.224

Ruggedness study of MIL and MET are carried out and results are found to be S.D. is not less than0.378 and % R.S.D is not greater than accurate by statistical manner and obeys ICH guidelines.

LOD: Limit of detection of Myo-inositol and Metformin HCl were found to be 1.8025µg/ml and 1.9412µg/ml respectively.

LOQ: Limit of Quantitation of Myo-inositol and Metformin HCl were found to be 5.4622µg/ml and 6.4707µg/ml respectively.

Results and Discussion

A simultaneous UV Spectrophotometric Estimation method was developed for Myo-inositol and Metformin HCl. The method employs 278 nm as λ1 and 231 nm as λ2 for formation of equations. Myo-inositol and Metformin HCl obeys Beer's law in the concentration range 15-75µg/ml (R^2=0.0.9996) and 10-50µg/ml (R^2=0.0.9987) respectively. The mean recovery for Myo-inositol and Metformin HCl was found to be **99.91 and 99.67 %** respectively. The developed method was validated according to ICH guidelines and values of accuracy, precision and other statistical analysis were found to be in good accordance with the prescribed values.

Conclusion

A validated simultaneous UV spectrophotometric method was successfully developed for the estimation of Myo-inositol and Metformin Hcl, demonstrating high accuracy, precision and reliability within the concentrations. The method complies with ICH guidelines and is suitable for routine analysis in labs.

Acknowledgement

Dr. Vijay R. Patil, Dr. Rajesh Y. Chaudhari, Dr. Sachin S. Rane.

Thank You for their valuable guidance providing the necessary resources and facilities to carried out this research and I am very Grateful to Everyone.

National Conference on «Modern Perspectives In Physical and Chemical Sciences » (MPPCS-2024) DOI: **10.13140/RG.2.2.13272.40962**

References

1. Karen Schimpf Determination of Myo-Inositol (Free and Bound as Phosphatidylinositol) in Infant Formula and Adult Nutritionals by Liquid Chromatography/Pulsed Amperometry with Column Switching: First Action 2011.18. Journal of AOAC International, 2012; 95: 4.
2. Knochenhauer ES, Key TJ, Kahsar-Miller M, Waggoner W, Boots LR, Azziz R. Prevalence of the polycystic ovary syndrome in unselected black and white women of the southeastern United States: a prospective study. J Clin Endocrinol Metab, 1998; 83(9): 3078–3082.
3. Rotterdam ESHRE/ASRM-Sponsored PCOS wonsensus workshop group, Revised 2003 consensus on diagnostic criteria and long-term health risks related to polycystic ovary syndrome (PCOS). Hum Reprod, 2004; 19(1): 41–47.
4. Vrbikova J, Hainer V. Obesity and polycystic ovary syndrome. Obes Facts, 2009; 2(1): 26–35
5. Legro RS, Kunselman AR, Dodson WC, Dunaif A. Prevalence and predictors of risk for type 2 diabetes mellitus and impaireglucose tolerance in polycystic ovary syndrome: a prospective, controlled study in 254 affected women. J Clin Endocrinol Metab, 1999; 84(1): 165–169.
6. Cattrall FR, Healy DL. Long-term metabolic, cardiovascular and neoplastic risks with polycystic ovary syndrome. Best Pract Res Clin Obstet Gynaecol, 2004; 18(5): 803–812.
7. Zawadsky JK, Dunaif A. Diagnostic criteria for polycystic ovary syndrome: towards a rational approach. In: Dunaif A, Givens JR, Haseltine FP, Merriam GR, editors. Current Issues in Endocrinology and Metabolism: Polycystic Ovary Syndrome. Cambridge, UK: Blackwell Scientific Publications, 1992; 377–384.
8. De Leo V, la Marca A, Petraglia F. Insulin-lowering agents in the management of polycystic ovary syndrome. Endocr Rev., 2003; 24(5): 633–667.
9. Genazzani AD, Ricchieri F, Lanzoni C. Use of metformin in the treatment of polycystic ovary syndrome. Womens Health (Lond Engl), 2010; 6: 577–593.
10. https://pubchem.ncbi.nlm.nih.gov/compound/inositol
11. https://pubchem.ncbi.nlm.nih.gov/compound/Metformin-hydrochloride
12. Arayne MS, Sultana N, Zuberi MH. Development and validation of RP-HPLC method for the analysis of metformin. Pakistan journal of pharmaceutical sciences., 2006; 19(3): 231-5.
13. Madhukar A, Prince A, Vijaykumar R, Sanjeev Y, Raghuprata D, Hplc. Jagadeeswar.K, Simple and Sensitive analytical method development and validation of Metformin hydrochloride by RP., Journal of Pharmacy and Pharmaceutical Sciences. Journal of chromatographic science, 2011; 3(3 SRC -): 117-20.
14. Narendra KT, Mohan RK, Sreenivasulu K, Novel RP, Raju R, V. NS, et al. Chandra for the Estimation of metformin hydrochloride In pharmaceutical dosage forms International Journal of Science Innovations and Discoveries. Journal of chromatographic science., 2011; 1(3): 395-421.
15. Mousumi K, Choudhury PK, Indian J. HPLC method for estimation of metformin hydrochloride in formulated microspheres and tablet dosage form Pharm. Sci., 2009; 71(3): 318-20.
16. Florentin T, Monica A. specificity of an analytical hplc assay method of metformin hydrochloride Revue Roumaine de Chimie. Journal of chromatographic science, 2007; 52(6): 603-9.
17. Arayne MS, Sultana N, Zuberi MH, Siddiqui FA. Spectrophotometric Quantitation of Metformin in Bulk Drug and Pharmaceutical Formulations using Multivariate Technique. Indian journal of pharmaceutical sciences, 2009; 71(3): 331-5.
18. Yunbiao W, Fawcettb J, Chromatography B. Yingwu Jingkai Gua,, Paul Xu Bai. Rapid and sensitive liquid chromatographytandem mass spectrometric method for the quantitation of metformin in human plasma Journal of, 2004; 808(2): 215-9.
19. AbuRuza S, Millershipb BJ, McElnayb J, Chromatography B. The development and validation of liquid chromatography method for the simultaneous determination of metformin and glipizide, gliclazide, glibenclamide or glimperide in plasma. Journal of, 2005; 817(2): 277-86.
20. Sultana N, Arayne MS, Shafi N, Siddiqui FA, Hussain A. Development and validation of new assay method for the simultaneous analysis of diltiazem, metformin, pioglitazone and rosiglitazone by RP-HPLC and its applications in pharmaceuticals and human serum. Journal of chromatographic Science, 2011; 49(10): 774-9.
21. Narsimha RD, Chandana M, Hplc, Pioglitazone H. Method Development and Validation of RP-for Simultaneous Analysisof Three Component Tablet Formulation containing Metformin and Glibenclamide. International Journal of PharmTech Research, 2012; 4: 948-56.
22. Ajay S, Bhatt A. Training needs of clinical research associates. Perspectives in clinical research, 2010; 1(4): 134-8.
23. Narasimha RD, Prasada RM, Hussain J, Sumanoja S, Rajeswara RV. Naga Lakshmi Method development and validation of forced degradation studies of metformin hydrochloride by using uv spectroscopy. IJPCBS, 2013; 3(3 SRC -): 546-53.
24. Amruta B, Minal R, Ghante SD, V. U. Loni, Sawant . Simultaneous Method for Estimation of Sitagliptin phosphate and Metformin Bhoomaiah et al. Int J Pharm Pharm Sci, Vol 6, Issue 6, 135-141 141 hydrochloride in Bulk and Tablet Dosage Form. Der Pharma Chemica, 2012; 4(3SRC - GoogleScholar): 854-9.
25. B. Bhoomaiah et al development and validation of RP-HPLC method for simultaneous determination of Metformin and Miglitol in bulk and pharmaceutical formulation. International Journal of Pharmacy and Pharmaceutical Sciences, 2014; 6: 6.

Content is available at: CRDEEP Journals
Journal homepage: http://www.crdeepjournal.org/category/journals/ijbas/

International Journal of Basic and Applied Sciences
(ISSN: 2277-1921) (Scientific Journal Impact Factor: 6.188)

UGC Approved-A Peer Reviewed Quarterly Journal

Synthesis and Characterization of Novel Activated Carbons derived from different parts of *Casuarina Cunninghamiana* Miq plant by using $ZnCl_2$ activating agent

Gunwant Hari Kurhade[1*] and Farooque Haider Zulfequar Haider[2]
[1,2]*Department of chemistry, Vidnyan Mahavidyalaya, Malkapur, District - Buldhana, M.S, India*

Abstract
This proposed work was used to synthesized fine powdered novel activated carbons which were synthesized from different parts of plant Casuarina Cunninghamiana Miq. Particularly cone and leaves were used as starting material. Carbonization was done at 300°C for one hour and allowed to cool at room temperature, after washing it the chemical activation was achieved by impregnating the charcoal with $ZnCl_2$ as an activating agent and further heated to 400°Cand 500°C for one hour. Synthesized six compounds were characterized by FTIR and four novel activated carbons further studied with respect to FTIR of their corresponding precursors.

Keywords: Casuarina Cunninghamiana Miq, Activation at 400°C, 500°C

Introduction:
Activated carbon (AC) is a carbonaceous material having high degree of the parameters like porosity and internal surface area[1] along with good thermal stability[2] and it has amorphous micro crystalline structure[3]. AC is non graphitic form with small number of hydrogen and much number of oxygens in their structures[4]. Pore structure of AC is its important property, practically porosity is dictated by the starting material used but the final pore size distribution is influenced by method of activation[5]. Activated carbons were recognized safe in the treatment of water, it can be used as decolorizing agent, odour and test removing agent, as purification agent in processing of food products[6]. The activated carbons also have numerous applications in the non-food products like filter for tobacco smoke, in cosmetic and pharmaceutical industry as well as in veterinary. Activated carbon is used as soil conditional and used for controlling acidity and alkalinity in agricultural soil, also used as agent in fuel gas desulphurization, in gas masks and in pollution control divices[7].

Materials and Methods:
A) Sample collection and preparation. The material which belongs to plant origin show high carbon content and low ash content. In present study Casuarina Cunninghamiana Miq used for the preparation of activated charcoal it was collected from different area which are 5-10 km away from Malkapur. The different parts of Casuarina Cunninghamiana Miq material like leaves and cone were washed thoroughly with water in order to remove the foreign particles. After washing all material were sun dried for 5 days. Sun dried materials were ground into a fine powder with the help of mortar and pestle. Before achieving carbonization, the moisture of material removed by heating at 110°C for an hour in hot air oven.

B) Carbonization and Activation.
Carbonization of dried sample was then carried out in a muffle furnace (Bio techno Lab, Model AI 7081) by placing a sample in a silica crucible at temperature of 300°C for one hour each. The charcoal thus formed was removed from the furnace, washed with water and dried at 110°C and converted into fine powder with help of mortar pestle by applying moderate pressure. Further sieved through 100-200 mesh. Ultimately chemical activation was done according to the Grigis et al method with slight modification. The aqueous solution of Zinc Chloride ($ZnCl_2$) was mixed with 25 g sample in the ratio 1:5 the mixture was soaked for twelve hours and later heated to form a paste. The paste was placed in the muffle furnace and heated at 400 and 500°C temperature for one hour. The ACs was cooled to room temperature. Further washed with the distilled water and dried at 110°C in an oven and allow to cool at room temperature[8]. The ACs produced was sieved with 150-micron mesh, kept in an air tight bottle and labelled as follows.

National Conference on «Modern Perspectives In Physical and Chemical Sciences » (MPPCS-2024) DOI: **10.13140/RG.2.2.13272.40962**

Result and Discussion:

Table :1 List of samples collected and synthesized activated carbons with their codes.

Sr. No.	Sample Name	Code for Raw Samples	Code for carbonized carbons at 300 ^{0}C	Code for Activated carbons at 400 ^{0}C	Code for Activated carbons at 500 ^{0}C	Activation Method
1	Casuarina Cunninghamiana Miq Cone	CCCRM	CCC300	CCCAC400	CCCAC500	Chemical activation by using 1N $ZnCl_2$ at 400 and 500 ^{0}C
2	Casuarina Cunninghamiana Miq Leaves	CCLRM	CCL300	CCLAC400	CCLAC500	

Table :2 Various functional groups found for Casuarina Cunninghamiana Miq Cone samples and their frequencies.

Sr. No.	Functional group	CCCRM	CCC300	CCCAC400	CCCAC500
		Wavenumbers cm^{-1}	cm^{-1}	cm^{-1}	cm^{-1}
1	O-H str.	3932.45 3871.59 3833.86 3730.04 3623.94 3441.92	--	3954.09 3705.21 3700.01 3594.96	--
2	C-H in -CH_3 and -CH_2	2978.87 2892.37	2977.96 2880.22	2981.98 2881.45	2976.39
3	Aromatic -C=C-	1516.08	--	1541.20	1584.59

Table:3 Various functional groups found for Casuarina Cunninghamiana Miq leaves samples and their frequencies.

Sr. No.	Functional group	CCLRM	CCL300	CCLAC400	CCLAC500
		cm^{-1}	cm^{-1}	cm^{-1}	cm^{-1}
1	O-H str.	3995.78 3901.59 3870.46 3729.61 3626.56 3596.22 3441.32	--	3728.65	3920.76 3724.63
2	C-H in CH_3 and CH_2	2977.54	2980.45	2980.73 2878.34	3043.23 2830.31
3	-C=O Str.	--	--	1797.58	--
4	Aromatic C=C	--	--	--	1591.51

FTIR spectroscopy was used to characterized the functional groups present on the surface of activated carbons. The raw samples, carbonized and activated carbons contains various functional groups. The adsorption capacity of activated carbon depends not only on porosity but also depends on the functional group present on the surface of activated carbons. From IR spectrum of various samples, the observed frequencies were tabulated in table number 2 and 3. The IR spectrums of Casuarina Cunninghaminana Miq cone raw sample (CCCRM) and Casuarina Cunninghaminana Miq leaves raw sample (CCLRM) shows the band at 3441.92 cm^{-1} and 3441.32 $cm^{-1}$are attributed to frequency of O-H vibrations in the hydroxyl group also the low intensity band around 3740 cm^{-1} is assigned for the stretching vibration of O-H bonds in phenol and alcohols[9]. The sharp bands are observed in the range of 3535.46 cm^{-1} to 3871.59 cm^{-1} and 3514.11 cm^{-1} to 3870.80cm^{-1} for CCCRM and CCLRM were observed respectively. The intensity of O-H stretching bands in the raw samples CCCRM and CCLRM decreases with increase in temperature that is carbonization at 300 ^{o}C[10].

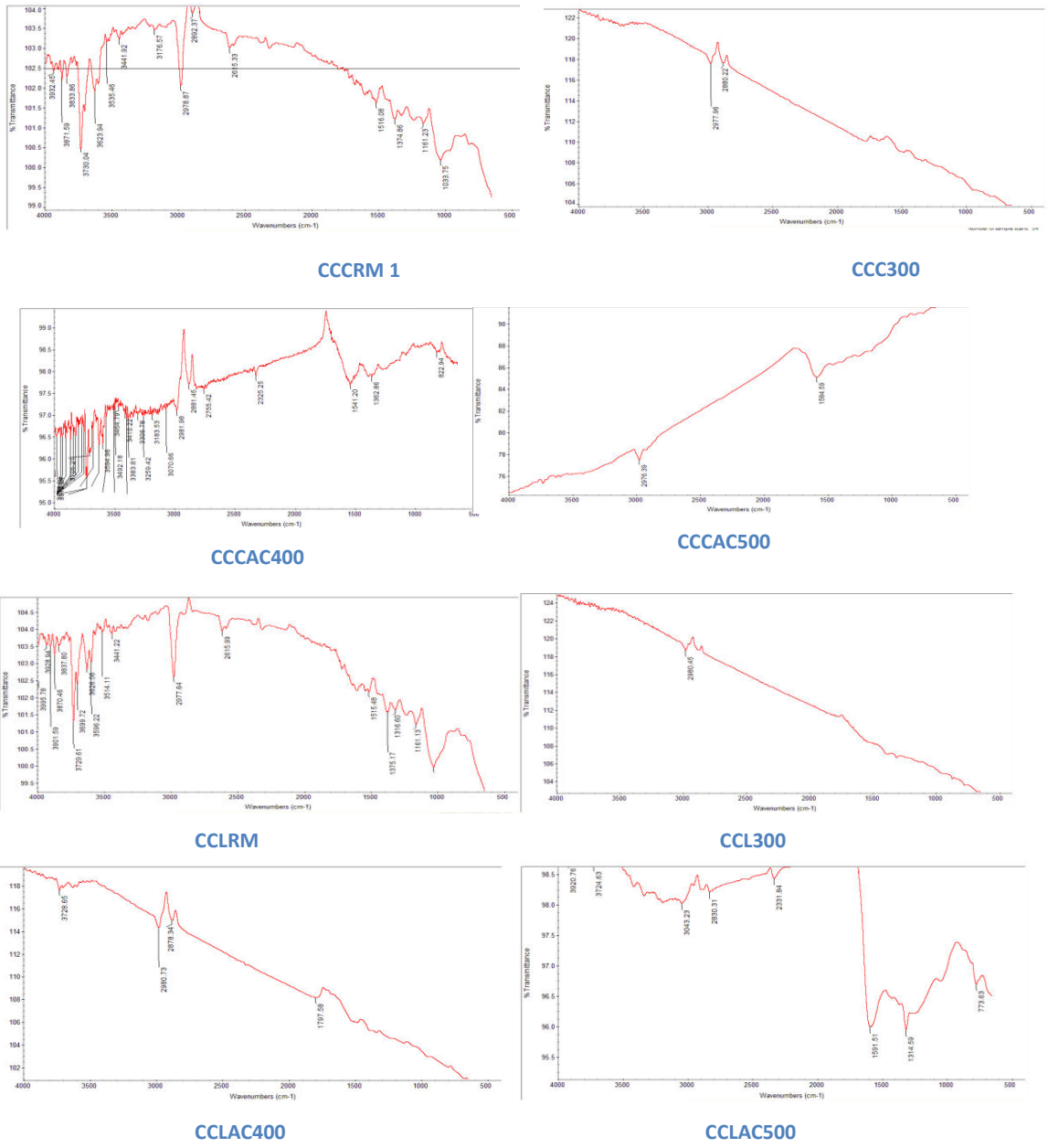

The band located around 2978.87 cm^{-1}, 2892.37 cm^{-1} and 2977.54 cm^{-1} in raw materials CCCRM and CCLRM belongs to C-H vibrations in methyl and methylene groups respectively[11,12]. These observed stretching vibrations in the raw materials are stronger as compare to stretching vibrations in their corresponding carbonized samples (2977 cm^{-1}, 2880.22 cm^{-1} and 2880.45cm^{-1}) it was the indication of completion of carbonization[13]. The peak at about 1516.08 cm^{-1}, 1541.20 cm^{-1} and 1584.59 cm^{-1} indicates the presence of an aromatic C=C ring stretching[14,15]. The band appearing at 1797.38 cm^{-1} was attributed to carbonyl group[16] (CO) in activated sample CCLAC400.

Conclusion:

The IR spectrum of novel synthesized activated carbons shows entirely different absorption intensities as compared to their corresponding precursors confirm the formation of activated carbons.

Activated carbons are porous and have high degree of surface area so they may be used for adsorption applications depending upon different activation conditions significantly conditions of activation temperature and activating agent.

Acknowledgments:

The authors gratefully acknowledge to the Board of directors of Gaurishankar Seva Samiti, Malkapur, Ex. Principal Dr. B. B. Wankhade and Principal Dr. Y. P. Patil Vidnyan Mahavidyalaya Malkapur for providing research facility. Authors also acknowledge assistance rendered by testing agencies Dr. Rajendra Gode College of Pharmacy, Malkapur for FTIR.

National Conference on «Modern Perspectives In Physical and Chemical Sciences » (MPPCS-2024) DOI: **10.13140/RG.2.2.13272.40962**

References

1. Baker, F.S., Miller, C.E., Repik, A. and Tolles, E., 1992. Activated Carbon: Kirk-Othmer *Encyclopedia of Chemical Technology*, pp. 1015-1037.

2. Han, X., Chu, L., Liu, S., Chen, T., Ding, C., Yan, J., Cui, L. and Quan, G., 2015. Removal of methylene blue from aqueous solution using porous biochar obtained by KOH activation of peanut shell biochar. *BioResources*, 10(2), pp. 2836-2849.

3. Yahya, M.A., Al-Qodah, Z. and Ngah, C.Z., 2015. Agricultural bio-waste materials as potential sustainable precursors used for activated carbon production: A review. *Renewable and sustainable energy reviews*, 46, pp. 218-235.

4. Sugumaran, P., Susan, V.P., Ravichandran, P. and Seshadri, S., 2012. Production and characterization of activated carbon from banana empty fruit bunch and Delonix regia fruit pod. *Journal of Sustainable Energy & Environment*, 3(3), pp.125-132.

5. Laine, J. and Yunes, S., 1992. Effect of the preparation method on the pore size distribution of activated carbon from coconut shell. *Carbon*, 30(4), pp. 601-604.

6. Burdock, G.A., 2014. Encyclopedia of food & color additives*. CRC press*. 32, pp. 310-329.

7. Ashford, R.D., 1994. Ashford's Dictionary of Industrial Chemicals: Properties. *Production, Uses, Wavelength, London*. pp. 34-35.

8. Ashtaputrey, P. D. and Ashtaputrey, S. D., 2020. Preparation and characterization of activated charcoal derived from wood apple fruit shell. *J. Sci. Res,* 64(01), pp.236-240.

9. Lua, A.C. and Yang, T., 2005. Characteristics of activated carbon prepared from pistachio-nut shell by zinc chloride activation under nitrogen and vacuum conditions. *Journal of colloid and interface science*, 290(2), pp. 505-513.

10. Kurhade, G.H. and Haider, F.H.Z., 2024. Synthesis and Characterization of Novel Activated Charcoal derived from Casuarina Cunninghamiana Miq Root. *Environment and Sustainable Development Perspectives and Issues*, pp.218-223.

11. Adhikaria, S., Pokharel, B., Gurung, V., Shrestha, R.M. and Rajbhandari, R., 2019, December. Preparation and characterization of activated carbon from walnut (jaglansregia) shells by chemical activation with zinc chloride (ZnCl2). *In Proceedings of the IOE Graduate Conference*,7, pp.15-20.

12. Astuti, E., Mufrodi, Z., Budiarti, G.I. and Dewi, A.C., 2020. Active Charcoal from Palm Kernel Shells as a Catalyst in The Production of Biodiesel. *Jurnal Bahan Alam Terbarukan*, 9(2), pp.120-125.

13. Haider, F. H. Z & Kurhade, G. H., 2024. Synthesis and Characterization of Novel Activated Carbons derived from different parts of Abutilon Indicum plant by using $ZnCl_2$ activating agent. Conference Proceedings, *Recent Advancements in Science & Technology*.1, pp.452-456.

14. Saka, C., 2012. BET, TG–DTG, FT-IR, SEM, iodine number analysis and preparation of activated carbon from acorn shell by chemical activation with $ZnCl_2$. *Journal of Analytical and Applied Pyrolysis*, 95, pp.21-24.

15. Bedmohata, M.A., Chaudhari, A.R., Singh, S.P. and Choudhary, M.D., 2015. Adsorption capacity of activated carbon prepared by chemical activation of lignin for the removal of methylene blue dye. *International Journal of Advanced Research in Chemical Science* (IJARCS), 2(8), pp.1-13.

16. Basrur, D. and Bhat, J.I., 2018. Preparation of activated carbon from mustard seed and its adsorption efficiency toward dye and acid. *Journal of Urban & Environmental Engineering*, 12(2), pp. 266-276.

National Conference on «Modern Perspectives In Physical and Chemical Sciences » (MPPCS-2024) DOI: **10.13140/RG.2.2.13272.40962**

Content is available at: CRDEEP Journals
Journal homepage: http://www.crdeepjournal.org/category/journals/ijbas/

International Journal of Basic and Applied Sciences
(ISSN: 2277-1921) (Scientific Journal Impact Factor: 6.188)

UGC Approved-A Peer Reviewed Quarterly Journal

A Review on Deep Learning Techniques for Disease Detection in Cotton Plants

P.U.Gadgil, L.B.Patle, K. D. Gaikwad
PG & Research Department of Electronics, MGSM's DDSGP College, Chopda , Jalgaon, India.

Abstract
Not In modern agricultural production, the severity of diseases plays a critical role in determining both the yield and quality of crops. To effectively monitor and control the entire production process, it is essential to identify not only the types of diseases but also their severity. Early detection and identification of plant diseases using machine learning from leaf images is a vital and promising area of research in agriculture. This need is particularly pronounced in India, where agriculture is a primary source of income, contributing seventeen percent to the total gross domestic product (GDP). This paper presents a thorough review of original research conducted in the field of plant disease detection, employing machine learning and deep learning techniques. We address the significant challenges faced when relying on handcrafted feature-based approaches for disease identification. The implementation of deep learning methods effectively overcomes these challenges, showcasing superior performance and accuracy. This survey emphasizes the substantial advancements in disease identification, illustrating the shift from traditional handcrafted techniques to advanced machine learning and deep learning models. Our findings demonstrate that deep learning approaches consistently achieve impressive accuracy rates across various datasets, solidifying their importance in modern agricultural practices,CNN

Keywords: *Plant Disease Detection, Deep Learning, Cotton Diseases, Machine Learning, Image Processing,*

Introduction

Agriculture is one of India's key sources of economic growth. Like humans, plants can also suffer from diseases that hinder their normal development [Hassan, Sk Mahmudul, et al,2022]. These diseases can affect any part of the plant, including the leaves, flowers, fruits, stems, and roots. Due to the complexity and diversity of crops and cultivated plants, the number of potential diseases is quite large [Ferentinos, Konstantinos P.,2018]. As a result, pathologists may sometimes struggle to diagnose diseases accurately. Timely and precise diagnosis of plant diseases is crucial to preventing both quantitative and qualitative losses in crops [Bharate, Anil A., and M. S. Shirdhonkar ,2017 - Bock, C. H., et al,2010]. Many farmers rely on their previous experiences to detect diseases, while some seek assistance from experts. However, experts often diagnose symptoms with only visual observation, which may lead to inaccuracies, especially with diseases that have very similar symptoms. Errors in diagnosing diseases can result in inappropriate control measures and excessive use of pesticides [Das, Rahul, V. Pooja, and V. Kanchana,2017]. Furthermore, many farmers lack adequate knowledge about effective plant disease detection techniques [Tlhobogang, Boikobo, and Muhammad Wannous,2018]. Therefore, automated disease identification can minimize human effort and provide more accurate results [Mutka, Andrew M., and Rebecca S. Bart,2015]. Automated detection is particularly beneficial for farmers, many of whom have limited knowledge about plant diseases. Symptoms of diseases are often visible on the leaves of cotton plants. This highlights the need for an automatic, accurate, and cost-effective machine vision system to detect diseases from images of cotton leaves and to recommend appropriate pesticide solutions [Nutter, Forrest W., Paul D. Esker, and Rosalee A. Coelho Netto,2006]. Image recognition and machine learning are essential fields of study because they can facilitate the monitoring of large crop fields and the automatic identification of symptoms as they appear [Rajasekar, Vani, et al,2021]. Deep learning represents a modern approach in machine learning, achieving state-of-the-art results across various research areas, including computer vision, pharmaceuticals, and bioinformatics. Deep learning has the advantage of utilizing raw data directly without the need for intricate preprocessing [Jackulin, C., and S. Murugavalli,2022]. In the agriculture sector, classification and recognition are two significant techniques with economic implications [Zang.J.,Wang, S.X,2007]. Several classifiers are employed to differentiate between diseased and healthy plant images. The most commonly used plant disease detection techniques include Artificial Neural Networks (ANN), Naïve Bayes (NB), k-Nearest Neighbors (k-NN), Support Vector Machines (SVM), Random Forests (RF), and Convolutional Neural Networks (CNN), among others. This paper surveys different

methodologies for identifying the most commonly occurring diseases in cotton plants using machine learning and deep learning techniques.

Types of diseases affecting cotton leaves and their characteristics

Cotton plant affected by various types of diseases are Bacterial, fungal and viral diseases. Disease not only appears on the leaf of plant but also on cotton balls, cotyledons, seedling, root etc. The accurate and timely detection of these diseases is essential for the farmers to take prompt action and maximize the crop yield.

1. Bacterial leaf blight Disease

Bacterial disease caused by the bacteria Xanthomonas campestis pv. Malvacearum.The spots on the lesion area of leaves may spread over the major veins of leaf and in later petioles stem get infected [8]. The disease symptoms start with dark green colour and leaf spot appear red to brown or dark brown to black in colours with angular in shape [12].

2. Anthracnose Disease

Anthracnose disease is one of the fungal diseases which may affect all the plant parts of the cotton plant. At seedling stage, the circular red coloured spots are noticed and seedling may even die. Circular, reddish to brown coloured spots on bolls and leaves are noticed at later stages of infection.

3. Cercospora Disease

Cercospora is caused by the cercosporin Gossiping [8]. The tainted leaf has red spot in unpredictable shape with yellowish, purple, dark brown or blackish spread out up to 2cm.The lesion region blackish leaf spot shows up through fine veins of the leaf that influences more seasoned leaves of developing plants [13].

4. Grey Mildew Disease

It is one of the diseases caused by the fungal of Ramularia Areola Atk [8]. At primary stage, the infection appears in whitish spots irregular angular. As disease increases, the small spot merge to form bigger spots and leaf tissue change yellowish brown while whitish frosty growth appears on lower surface [13].

5. Fusarium Wilt Disease

It is the fungal disease caused due to Fusarium Oxysprum [13]. The influenced plants are darker green and latterly show down as the yellow dark colour of the leaves. Which causes loss of foliage.

Fig-1 Bacterial leaf blight

Fig-2 Anthracnose

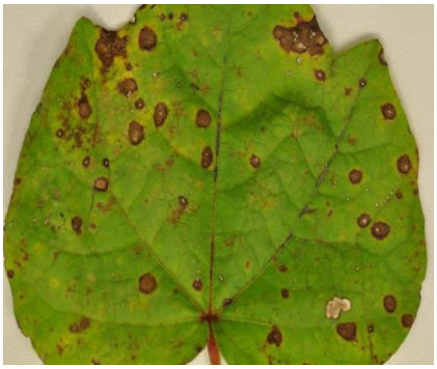

Fig-3 Cercospora

Fig-4 Grey Mildew

Fig-: 5 Fusarium Wilt

National Conference on «Modern Perspectives In Physical and Chemical Sciences » (MPPCS-2024) DOI: **10.13140/RG.2.2.13272.40962**

Literature survey:

Cotton plays a pivotal role as a cash crop, particularly given its extensive use in the textile industry. Unfortunately, various diseases can significantly degrade the quality of cotton, posing challenges for farmers and producers. To address this issue, numerous researchers have been actively working on developing automated methods for effectively detecting these diseases. The following is a detailed summary of several notable studies in this field. Hassan, Sk Mahmudul, and colleagues proposed a variety of machine learning approaches aimed at identifying plant diseases through analysis of leaf images. Their research highlighted the critical need for advanced processing and segmentation techniques, which they determined play a fundamental role in enhancing the accuracy of disease identification. By comparing different deep learning models, such as ResNet50, Inception V3, and DenseNet201 architectures, they concluded that these models are particularly suitable for the identification of plant diseases. Their comprehensive analysis underscores the importance of machine learning in agricultural disease detection [1]. In a separate study, Das Rahul and his team focused on the identification and classification of five prevalent cotton leaf diseases: bacterial blight, Alternaria, gray mildew, cercospora, and fusarium wilt. They utilized a Support Vector Machine (SVM) based regression system and developed an innovative Android app that not only displayed disease information but also provided sensor data to farmers. This app features real-time monitoring of critical soil parameters, including humidity, moisture, and temperature, as well as the water level in irrigation tanks. Their integration of a Raspberry Pi for the leaf disease detection system achieved an impressive classification accuracy of 83.26%, demonstrating the feasibility of mobile technology in agricultural applications [4]. Rajasekar, Vani, and co-authors presented a CNN-based deep learning approach tailored for identifying cotton leaf diseases. Their methodology employed a novel fully integrated softmax layer for image classification, enhancing the system's capacity to discern subtle variations in leaf images. By integrating a pretrained ResNet model with the Xception module, they aimed to refine the classification process further. Their implementation of the Cross Entropy Loss function improved the learning capacity for detecting smaller and less obvious features in the images, thus enhancing the overall accuracy of the model [9]. Kotian, Smruti, and colleagues explored a semi-supervised learning approach employing transfer learning to classify healthy and unhealthy cotton leaves. Their research specifically targeted diseases such as bacterial blight and leaf curl. They classified unhealthy leaves using the K-Nearest Neighbors (KNN) algorithm after initial identification through transfer learning with ResNet50. Remarkably, their combined approach achieved an accuracy rate of 95% in diagnosing diseased leaves, highlighting the effectiveness of their methodology in practical applications [12]. Shantkumari, M., along with their research team, introduced an Adaptive Snake Algorithm (ASA) designed to accurately identify and segment regions on grape leaves. This two-phase model operates by first locating potential disease areas and then achieving precise segmentation in the second phase. The ASA demonstrated high effectiveness in measuring performance through various metrics such as precision, recall, Jaccard index, Manhattan distance, and Dice score. Their evaluations on standard datasets confirmed the ASA's efficiency and robustness, validating its utility for leaf disease detection in diverse agricultural settings [14]. Ramesh, Shima, and their team tackled the issue of overfitting in training datasets by proposing a Random Forest classifier. This model effectively addresses both numeric and categorical data, enhancing disease prediction accuracy. The researchers extracted shape and texture features from leaves using Hu moments and Haralick texture descriptors. They also employed histogram techniques to analyze color image distribution. Although trained on a limited set of 160 images of papaya leaves—resulting in a 70% accuracy rate—they suggested that training with a larger dataset could yield even better results, enhancing the reliability of their classification method [15].

Prabhakar and their collaborators delved into deep learning with a focus on the Foldscope Deep Residual Network 101 (ResNet101) for detecting early blight in tomato leaves. Their dataset comprised 1,000 images representing various stages of early blight, including mild, moderate, and severe cases. They applied multiple deep learning architectures including VGG16, VGG19, GoogLeNet, AlexNet, ResNet50, and ResNet101 in their analysis. Their findings revealed a high training accuracy of 97.6% and a testing accuracy of 94.6%, demonstrating the potential of deep learning frameworks in plant disease detection [16]. Zhu, Juanhua, and colleagues employed an Image Analysis and Back Propagation Neural Network (BPNN) method for identifying various grape leaf diseases. Their approach focused on five specific conditions: leaf spot, Sphaceloma ampelinum de Bary, anthracnose, round spot, and downy mildew. To mitigate noise in the images, they converted color images to grayscale and utilized Wiener filtering for further denoising. The Otsu method facilitated effective segmentation of disease regions on the leaves. Their proposed system exhibited superior classification accuracy compared to existing methods, showcasing its potential for practical use in the agricultural sector [17]. Chopda, Jayraj, et al., developed an innovative system using a Decision Tree Classifier for detecting diseases in cotton crops. Their approach involved collecting vital parameters such as temperature and soil moisture through sensor data and human input via a mobile application. The data was subsequently uploaded to the Thingspeak server for analysis, allowing for accurate predictions regarding crop health. They developed a mobile app designed to provide farmers with crop-related alerts, offering real-time insights into their agricultural practices and enhancing decision-making for disease management [18]. Zambare, Rajani, and their team presented an approach utilizing Convolutional Neural Networks (CNN) for the identification of diseases in cotton plants. Their system included meticulous preprocessing and segmentation of images based on established teacher standards, thereby ensuring high accuracy in disease detection [19]. Shah, Nikhil et al. have developed an Artificial Neural Network (ANN) based system for detection of different diseases of cotton plant. For image processing MATLAB used to classify the quality of cotton leaf with or without defects with the help of RGB (Red, green, blue) and HSV (hue, saturation and value) components from the image [20]. Lastly ,Singh, et al. proposed novel deep

learning technique Heap Auto Encoders (HAE) for image classification of banana leaf disease. The dropout method and Rectified Linear Units (ReLU) are also applied HAE. YCbCr component used for segmentation of input image provide good results compared to RGB image. The proposed technique provides a decision support tool to assist farmers in identifying the disease on banana leaf. The system proposed classification accuracy is 99.35% with real data sets [21].This research emphasizes the continued advancement and application of deep learning techniques in agricultural disease management, paving the way for more sustainable and effective farming practices.

A Precautionary method for identifying and categorizing leaf diseases :
The two stages of the general strategy for leaf disease detection are image processing and machine learning-based disease classification. This section covers the image processing stages of picture acquisition, image pre-processing, image segmentation, and feature extraction. We also go through a few classification strategies. The disease detection take place in step wise manner to get high accuracy.

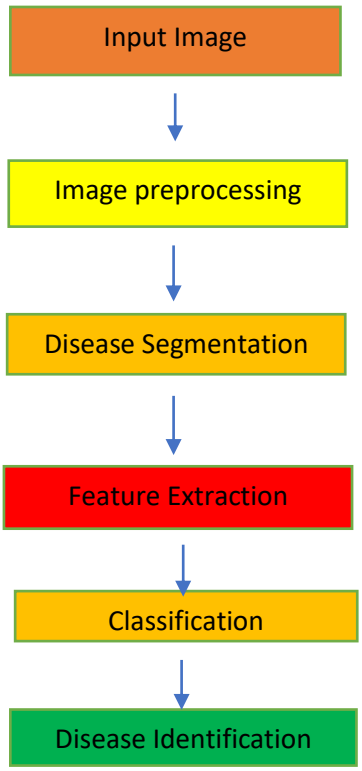

Fig. 6: Design Flow for Cotton leaf Disease Detection

The main steps of disease detection are as follows.

Image Acquisition:
For the image acquisition process, the user can capture high-quality photographs of cotton plants or leaves using a digital camera or a smartphone. It is important to ensure that the images are captured in a manner that minimizes any distortion or unwanted artifacts, such as by using proper lighting conditions, camera angles, and focusing techniques. For training the machine learning model, the researcher should curate a comprehensive dataset that includes images of both healthy and diseased cotton leaves, covering a wide range of disease symptoms and severity levels. This dataset should be carefully annotated and organized to enable effective model training and evaluation.

Image Pre-processing :
The input image undergoes a crucial pre-processing stage to enhance its quality and prepare it for further analysis. This pre-processing step involves several techniques to remove unwanted noise and distortions, while simultaneously highlighting the important visual features of the cotton leaf.
First, the image may be subjected to color space conversion, transforming it from the original RGB (red, green, blue) color space to alternative representations, such as HSV (hue, saturation, value) or LAB (lightness, red-green, blue-yellow). These color space transformations can help accentuate the distinctive color patterns associated with different cotton plant diseases. Next, the image is resized to a standardized dimension, ensuring compatibility with the input requirements of

National Conference on «Modern Perspectives In Physical and Chemical Sciences » (MPPCS-2024) DOI: **10.13140/RG.2.2.13272.40962**

the subsequent machine learning models. This resizing step may involve techniques like bilinear or bicubic interpolation to preserve the important visual details.
Additionally, various filtering operations, such as Gaussian blurring or median filtering, are applied to the image to remove noise and smooth out unwanted artifacts, while preserving the critical edge information and textural characteristics of the cotton leaf.
These pre-processing techniques work in tandem to enhance the quality of the input image, making it more suitable for the subsequent segmentation, feature extraction, and disease classification stages of the cotton plant disease detection pipeline.

Segmentation:
Image segmentation is a crucial step in the cotton plant disease detection process. It involves the extraction of the diseased or defected leaf region from the input image. The segmentation process separates the region of connected pixels with similar visual properties, such as color, texture, and intensity, by identifying the boundaries between these regions. This allows the isolation of the affected leaf area from the healthy parts, enabling a more focused analysis of the disease symptoms. Various segmentation techniques, such as thresholding, edge detection, and region-growing algorithms, can be employed to accurately delineate the diseased leaf region. The effectiveness of the segmentation step directly impacts the subsequent feature extraction and disease classification stages, as it provides a refined region of interest for further analysis.

Feature Extraction:
The extracted features play a crucial role in training the machine learning model for accurate disease classification. Some commonly used feature extraction techniques include:
Hu Moments: This method extracts translation, scale, and rotation-invariant features from the image, which can effectively capture the shape characteristics of the diseased leaf regions.
Haralick Texture: This technique analyzes the spatial relationship of pixels in the image, providing valuable information about the textural properties of the diseased areas, such as smoothness, coarseness, and regularity.
Color Histogram: By analyzing the distribution of pixel values in the RGB or other color spaces, the color histogram feature can help distinguish between healthy and diseased leaf regions based on their distinctive color patterns.
These feature extraction techniques, when combined, can provide a comprehensive representation of the visual characteristics of the leaf, enabling the machine learning model to learn the unique signatures of different plant diseases and improve the classification accuracy.

Classification:
The final step in the disease detection process is the classification of the leaf into different disease categories. Various machine learning and deep learning algorithms have been used for this purpose, including Support Vector Machines, Artificial Neural Networks, Convolutional Neural Networks, and Transfer Learning-based models. The choice of the classification algorithm depends on the complexity of the problem, the size and quality of the available dataset, and the desired performance metrics, such as accuracy, precision, and recall.
Some of the popular classification models used for plant disease detection include:

Plant disease detection using machine learning model:
Support Vector Machines
which can effectively handle non-linear and high-dimensional data, making them suitable for complex plant disease classification tasks [22]. In SVM, a hyper plane is utilized to divide data. Both linear and nonlinear classifications use SVM. Training samples and datasets can be classified with ease when using linear classification. In contrast to linear classification, non-linear classification makes it more difficult to differentiate training samples from data. SVM can be used for both multiclass and binary classification [23].

Neural Network (NN)
A neural network (NN) is a computing system composed of densely interconnected, basic processing components that use states to process information from external inputs. A limitation of NN is that, in a backpropagation neural network, the user essentially has no idea what steps are being taken by the classifier to categorize the dataset. When it comes to training, backpropagation networks take longer than other types of NN.[24]

KNN Classifier
KNN classifier is used to solve regression and classification problems, albeit it primarily aids in classification problems. KNN is a distribution tree algorithm diagnosis. It is called non-parametric, i.e., the structure derived from the qualities of the data collection, if there is no imagination for the distribution of the data. When data sets never comply with theoretical mathematical thoughts, KNN is utilized for prediction. To continue, KNN does not require any training data. Because all of the training data aids in the testing data, it is known as the Slow Learning (SL) algorithm [10].

National Conference on «Modern Perspectives In Physical and Chemical Sciences » (MPPCS-2024) DOI: **10.13140/RG.2.2.13272.40962**

RF Classifier

The supervised algorithm RF is capable of handling both regression and classification techniques. It is mostly focused on matters pertaining to classification. A forest is a collection of trees, and a forest with a high tree count is called a strong forest. The dataset-based decision tree approach is also found by the RF, similar to decision trees. It first chose a better result by selecting the specified method after obtaining the prediction results from the whole tree. It is known as an ensemble approach, and because the average performance reduces over-fitting, it performs better than a single DT classifier [10].

Plant disease diagnosis using deep learning:

Convolutional Neural Networks

which are well-suited for image-based plant disease detection, as they can automatically learn relevant features from the input images without the need for manual feature engineering. Among the particular classes of ANNs is the Convolutional Neural Network (CNN). These are deep networks that take in an image as input, apply internal weights and biases to various regions or objects, and attempt to distinguish between various items. When compared to more conventional methods, its unique feature—requiring little to no preprocessing—makes it a popular choice among researchers. CNN requires a lot less pre-processing than the other categorization algorithms [25].

Transfer Learning

where pre-trained models (such as VGG, ResNet, or InceptionV3) are fine-tuned on the plant disease dataset, leveraging the rich feature representations learned from large-scale image datasets, such as ImageNet.

InceptionV3

The 48-layered deep CNN network known as Inception V4 is an extension of the Image Net paradigm. Asymmetric and symmetric blocks make up the constructed model. Convolution is used to create a map of features when applying a filter to an image. Average computation of the feature map for every pixel, maximum pooling layer, average pooling (8 × 8), and maximum pixel are also covered. These blocks help reduce the computation cost parameters numbers for learning. Neurons in the fully-connected layer are connected to each layer by means of the same-sized inputs, which are typically dropouts merged after pooling to help reduce overfitting and increase accuracy. Softmax and batch norm are used to create the activation norm, which is used in loss computation.

VGG–16

The Oxford University, which created this kind of deep CNN model for the "Image Net," introduced the "visual geometry group," or VGG. In 2014 "Large-scale Recognition of Visual Challenge" (ILSVRC) was conducted. When compared to other deep neural networks, this structure has the best function available as of right now. Even though there are many other types of parameters, this structure only pays attention to the max pool, fully connected layer, and padding convolution layer, which provide the softmax layer's output.

ResNet

ResNet refers to residual network, researchers focused more on creating a deeper network with additional layers. But there are more and more of them. Additionally, layers raise the rate of test and training errors. The issue of vanishing gradient is also lessened by residual network architecture. In ResNet, a unique approach known as skip connection is employed to connect to the outputs without connecting to certain levels. Because skip connection approaches eliminate layers that perform poorly due to regularization, the network performs better overall. As a result, the vanishing gradient issue can be resolved. One convolution layer, one average pool layer, and 48 convolution layers make up the ResNet50 variation of the ResNet model [25].

The performance of these classification models can be further improved by employing ensemble techniques, where multiple models are combined to make more robust and accurate predictions.

In summary, the key steps in the detection of cotton plant diseases include image preprocessing, segmentation, feature extraction, and classification using advanced machine learning and deep learning algorithms. These techniques have shown promising results in accurately identifying and diagnosing various cotton plant diseases, aiding farmers and agricultural experts in timely intervention and effective disease management [26][27][28].

Validation:

The method is confirmed by running it on a fresh set of photos that have unidentified labels after it has been tested. Verifying the accuracy and dependability of the algorithm will be the goal of validation. Finding any flaws or restrictions in the algorithm also helps, since these can be leveraged to enhance its functionality.

Conclusion:

In this paper, we conducted a comprehensive survey of the various machine learning-based approaches that have been developed for the identification and detection of plant diseases using leaf images. As with human health, plants are susceptible to a wide range of diseases that can significantly impact their growth and productivity. This survey explored

both the traditional handcrafted-feature-based methods as well as the more recently emerged deep learning-based techniques for plant disease classification.

The literature review revealed that one of the key challenges in reliable plant disease detection is the fact that the visual symptoms can change significantly across different stages of disease progression. This dynamic nature of the disease symptoms can adversely impact the performance and accuracy of the detection models, particularly when they are trained on a limited dataset. However, the proposed systems have shown promising potential in identifying the diseases at an earlier stage, even before the visible symptoms become prominent. This early detection capability can help minimize crop losses and reduce the dependence on expert human intervention to a considerable extent.

Furthermore, the survey highlighted the importance of these automated plant disease detection systems in assisting individuals with limited domain knowledge, providing them with valuable insights and support in accurately diagnosing and managing plant diseases. The integration of these advanced machine learning techniques into practical, user-friendly applications can significantly enhance the accessibility and impact of such technologies in the agricultural sector.

.

References

Journal

[1] Hassan, Sk Mahmudul, et al. "A Survey on Different Plant Diseases Detection Using Machine Learning Techniques." Electronics 11.17 (2022): 2641.

[2] Ferentinos, Konstantinos P. "Deep learning models for plant disease detection and diagnosis." *Computers and electronics in agriculture* 145 (2018): 311-318.

[3] Bharate, Anil A., and M. S. Shirdhonkar. "A review on plant disease detection using image processing." *2017 International Conference on Intelligent Sustainable Systems (ICISS)*. IEEE, 2017.

[4] Das, Rahul, V. Pooja, and V. Kanchana. "Detection of diseases on visible part of plant—A review." *2017 IEEE Technological Innovations in ICT for Agriculture and Rural Development (TIAR)* (2017): 42-45.

[5] Bock, C. H., et al. "Plant disease severity estimated visually, by digital photography and image analysis, and by hyperspectral imaging." *Critical reviews in plant sciences* 29.2 (2010): 59-107.

[6] Tlhobogang, Boikobo, and Muhammad Wannous. "Design of plant disease detection system: A transfer learning approach work in progress." *2018 IEEE International conference on applied system invention (ICASI)*. IEEE, 2018.

[7] Mutka, Andrew M., and Rebecca S. Bart. "Image-based phenotyping of plant disease symptoms." *Frontiers in plant science* 5 (2015): 734.

[8] Nutter, Forrest W., Paul D. Esker, and Rosalee A. Coelho Netto. "Disease assessment concepts and the advancements made in improving the accuracy and precision of plant disease data." *European Journal of Plant Pathology* 115 (2006): 95-103.

[9] Rajasekar, Vani, et al. "Detection of cotton plant diseases using deep transfer learning." *Journal of Mobile Multimedia* 18.2 (2021): 307-324.

[10] Jackulin, C., and S. Murugavalli. "A comprehensive review on detection of plant disease using machine learning and deep learning approaches." *Measurement: Sensors* (2022): 100441.

[11] Zang.J.,Wang, S.X.:A study on the segmentation Method in Image Processing for Plant Disease of Greenhouse (in Chinese). Journal Of Inner Mongolia Agricultural University 28 (2007):19-22

[12] Kotian, Smruti, et al. "Cotton Leaf Disease Detection Using Machine Learning." *Available at SSRN 4159108* (2022).

[13] Sarangdhar, Adhao Asmita, and V. R. Pawar. "Machine learning regression technique for cotton leaf disease detection and controlling using IoT." *2017 international conference of electronics, communication and aerospace technology (ICECA)*. Vol. 2. IEEE, 2017.

[14] Shantkumari, M., and S. V. Uma. "Grape leaf segmentation for disease identification through adaptive Snake algorithm model." *Multimedia tools and applications* 80.6 (2021): 8861-8879.

[15] Ramesh, Shima, et al. "Plant disease detection using machine learning." *2018 International conference on design innovations for 3Cs compute communicate control (ICDI3C)*. IEEE, 2018.

[16] Prabhakar, Maheswari, Raja Purushothaman, and Durga Prasad Awasthi. "Deep learning-based assessment of disease severity for early blight in tomato crop." *Multimedia Tools and Applications* 79 (2020): 28773-28784.

[17] Zhu, Juanhua, et al. "Identification of grape diseases using image analysis and BP neural networks." *Multimedia tools and applications* 79 (2020): 14539-14551.

[18] Chopda, Jayraj, et al. "Cotton crop disease detection using decision tree classifier." *2018 International Conference on Smart City and Emerging Technology (ICSCET)*. IEEE, 2018.

[19] Zambare, Rajani, et al. "Deep Learning Model for Disease Identification of Cotton Plants." *Specialusis Ugdymas* 1.43 (2022): 6684-6695.

[20] Shah, Nikhil, and Sarika Jain. "Detection of disease in cotton leaf using artificial neural network." *2019 Amity International Conference on Artificial Intelligence (AICAI)*. IEEE, 2019.

[21] Ani brown mary,Singh, Robert, and Suganya Athisayamani. "Banana leaf diseased image classification using novel HEAP auto encoder (HAE) deep learning." *Multimedia Tools and Applications* 79.41-42 (2020): 30601-30613.

[22] Pukkela, Pragati, and Surekha Borra. "Machine learning based plant leaf disease detection and severity assessment techniques: State-of-the-art." *Classification in BioApps: Automation of Decision Making* (2018): 199-226.

[23] Kim, Jinho, Byung-Soo Kim, and Silvio Savarese. "Comparing image classification methods: K-nearest-neighbor and support-vector-machines." *Proceedings of the 6th WSEAS international conference on Computer Engineering and Applications, and Proceedings of the 2012 American conference on Applied Mathematics*. 2012.
[24] Prajapati, Bhumika S., Vipul K. Dabhi, and Harshadkumar B. Prajapati. "A survey on detection and classification of cotton leaf diseases." *2016 international conference on electrical, electronics, and optimization techniques (ICEEOT)*. IEEE, 2016.
[25] Dahiya, Sachin, Tarun Gulati, and Dushyant Gupta. "Performance analysis of deep learning architectures for plant leaves disease detection." *Measurement: sensors* 24 (2022): 100581.
[26] Foysal, Md Aziz Hosen, Foyez Ahmed, and Md Zahurul Haque. "Multi-Class Plant Leaf Disease Detection: A CNN-based Approach with Mobile App Integration." *arXiv preprint arXiv:2408.15289* (2024).
[27] Gong, Xulu, and Shujuan Zhang. "An analysis of plant diseases identification based on deep learning methods." *The plant pathology journal* 39.4 (2023): 319.
[28] Kumar, Raj, et al. "[Retracted] A Systematic Analysis of Machine Learning and Deep Learning Based Approaches for Plant Leaf Disease Classification: A Review." *Journal of Sensors* 2022.1 (2022): 3287561.

Content is available at: CRDEEP Journals
Journal homepage: http://www.crdeepjournal.org/category/journals/ijbas/

International Journal of Basic and Applied Sciences
(ISSN: 2277-1921) (Scientific Journal Impact Factor: 6.188)

UGC Approved-A Peer Reviewed Quarterly Journal

Determination of M-Ligand Stability Constants for Lanthanide(III) Complexes with Substituted Heterocyclic Drugs.

R. D. Khalapure[1], S. R. Ingale[2], K. N. Sonune[2], R. S. Khedekar[2]
1. Lal Bahadur Shastri Sr College Partur
2. Jijamata Mahavidhyalaya Buldana
3. Swami Vivekanand Mahavidhyalaya Mantha

Abstract:
The lanthanide metal ions of Ce^{3+}, Gd^{3+}, Pr^{3+}, Nd^{3+}, Yb^{3+}, Sm^{3+}, Lu^{3+} and Dy^{3+}. interactions with ligands Oxymetazoline 6-tert-butyl-3-(4,5-dihydro-1H-imidazol-2-ylmethyl)-2,4- dimethylphenol Ligand-1 and Amikacin (2S)-4-amino-N-[(1R,2S,3S,4R,5S)-5-amino-2-[(2S,3R,4S,5S,6R)-4-amino-3,5-dihydroxy-6-(hydroxymethyl)oxan-2-yl]oxy-4-[(2R,3R,4S,5S,6R)-6- (aminomethyl)-3,4,5-trihydroxyoxan-2-yl]oxy-3-hydroxycyclohexyl]-2- hydroxybutanamide. Ligand-2 was one by one simultaneously, systematically investigated by using pH-metric techniques, under controlled conditions at ionic strength 0.1 M and temperature ±0.1 °C in a 70% dioxane-30 % water mixture. The experimental data obtained were utilised to determine the proton-ligand stability constants (pK) and the metal-ligand stability constants (log K). The findings reveal that the Inner transition metal or lanthanide metal ions like Ce^{3+}, Gd^{3+}, Pr^{3+}, Nd^{3+}, Yb^{3+}, Sm^{3+}, Lu^{3+} and Dy^{3+}. Form both 1:1 and 1:2 complexes with investigated heterocyclic substituted ligands.

Keywords: Metal-ligand stability constant, lanthanide (III) Substituted drugs, Heterocyclic drugs, Inner transition metal,proton-ligand Stability.

Introduction:
Recent research in coordination chemistry has focused on studying the stability constants of metal-ligand complexes, particularly those involving trivalent metal ions and various organic compounds. Understand there are many applications in medicine, catalysis, and environmental science. S Muthaiah et al. &T Patekar et al.[1] Organic molecules such as substituted sulphonic acids,aromatic ketones, coumarins,alkyl monoamines, isoxazolines, pyrazolines and benzothiazoles have beenwidely studied and investigated due to their ability to form stable complexes with metal ions. V Solov'ev, & J Sattar et al. [2,3] This study focused on the stability constants of metal complexes formed by two specific drugsOxymetazoline (Ligand-1), a widely used decongestant, and Amikacin (Ligand-2), an aminoglycoside antibiotic. These drugs were tested for their interactions with trivalent metal ions, includingCe^{3+},Gd^{3+}, Pr^{3+},Nd^{3+}, Yb^{3+}, Sm^{3+},Lu^{3+} andDy^{3+}. The stability constants were determined using the pH-metric method, a reliable technique for studying metal-ligand complexes. A Sonar et al, A Vyas et al. & K Sonune et al. [4,5,6]

Experimental Work:
This study were used inTwo ligands Oxymetazoline; 6-*tert*-butyl-3-(4,5-dihydro-1*H*-imidazol-2-ylmethyl)-2,4-dimethylphenol Ligand-1 and Amikacin;(2*S*)-4-amino-*N*-[(1*R*,2*S*,3*S*,4*R*,5*S*)-5-amino-2-[(2*S*,3*R*,4*S*,5*S*,6*R*)-4- amino-3,5-dihydroxy-6-(hydroxymethyl) oxan-2-yl]oxy-4-[(2*R*,3*R*,4*S*,5*S*,6*R*)-6- (aminomethyl)-3,4,5-trihydroxyoxan-2-yl]oxy-3-hydroxycyclohexyl]-2- hydroxybutanamide.Ligand-2. The above ligands were synthesised according to previously reported methods.[7,8]

Preparation of Solutions:
Solvent - the ligands were dissolved in a solvent mixture of 70% dioxane-water (v/v), used as the solvent for all experiments.[9]Rear earth, Inner transition, and lanthanide Metal Nitrate Solutions(from BDH Chemicals) were dissolved in perchloric acid. Their maintained concentrations were using volumetric and spectrophotometric methods1.[10] The solution was prepared with well-purified water to ensure purity. The Solution 0.1 M sodium perchlorate solution was prepared with constant ionic strength during titration.[11]

Potentiometric Titration

Potentiometric titrations were performed by using an Elico (L1-613) pH meter with glass and calomel electrode, ensuring an accuracy of ±0.01 pH units.[12] The instrument was calibrated by using0.05 M potassium hydrogen phthalate (pH 4) and a standard buffer tablet (pH 9).[13]

All titrations with constant temperature, maintaining at 0.1 Mionic strength of$NaClO_4$ solution. The volume of the solutions was fixed at 50 mL. Metal ions involved in the study included Ce^{3+},Gd^{3+}, Pr^{3+},Nd^{3+}, Yb^{3+}, Sm^{3+},Lu^{3+} andDy^{3+}. Each titration was repeated at least twice to ensure accuracy.

Titration Protocol

The solution was titrated PH-metricallywith 0.2 M sodium hydroxide (carbonate-free).

1. Free Acid Solution: 5 mL $NaClO_4$ solution, 5 mL $HClO_4$ solution, 15 mL dioxane solvent, 5 mL double-distilled water.[6]
2. Free Acid + Ligand solution: 5 mL $NaClO_4$ solution, 5 mL $HClO_4$ solution, 35 mL dioxane solvent, 3 ml double-distilled water, 2 mL ligand solution[6].
3. Free Acid + Ligand + Metal Ion Solution: 5 mL $NaClO_4$ solution, 5 mL $HClO_4$ solution, 15 mL dioxane solvent, 1 mL distilled water, 2 mL ligand solution, 2 mL metal ion solution[6].

The Irving and Rossotti method[14] was used to calculate (pK) the proton-ligand stability constant and(log β) the metal-ligand stability constant. The ionic strength of a solution was calculated by using the formula $\mu=\frac{1}{2}\Sigma CiZi$. The ionic strength ofsolutions was maintained at 0.1 M, accounting for contributions from all ions, including ClO_4^-andNa^+.

Results and discussion:

Proton-Ligand Stability Constants

Substitutedheterocyclic drugs can be categorized as monobasic acids due to their single replaceable proton originating from the hydroxyl (-OH) group. This group dissociates completely at pH above 9, making these compounds chemically representable as HL. H represents the dissociable proton and L represents the remaining molecular structure of Substitutedheterocyclic drugs.

$$HL \leftrightarrow H^+ + L^-$$

In this experiment, titration was conducted to study the dissociation and stability of these heterocyclic compounds. The titration data was used to create graphs plotting the volume of sodium hydroxide (NaOH) added against pH. These graphs were generated for the acid-ligand system and the acid-ligand-metal system. The titration data was used to conduct curves between the volume of sodium hydroxide vs. pH-free acid, acid ligand and acid ligand metalcurved.[6] It was observed that ligand curves start deviating from free acid (HClO4) curves at approximately pH 7, and this deviation continues up to pH 12. This indicates the dissociation of the -OH group in substituted heterocyclic drugs, a key factor in their proton-ligand interaction. To determine the dissociation, the degree of protonation, denoted as nA, was calculated at different pH levels using (curve A) denoted acid titration curves and (curve B) denoted ligand titration curves. These calculations were performed using the formula proposed by Irving and Rossotti[14], a widely accepted method for such studies.

The proton-ligand stability constants (pK values) by plotting nA against pH. The pK values were specifically calculated using two methods:

1. Half-integral method: In this approach, the pK is determined by identifying the pH at which nA = 0.5.
2. Pointwise calculation method: This involves calculating pK values for each data point, ensuring a more precise result.

ThepK values of studied ligands are summarized in Table 1.

Table 1: Proton-Ligand Stability Constant (pK) of Substituted heterocyclic ligands.

Systems	**Constant pK**	
	Half integral	**Point wise calculation**
Oxymetazoline Ligand-1	11.60	11.63 ± 0.05
Amikacin Ligand-2	11.80	11.82 ± 0.03

The results indicate that Ligand-2 has a higher stability constant compared to Ligand-1. This can be the presence of a strong proton-withdrawing chlorine (Cl) group in Ligand-2. The Cl group stabilizes the conjugate base, thereby increasing the acidity of Ligand-2. Consequently, Ligand-2 dissociates more readily than Ligand-1. The observed order of dissociation is Ligand-2 greater than Ligand-1.

Metal-Ligand Stability Constants

The stability constants of metal-ligand complexes involving Ce^{3+},Gd^{3+}, Pr^{3+},Nd^{3+}, Yb^{3+}, Sm^{3+},Lu^{3+} andDy^{3+}, with substituted heterocyclic drugs, were calculated using the Bjerrum-Calvin pH titration technique, as adapted by Irving and Rossotti[14].

This technique allows for precisely determining stability constants by analyzing the behaviour of metal-ligand interactions in solution.

Evidence of Complex Formation

1. Titration Curve Deviations:

For Ce^{3+}, Gd^{3+}, and Pr^{3+}, significant deviations in the metal-ligand titration curves from the free ligand were observed starting at pH 3.

For Nd^{3+}, Yb^{3+}, Sm^{3+}, and Lu^{3+}, deviations began at pH 4.5.

For Dy^{3+}, the deviation occurred at pH 5.

2. Color Changes:

The solutions displayed distinct colour changes, transitioning from yellowish-white to light brown to dark brown as the pH increased from 2.5 to 8.5.

These deviations and colour changes indicate the release of protons during chelation, confirming the formation of stable metal-ligand complexes.

Calculation of Stability ConstantsLog K_1 and Log K_2

The formation curves calculated the primary stability constant (log K_1) and secondary stability constant (log K_2). These constants correspond to specific values of n, with n = 0.5 for log K_1 and n = 1.5 for log K_2. Calculated stability constants are shown in Table 2 below.

Table 2: Metal-Ligand Stability Constants (log K) for Substituted heterocyclic drugs.

System	Constant	
	logK_1 i.e. pL_1	**logK_2 i.e. pL_2**
Ce (III) Ligand-1	07.64	09.74
Pr (III) Ligand-1	08.52	10.17
Nd (III) Ligand-1	08.92	09.97
Sm (III) Ligand-1	07.61	10.26
Gd(III) Ligand-1	09.96	10.99
Dy (III) Ligand-1	08.17	10.37
Yb (III) Ligand-1	07.16	09.98
Lu (III) Ligand-1	08.06	10.56
Ce (III) Ligand-2	07.96	10.22
Pr (III) Ligand-2	07.35	10.85
Nd (III) Ligand-2	09.05	10.35
Sm (III) Ligand-2	07.24	09.78
Gd(III) Ligand-2	09.76	11.76
Dy (III) Ligand-2	07.39	09.99
Yb (III) Ligand-2	08.59	10.29
Lu (III) Ligand-2	09.28	10.68

The data shows that the difference between log K_1 and log K_2 is relatively small, suggesting a trans-structure for the complexes. This structure facilitates the addition of secondary ligands without steric hindrance, as indicated by the positive ratio of log K_1/log K_2 for all systems.

Stability Trends

The order of stability for metal-ligand complexes based on log K_1 is as follows:

1. Ligand-1:

Gd^{3+}> Nd^{3+}> Pr^{3+} > Dy^{3+} > Lu^{3+}> Ce^{3+}> Sm^{3+}> Yb^{3+}

2. Ligand-2:

Gd^{3+}> Lu^{3+}> Nd^{3+}> Yb^{3+}> Ce^{3+}> Dy^{3+}> Pr^{3+}> Sm^{3+}

These results align with prior research by Tambatkar et al[15]. andK. N. Sonune et al[6]., further validating the observed trends.

Table 3: Stability Constant Differences.

System	logK_2 -logK_1	logK_2 /logK_1
Ce (III) Ligand-1	02.10	01.27
Ce (III) Ligand-2	02.26	01.28
Pr (III) Ligand-1	01.65	01.19
Pr (III) Ligand-2	03.50	01.47

Nd (III) Ligand-1 **Nd (III) Ligand-2**	01.05 01.30	01.11 01.14
Sm (III) Ligand-1 **Sm (III) Ligand-2**	02.65 02.54	01.34 01.35
Gd(III) Ligand-1 **Gd(III) Ligand-2**	01.03 02.00	01.10 01.20
Dy (III) Ligand-1 **Dy (III) Ligand-2**	02.20 02.60	01.27 01.35
Yb (III) Ligand-1 **Yb (III) Ligand-2**	02.82 01.70	01.39 01.19
Lu (III) Ligand-1 **Lu (III) Ligand-2**	02.50 01.40	01.31 01.15

Acknowledgement

The authors express their sincere gratitude to the principal and department of Chemistry, Jijamata Mahavidyalaya, Buldhana and HOD, Department of Chemistry, SVC College, Mantha, for providing the facilities and support for this research work.

References

1. Trupti A Patekar, Abdul Rahim Shaikh, *Int J Sci Res Sci & Technol. March-April 11 (15), 828-840, (2024), research gate.net.*
2. Vitaly Solov'ev, Natalia Kireeva, Svetlana Ovchinnikova, Aslan Tsivadze, *Journal of Inclusion Phenomena and Macrocyclic Chemistry 83, 89-101, (2015), Springer.*
3. Jwan Oday Abdulsattar, Hind Hadi, Samantha Richardson, Alexander Iles, Nicole Pamme, *Analytica Chimica Acta 1136, 196-204, (2020). Elsevier.*
4. A. N. Sonar, N. S. Pawar, *Journal of Chemistry 8 (2), 517-522,* (2011). *wily online library.*
5. Alok Vyas, RP Mathur, *Journal of Rare Earths* 27 (3), 457-460, (2009)*, Elsevier.*
6. K. N. Sonune, Y. K. Meshram, J. B. Devhade, *international journal of chemical and physical science,* 3, No. 1, Jan-Feb (2014).
7. H. Alghamdi, M. Alsaeedi, P. Hayes, J. Glennon, *Journal of Pharmaceutical and Biomedical Analysis* 214, 114717, (2022).
8. Ryu, Eunji Kim, Je Won Park, Dong Gun Lee, Yeo Joon Yoon, *Frontiers in Microbiology* 12, 725916, (2021).
9.J. N. Nayak, M. I. Aralaguppi, B. V. Naidu, T. M. Aminabhavi, *Journal of Chemical & Engineering Data, Vol 49/Issue 3,* (2004).
10.G. H. Jeffery, *Vogel's Textbook of Quantitative Chemical Analysis 5th Ed, INC,* (2022).
11.Vogel, A. I. *Textbook of Quantitative Chemical Analysis. Longman Group Ltd., London,* (1978).
12. Sonu Sharma, TV Ramana Rao, *LWT-Food Science and Technology* 62 (1), 791-800, (2015).
13. Alicja Kicińska, Radosław Pomykała, Miguel Izquierdo-Diaz, *European Journal of Soil Science* 73 (1), e13203, (2022).
14. Irving, H. M, &Rossotti, H. S. *Journal of the Chemical Society,* 76, 2904–2910*,* (1954).
15. G.D. Tambatkar, Y. K. Meshram, M.R. Gadpale, P.G. Bhutyada and G.H. khurhade, *Asian J. Chem.*,20,5414, (2008).

Content is available at: CRDEEP Journals
Journal homepage: http://www.crdeepjournal.org/category/journals/ijbas/

International Journal of Basic and Applied Sciences
(ISSN: 2277-1921) (Scientific Journal Impact Factor: 6.188)

UGC Approved-A Peer Reviewed Quarterly Journal

Effect of Calcination Temperature on Different Phases of Iron Oxide Nanoparticles

Priyanka A. Patil*, Shanabhau D. Bagul, Nitesh S. Koche
Nanomaterials Research Laboratory, Department of Physics Pratap College Amalner.Dist.: Jalgaon, Maharashtra. 425401

Abstract
Structural, Microstructural and phase transformation properties of magnetite (Fe_3O_4) nanostructured powder prepared from sol gel technique. The nontoxic and inexpensive Fe $(NO_3)_3.9H_2O$ is used as iron precursor, ethanol as a solvent and glycerol, triethylamine (TEA) as gelation agent. The dried gel was calcined at 400°C and 600°C. The obtained nanoparticles were characterized by x-ray diffraction (XRD), field emission scanning electron microscopy (FESEM) and therrmogravimetric analysis (TGA)/differential scanning calorimetry (DSC). The DSC study showed that the phase transformation of magnetite (Fe_3O_4) to hematite (α-Fe_2O_3) was taken place at 542°C. The phases of iron oxide were monitored by just changing calcinations temperature.

Keywords: Sol gel method; iron oxide; calcinations temperature; x-ray diffraction (XRD); differential scanning calorimetry (DSC).

Introduction

Now days the synthesis and applications of iron oxide nanomaterials are have been extensively studied because of their novel and unique properties [E. Eken *et.al.*, 2009]. There are sixteen pure phases of iron oxides i.e. oxides, hydroxides and oxyhydroxides. Among all these phases magnetite (Fe_3O_4), maghemite (γ-Fe_2O_3) and hematite (α-Fe_2O_3) are most common phases [R. M. Cornel *et. al.,* 1996]. Magnetite and maghemite is the promising candidate for biomedical applications since its biocompatibility has already proven [A. K. Gupta *et. al.*, 2005]. Hematite is most thermodynamically stable phase under ambient conditions. Due to which hematite has been used as gas sensors, lithium ion batteries, pigments [P. Sun *et. al.,* 2012; Y. Cao *et. al.,* 2013; P. Zhang *et. al.,* 2010]. It is reported that synthesis methods play an important role in determining the various properties of nanomaterials such as structural, morphological, chemical etc. [P. Xu *et. al.,*2012]. It is very difficult to synthesize iron oxide nanoparticles with desired properties and phases. Magnetite phase is synthesized by the reactions in the mixture of Fe^{+2} and Fe^{+3} precursor solutions under various conditions, hematite phase is synthesized by hydrolysis of $FeCl_3$ [H. Cui *et. al.,*2013]. Herein we report sol gel method for synthesis of iron oxide nanoparticles and their characterization. Sol gel method is employed to synthesize iron oxide nanoparticles because it takes place at low temperature; it is simple and cost effective; it controls the stoichiometry of the products [C. J. Brinker 1990, L .Duraes *et. al.,* 2005]. The pretty of the present work is that the same chemicals and experimental conditions facilitate the synthesis of magnetite (Fe_3O_4) and hematite (α-Fe_2O_3) just by monitoring calcination temperature.

Materials and methods:

Materials:

Fe $(NO_3)_3.9H_2O$, ethanol, glycerol and triethylamine (TEA) were of AR grade.

Methods:

20.8 gm of Fe $(NO_3)_3.9H_2O$ was dissolve in 20 ml ethanol under magnetic stirring at 60°C in water bath. 20 drops of glycerol were added to the solution following by the addition of 3 ml of TEA. The color of solution changed from orange to reddish brown with heat release and after 2 hours the gel was set completely. After 4 hours the gel was completely dried and xerogel was obtained. The obtained xerogel was calcined at temperature 400°C and 600°C for 2 hours in air atmosphere.

National Conference on «Modern Perspectives In Physical and Chemical Sciences » (MPPCS-2024) DOI: **10.13140/RG.2.2.13272.40962**

Characterization:

The structural characterization of the obtained particles were carried out using X-ray diffraction technique (Bruker D8 ADVANCE model) with CuKα radiation (λ= 1.5406 Å). Morphological analysis of the samples was performed using field emission scanning electron microscopy (FESEM model S4800 type II, Hitachi High Technologies). Thermo gravimetric analysis (TGA) and differential scanning calorimetry (DSC) study of samples is done by STA-6000 (Perkin Elmer) in the temperature range 50-800^{o}C under nitrogen atmosphere.

Results and discussion:

Structural Properties: XRD study

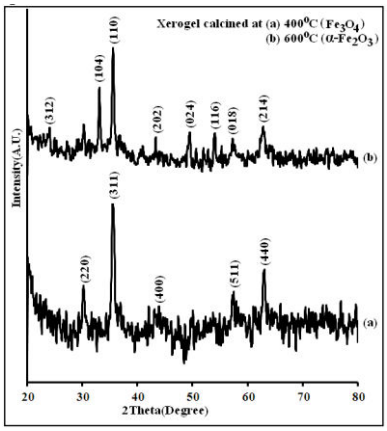

Fig. 1. XRD patterns of xerogel calcined at (a) 400^{o}C and (b) 600^{o}C

The XRD patterns of xerogel calcined at (a) 400^{o}C and (b) 600^{o}C for 2 hours is shown in Fig. 1. According to the JCPDS data, the xerogel calcined at 400^{o}C was found to be magnetite (Fe_3O_4) phase of iron oxide (JCPDS card no. 85-1436). The strong diffraction peaks of xerogel calcined at 600^{o}C were observed to be hematite (α- Fe_2O_3) phase of iron oxide (JCCPDS card no.72-0469).

- **Microstructural Properties: FESEM study**

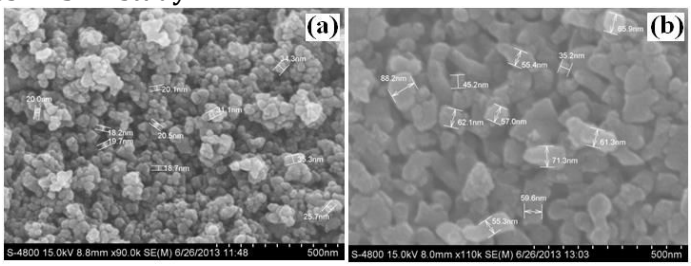

Fig. 2. FESEM images of (a) Fe_3O_4 and (b) α- Fe_2O_3 nanoparticles.

Fig. 2 shows field emission scanning electron microscopic (FESEM) images of (a) Fe_3O_4 and (b) α- Fe_2O_3 nanoparticles. From Fig. 2 (a) it is seen that the particles are nearly spherical in shape and average particles size is about 24nm. Fig. 2 (b) indicates wormlike morphology [L. Wan *et al.,* 2008] with increase in particle size. Due to increase in temperature the spherical particles may agglomerate and result in increase in particle size. The average particle size found to be 60nm. The scheme of change in morphology of iron oxide nanoparticles with temperature may be described as shown in is shown in Fig. 3. From FESEM study it is noted that the morphology of iron oxide nanoparticles can be tuned by tuning the calcination temperature.

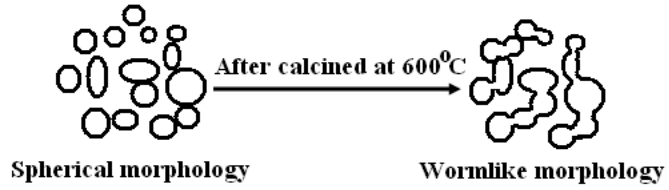

Fig. 3. Scheme of change in morphology of iron oxide nanoparticles with temperature

Phase transformation properties : TGA/DSC analysis

Thermal stability and phase transformation temperature of sol gel synthesized powder was studied using TGA/DSC technique. The TGA curve of the powder heated from 50 ^{o}C to 800 ^{o}C is shown in Fig. 4. During the temperature range of 50 ^{o}C to 800 ^{o}C, there is weight loss of only 2.4%. It means the iron oxide powder is thermally stable except change in phase at 542.72^{o}C. The DSC curve with endothermic peak at 87.26^{o}C between 50-120^{o}C may be ascribed to the removal of

physically adsorbed water molecules on the surface of magnetite (Fe_3O_4) nanoparticles [X.Q. Liu *et. al.,* 1997]. The two exothermic peaks on DSC curve at 165.40°C and 271.20°C corresponds to the recrystallization of magnetite (Fe_3O_4) nanoparticles.

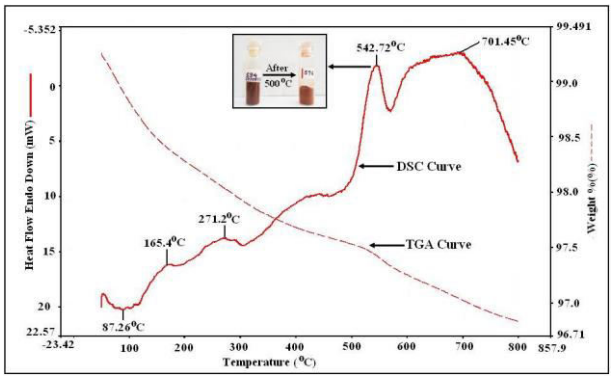

Fig. 4. TGA/DSC analysis of xerogel calcined at 400°C

The sharp exothermic peak at 542.72°C without corresponding weight loss attributed to the transformation of magnetite (Fe_3O_4) to hematite (α-Fe_2O_3) which was also confirmed by XRD study [R. M. Cornel *et. al.,* 2000]. The phase transformation of magnetite (Fe_3O_4) to hematite (α-Fe_2O_3) is also confirmed by color change observed from blackish brown to reddish brown [D. Maiti *et. al.,* 2013]. The exothermic peak at 701°C corresponds to the recrystallization of α-Fe_2O_3 nanoparticles.

Conclusions:

Sol gel method can be successfully used to synthesize magnetite phase of iron oxide nanocrystalline powder. Hematite phase of iron oxide may be obtained just by heating the magnetite powder above 542°C. The XRD study confirms the magnetite and hematite phases of iron oxide nanoparticles. TGA analysis showed that the obtained iron oxide nanoparticles are thermodynamically stable except the change in phase. The DSC curve of iron oxide nanoparticles indicated that the phase transformation of magnetite and hematite takes place at 542°C. FESEM analysis revealed that the calcination temperature changes the morphology and the size of nanoparticles associated in powder.

Acknowledgements:

Authors are thankful to RUSA (Rashtriya Uchchattar Shiksha Abhiyan) for finicial and all kind of support. The authors also would like to thank Head of Physics Department and Principal Pratap College Amalner, Dist: Jalgaon, Maharashtra for providing laboratory facilities.

References:

E. Eken, M. Ozenbas, Characterization of nanostructured magnetite thin films produced by sol–gel processing, J. Sol-Gel Sci. Technol. 50 (2009) 321-327.

R. M. Cornel, U. Schwertmann, The Iron Oxides: Structure, Properties, Reactions, Occurrences and Use, New York Weinheim, 1996.

A. K. Gupta, M. Gupta, Synthesis and surface engineering of iron oxide nanoparticles for biomedical applications, Biomaterials, 26 (2005) 3995–4021.

P. Sun, W. Wang, Y. Liu, Y. Sun, J. Ma, G. Lu, Hydrothermal synthesis of 3D urchin-like α-Fe_2O_3 nanostructure for gas sensor, Sens. Actuators B: Chem. 173 (2012) 52–57.

Y. Cao, H. Luo, D. Jia, Low-heating solid-state synthesis and excellent gas-sensing properties of α-Fe_2O_3 nanoparticles, Sens. Actuators B: Chem. 176 (2013) 618-624.

P. Zhang, Z. P. Guo, H. K. Liu, Submicron-sized cube-like α-Fe_2O_3 agglomerates as an anode material for Li-ion batteries, Electrochim. Acta 55 (2010) 8521-8526.

P. Xu, G. M. Zeng, D. L. Huang, C. L. Feng, S. Hu, M. H. Zhao et al., Use of iron oxide nanomaterials in wastewater treatment: A review, Sci. Total Environ. 4 24 (2012) 1-10.

H. Cui, Y. Liu, W. Ren, Structure switch between α-Fe_2O_3, γ-Fe_2O_3 and Fe_3O_4 during the large scale and low temperature sol–gel synthesis of nearly monodispersed iron oxide nanoparticles Adv. Powder Technol. 24 (2013) 93-97.

C. J. Brinker, G. W. Scherer, Sol–Gel Science-The Physics and Chemistry of Sol–Gel Processing, Boston: Academic Press: 1990.

L .Duraes, B. F. O. Costab, J. Vasquesa, J. Camposc, A. Portugala, Phase investigation of as-prepared iron oxide/hydroxide produced by sol–gel synthesis, Mater. Lett. 59 (2005) 859-863.

L. Wan, K. Shi, X. Tian, H. J. Fu, Facile synthesis of iron oxide with wormlike morphology and their application in water treatment, Solid State Chem. 181 (2008) 735-740.

X.Q. Liu , S.W. Tao, Y.S. Shen, Preparation and characterization of nanocrystalline α-Fe_2O_3 by a sol-gel process, Sens. Actuators B: Chem. 40 (1997) 161-165.

Content is available at: CRDEEP Journals
Journal homepage: http://www.crdeepjournal.org/category/journals/ijbas/

International Journal of Basic and Applied Sciences
(ISSN: 2277-1921) (Scientific Journal Impact Factor: 6.188)

UGC Approved-A Peer Reviewed Quarterly Journal

To Investigate Thermal and Mechanical Properties of Binary Epoxy Nanocomposites

Sandip.S. Nandre*[1], Atul.A. Patil[2], Umesh.B. Gawai,[3] Sandip R. Patil [4]
[1&3]Late Annasaheb R. D. Deore Arts & Sci. College Mhasadi,Tal.-Sakri, Dist. Dhule
[2] SSVPSs L. K. Dr. P. R. Ghogerey Science College, Dhule, Maharashtra
[4] MGSM's Dadasaheb Dr. S. G. Patil Arts and Sci. College Chopda, Dist. Jalgaon

Abstract
The preparation of epoxy nanocomposites Sodium Dodecyl Sulphate (DDS) intercalated magnesium aluminium layered double hydroxide (Mg Al SDS LDHs) were synthesized and used as additives. The properties of the additives and their epoxy nano-composites were characterized by X-ray diffractometer (XRD), SEM, UTM and TGA. The Mg-Al SDS LDH additions into the epoxy resin, which was shown by a constant improvement of the thermal properties of the nanocomposites as to relationship to virgin epoxy resin. Due to the presence of Mg-Al SDS LDH, the epoxy nano-composites developed a rigid and dense upper layer, with stable charring, which prevented the escape of the decomposed flammable volatiles and protected the lower layer of the nanocomposites from further decomposition. The mechanical strength of these composites was also assessed. The strength of the composites was found to increase linearly on increasing the Mg Al SDS LDHs content. An enhancement in the properties was observed after toughening the epoxy resin.

Keywords Sodium Dodecyl sulphate, X-ray diffractometer, Thermal and Mechanical Properties

Introduction

Epoxy matrix are one of the most fundamental types of thermosetting polymers resin and have broadly use as structural materials, structural adhesives, and matrix resins for fiber reinforced nanocomposites. They are easily breakable and have poor resistance to crack propagation. The toughness of bi-functional epoxy matrix such as DGEBA has been increased by blending with many type materials [1-4]. The investigated showed that the addition of nano fillers into the epoxy matrix can significantly progress the mechanical and thermal properties [5-6]. The reinforcement of epoxy polymer matrix by the inorganic nanofillers such as Titanium dioxide (TiO_2), Zinc Oxide (ZnO), nano-clay, carbon nano-tubes, Carbon blacks and Calcium Carbonate ($CaCO_3$) were attracted to many research scholar and scientists. The addition of nano fillers (particle size less than 100 nm) into the epoxy polymer matrix affects very much to the properties of nano-composites due to their larger surface area and the homogeneous dispersion within the macro molecules up to certain extent [7-8]. However, one of the basic problems associated with the nanofillers is the tendency to agglomerate during the mixing with the polymer resin matrix [9]. This shortfall can be bridged by prolong mechanical mixing and followed by ultra-sonication of the nanofiller/resin mixture [10].

Various literature survey focused on epoxy nanocomposites such as Ng et al. [11] developed epoxy nano-composites containing TiO_2 and result shows that the toughness of the nanocomposites is better than that traditional material filled epoxy composites. Wetzel et al. [12] introduced two nanofiller like $CaSiO_3$ and Al_2O_3 into epoxy resin matrix. They found nanoparticles can deviate and branch the crack front or even pin it, forcing a higher energy absorption in the composite when crack occurred. Chen *et al.* [13] reported the effect of $CaCO_3$ concentration on the mechanical properties of blocked polyurethane/epoxy interpenetrating polymer networks and they reported that mechanical properties like tensile strength, flexural strength, tensile modulus, and flexural modulus of IPNs improved with $CaCO_3$ concentration to a utmost value at 5, 10, 20, and 25 phr, respectively. Wang *et al.* [14] developed epoxy resin/$CaCO_3$ composites by the methods of extruding, solution, blending, as well as *in situ* and inclusion polymerization. In this paper study, the nanocomposites were prepared by mechanical mixing of epoxy resins and Sodium Dodecyl Sulphate. The effect of nano size of filler on the mechanical properties viz., tensile strength, elongation-at-break, impact strength and hardness were studied.

National Conference on «Modern Perspectives In Physical and Chemical Sciences » (MPPCS-2024) DOI: **10.13140/RG.2.2.13272.40962**

Materials and Methods

Materials:

Epoxy resin was commercially available and was used without any further purification (Pliogrip resin and Chemicals Pvt. Ltd, Dombivali, Mumbai, (India)). Grade PG-100; equivalent weight 182 eq/g; trade name: Resinova ; Viscosity: 9000-12000cps. The Mg-Al based Layered Double Hydroxides and Sodium dodecyl sulfate was obtain from Alderich Chemical Co.; Mumdai (India)

Preparation of the Layered Double Hydroxides Sodium Dodecyl Dulfate (LDH-SDS):

LDH was calcined in a muffle furnace at 440- 450^{0}C for about 6 hr to alter it into metal oxide. The calcined product (LDH) 38 g was dispersed in a 120 ml of aqueous solution containing Sodium dodecyl sulfate (LDH-SDS) and the dispersion was stirred by magnetic stirrer for 24 hr at room temperature at 25^{0}C. The regenerated SDS intercalated LDH (LDH-SDS) was filtered out followed by drying in oven at 100^{o}C.

Preparation of Epoxy Nanocomposites:

For Preparation of the Epoxy Mg-Al LDH-SDS Nanocomposites system, the stoichiometric amount of Epoxy resin (27 g) was taken in beaker and then different % of LDH-SDS (1.0 to 5.0% with respective to epoxy resin) were added into beaker and mechanically stirred at room temperature for 1.5 hrs at 300 rpm and mixed thoroughly. Subsequently after through mixing of epoxy resin and LDH- SDS a stoichiometric amount of the curing agent (9 g) was added in each system and then again mechanically stirred at room temperature for 15 min at 300 rpm. After through mixing of epoxy resin-LDH-SDS and curing agent, the viscous mixture was obtained, which were poured into flat aluminium foil mould and cured at room temperature for 24 hrs. Then sample plaque of cured product with different % LDH-SDS content were obtained and will keep as such for further characterization.

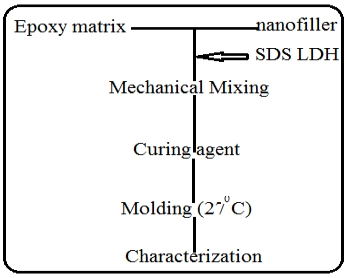

Figure 1. Schematic representation for preparation of epoxy nanocomposites.

Table No. 1 Preparation of (epoxy/SDS-LDH) nanocomposites.

Sample Code	Epoxy resin (g)	Curing Reagent(g)	Mg-Al SDS LDH (g)
SAP-0	27	9	-
SAP-1	27	9	0.27
SAP-2	27	9	0.54
SAP-3	27	9	0.83
SAP-4	27	9	1.08
SAP-5	27	9	1.35

Characterization of Nano Composites:

***X-ray diffraction (XRD)*:**

X-ray diffraction (XRD) pattern was recorded on a Shimadzu SD-D1 diffractometer with Cu target (λ =1.54 Å). The d spacing of the epoxy nanocomposites was analyzed by using Bragg's equation (nλ =2d sin θ).

***Mechanical Properties*:**

Determination of Tensile Strength, Elongation-at- break and elastic modulus:

The Dumb-bell shaped samples were prepared and was used for the determination of the tensile strength, elongation-at-break and elastic modulus. The samples were prepared in a self-designed teflon mould as per ASTM D638 standardization.

Thermogravimetric Analysis (TGA):

Thermo-gravimetric analysis (TGA) was carried out using a Shimadzu Thermogravimetric Analyzer (TGA-50, Japan), in the temperature range between room temperature and 800^{0}C at a heating rate of 10^{0}C per min in nitrogen atmosphere with a flow rate of 50 mL/min. TG traces were obtained by plotting per cent residual weight against temperature.

Morphological Properties:

The Scanning Electron Microscope (SEM) images of the fractured surface of samples were obtained by using high resolution and low vacuum SEM equipment (M/s FEI Company, USA; model: Quanta 200 FEG) to examine the microstructure and fractured surfaces of nano- composites. The samples were mounted on aluminium stubs using carbon tape. The samples were coated with a thin layer of platinum to prevent charging before the observation by SEM.

National Conference on «Modern Perspectives In Physical and Chemical Sciences » (MPPCS-2024) DOI: **10.13140/RG.2.2.13272.40962**

Results and Discussion

X-ray diffraction (XRD):

XRD is a powerful technique for detect the exfoliation of SDS-LDH structures. **Fig. 2** shows the XRD patterns of the SDS-LDH /epoxy composites for distinct SDS-LDH content and dispersion agent [15].

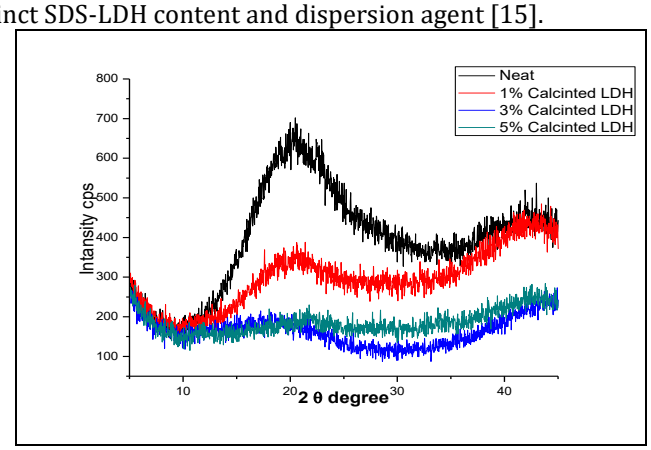

Figure 2: X-ray diffraction patterns of various epoxy nanocomposites

Characteristic maxima of SDS-LDH (2ϑ = 32° and 37°) are present in XRD spectra of all epoxy/SDS-LDH systems indicating successful incorporation of SDS-LDH into polymer matrix

(**Fig. 2**). On the other hand, the disappearance of maxima at 7°, 11°, 20° and 23°, which originate from the layered structure of the filler, indicate intercalation and possibly exfoliation of SDS-LDH to form the epoxy nanocomposites.

Studies on Mechanical Properties:

The results of tensile strength and elongation-at-break are summarized in the **Table 2** it is evidence from the results that the increase in loading of SDS-LDHs in epoxy matrix increased both the tensile strength and elongation-at-break.

Table 2: Experimental data sheet for mechanical properties of nano-composites

Sr. No	Sample Code	Tensile Strength in Kg/cm²	Elongation at break (%)
1	**SAP-0**	75.91	0.97
2	**SAP-1**	78.52	1.27
3	**SAP-2**	84.36	1.46
4	**SAP-3**	89.82	1.67
5	**SAP-4**	90.94	1.99
6	**SAP-5**	95.21	2.37

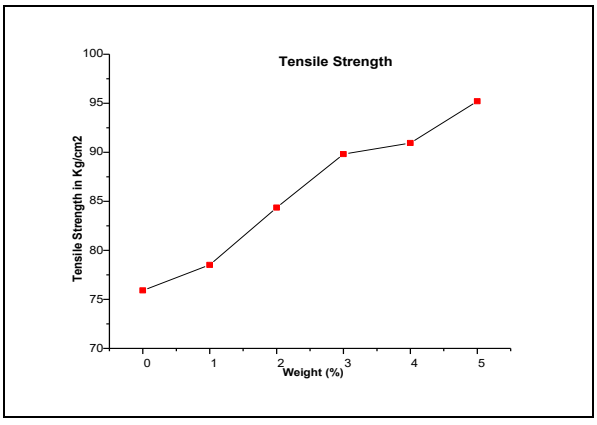

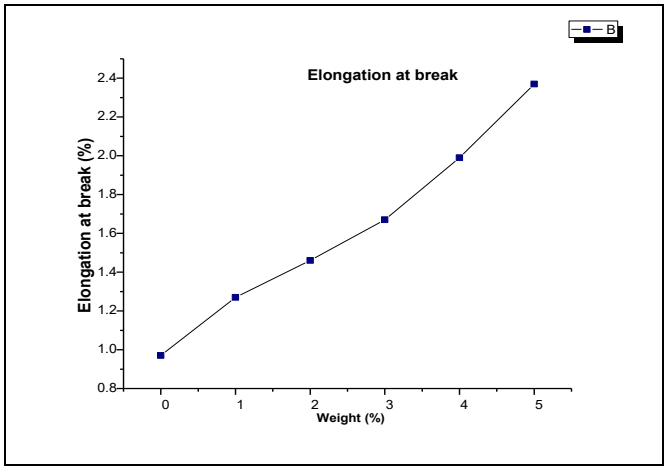

Figure 3[a-b]: Variation of tensile strength and elongation-at-break with percentage loading of SDS-LDHs in epoxy matrix.

The values of tensile strength and elongation-at-break was found to be greatest in 5 wt% **(SAP-5)** SDS-LDHs loaded nanocomposite sample. The enhance of tensile strength and elongation-at-break might be due to the filling of SDS-LDHs into the amorphous region of matrix via uniform scattering up to 5 wt% **(SAP-5)**[16,17]. When the amorphous region of epoxy polymer matrix had been completely filled by the nano particles, the sample achieved highest tensile strength due to the load shearing by SDS-LDHs. The nanocomposite samples also showed the toughening behavior on addition of nano-filler for same composition, which led to enhance the elongation-at-break values.

***Thermal stability*:**

The thermal stabilities of the Epoxy/SDS-LDH nanocomposites were studied by means of TGA. The TGA thermograms for the virgin epoxy resin and Epoxy/SDS LDH nanocomposites are shown in **Fig 4:**

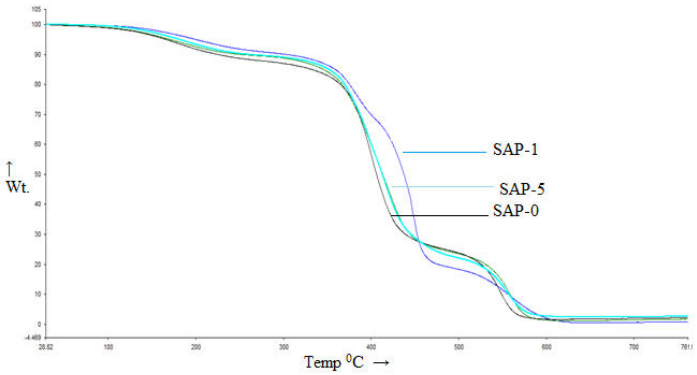

Figure 4: TGA thermograms of Epoxy/SDS-LDH nanocomposites as a function of SDS- LDH content.

The thermal stability of the nanocomposites was significantly enhanced by the addition of SDS-LDH. In the virgin epoxy system, the degradation started at around 290^{o}C. When SDS-LDH was added to the epoxy matrix, the IDT of the nanocomposites was at least 20^{o}C higher than that of the virgin epoxy system. The *T*max of the virgin epoxy system was 370^{o}C, whereas upon addition of SDS-LDH into the epoxy matrix, the *T*max of the nanocomposites appeared within the range of 400-410^{o}C. These results can be interpreted with reference to the addition of SDS-LDH to the epoxy polymeric matrix system [18,19], which increased the surface contact area between the SDS-LDH particles and the epoxy matrix, which in turn prevented the heat diffusion during decomposition of the Epoxy/SDS LDH nanocomposites. The results can be attributed also to the increased cross-linking density of the nanocomposites. The char content for the nanocomposites at 800^{o}C also was increased with the addition of SDS-LDH. A similar observation was reported by Chen *et al*. using rigid poly (vinyl chloride)/calcium carbonate nanocomposites.

Surface morphology of epoxy/SDS-LDHs nanocomposites was further studied by the SEM analysis (Figure 5). With smaller magnification (Figure 3a) it can be seen that SDS-LDHs is consistently dispersed within the epoxy matrix. Larger magnification confirms intercalation of epoxy matrix within layered structure of LDH-B, but no complete exfoliation in any of the nanocomposites [20,21]. Only nanocomposite with 5 % of nanofiller shows partial exfoliation.

Morphological Studies:

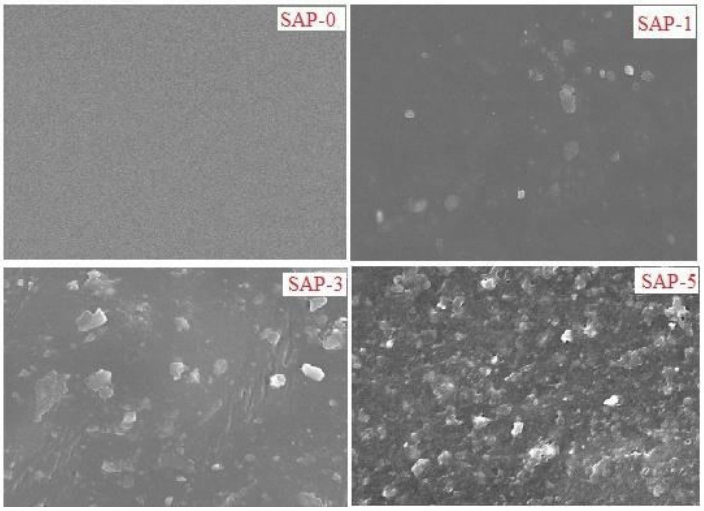

Figure 5: SEM image of samples SAP-0, EPC-1, SAP-3, and SAP-5 respectively.

Conclusion

The following conclusions can be drawn: -

1) As the concentration of Sodium Dodecyl Sulphate double hydroxide (Mg-Al SDS-LDHs) increased in the nanocomposite samples, the tensile strength, elongation-at-break, increased and found maximum in SAP-5 sample. The enhancement in the mechanical properties of nanocomposite samples were because load sharing by nano-particles, when subjected under load.

2) The high degree of intercalation of nano-particles was observed in SAP-5 sample than other nanocomposites, which showed the higher roughness and surface area to divert the crack initiation and propagation.

3) As the concentration of Sodium Dodecyl Sulphate Layered double hydroxides (Mg-Al SDS-LDHs) increased into the nanocomposite samples, the thermal properties also increase and found maximum in SAP-5 sample. The enhancement in the thermal properties of nanocomposite samples thus increasing the surface contact area between the SDS-LDHs particles and the epoxy matrix.

References

Harani, H., Fellahi, S. and Bakar, M. (1999). J. of App. Poly. Sci., 71: 29–38.

Mimura, K., Ito, H. and Fujioka, H. (2001). Polymer, 42: 9223–9233.

Mimura, K., Ito, H. and Fujioka, H. (2000). Polymer, 41: 4451–4459.

Wetzel, F., Haupert, M.Q. Zhang. (2003) Compos Sci Technol, 63: 2055

Quan, shi., Wang, Li., Haojie, Yu., Song, J., Dong, X. (2006) Macro Mater Eng, 291: 53-58.

He, H., Li, K.,Wang, J., Sun, G. (2001) Mater. And Desgn 32: 4521-4527.

Dihayati, Y., Aziz, A.R., Leong, Y. C., Harcharan, S. (2004) Um-repository proceeding, 629-01.

Zhang, K., Wang, L., Wang, F., Li, Z. (2004) J Appl Polym Sci 91: 2649-2652

Shao-Yun, Fu., Xi-Qiao, Feng., Lauke, B., Mai, Y. W. (2008) Compo Part B 39: 933- 961.

Harishanand, K. S., Nagabhushana, H., Nagabhushana, B. M., Muruli, M.S., Raghavendra, N., Vishnu Mahesh; K.R. (2013) Adv. Polym Sci and Tech.: An Inter J 3(1): 7-13.

Wetzel, F., Haupert, M.Q. Zhang. (2004) Compos Sci Technol, 63: 2055

Ng, C.B., Ash, B.J., Schadler, L.S., Siegel, R.W. (2001). Advanced Composites Letters, 12, 507.

Chen, C.H., Sun, Y.Y. (2006) J. Appl. Polym. Sci*., 99*, 1826.

Shi, Q., Wang, L., Yu, H., Jiang, S., Zhao, Z., Dong X. (2006). Macromol. Mater. Eng. 291(1), 53.

Jain, R., A. K. Narula, A. K., Choudhary, V. (2009) Journal of Applied Polymer Science, 114: 2161–2168.

Mishra, A., Shukla, M. K., Lodha, R (2016) International Journal of Innovative Research in Science, Engineering and Technology 5(7): 13678-13684

Rungruang, P., Grady, B. P., Supaphol, P. (2006) Colloids Surf A:Physicochem Eng Aspects 275: 114.

Jin, F. L., Park, S. J. J.(2006) Polym. Sci. Part B: Polym. Phys 44: 3348.

Jin, F. L.; Park, S. J. (2007) Polym. Degrad. Stab 92: 509.

Mu, Y.L., Yao, G.C., Liang, L. S., Luo, H.J., Zu, G.Y. (2010) Scripta Mater 63: 629–632.

Jiang, Z.Y., Zhang, H., Zhang, Z., Murayama, H., Okamoto, K. (2008) Compos Part A 39:1762–7.

National Conference on «Modern Perspectives In Physical and Chemical Sciences » (MPPCS-2024) DOI: **10.13140/RG.2.2.13272.40962**

Content is available at: CRDEEP Journals
Journal homepage: http://www.crdeepjournal.org/category/journals/ijbas/

International Journal of Basic and Applied Sciences
(ISSN: 2277-1921) (Scientific Journal Impact Factor: 6.188)

UGC Approved-A Peer Reviewed Quarterly Journal

Development and Validation of UV Spectrophotometric Method For the Simultaneous Estimation of Repaglinide and Metformin Hcl in Bulk Drugs and Pharmaceutical Dosage Form

Ashwini Dilip Patil, Hemangiv.Changare Dr. Sachin S. Rane, Dr. Rajesh Y. Chaudhari, Dr.Vijay R. Patil

TVES's Honorable Lokasevak Madhukarrao Chaudhari College of Pharmacy, Faizpur, Tal-Yawal, Dist- Jalgaon, Maharashtra, PIN-425503

Abstract:
A simple, robust, precise, UV spectroscopic method has been developed for the simultaneous estimation of Repaglinide and Metformin HCL sodium in bulk and tablet dosage forms. In this paper the estimation of those drugs was carried out by simultaneous equation method. This method is based on measurement of absorption at 281nm and 231 nm i.e, λmax of Repaglinide and Metformin HCL respectively. The linearity observed for Repaglinide is in the range of 2-10µg/ml and for Metformin is in the range of 10-50 µg/ml. The accuracy of methods was assessed by recovery studies and was found to be within the range of 99%-101% for both Repaglinide and Metformin HCl.The developed methods were validated with respect to linearity, accuracy (recovery), and precision. The method can be employed for estimation of pharmaceutical formulations with no interference from any other excipients and diluents. The results were validated as per ICH guidelines.

Keywords: Repaglinide and Metformin HCl, ICH, Validation, UV Visible Spectrophotometer etc.

Introduction

Metformin hcl and Repaglinide are given to diabetic patients suffering from high blood glucose levels. This combination is used to manage high blood sugar in diabetic individuals combined with a diet and exercise program .By promoting the release of your body's endogenous insulin, repaglinide works [15]. As a biguanide, metformin reduces the amount of sugar produced by your liver and absorbed by your stomach and intestines [14]. Both of these drugs work by assisting in the restoration of your body's appropriate reaction to the insulin you naturally make Blood sugar control can avoid kidney damage, blindness, nerve problems, limb loss,and problems with sexual function.[16] An innovative, cost-effective Spectrophotometric bioanalytical technique for measuring Metformin HCl and Repaglinide has been developed. The validation of bioanalytical methods used for the quantitative measurement of medicines and their metabolites in biological fluids. The study is important in the assessment and interpretation of data from bioavailability, bioequivalence, pharmacokinetic, and toxicokinetic studies [18]. The quantitative measurement of analytes in a specific biological matrix, such as blood, plasma, serum, or urine, is required for bioanalytical technique validation.

Diabetes mellitus a chronic diseases across the world is a key disease for the exploring the therapeutic value of the drug .The combined use of metformin and Repaglinide for type 2 diabetes mellitus was shown improved patient compliance by controlling the post prandial glucose levels and reaches normal glycemic levels[4]. Metformin Hydrochloride (MET) (Figure 1) is a biguanide class of antidiabetic drug; chemically is N, N-dimethylimidodicarbonimidicdiamide hydrochloride. It is an oralanti-antidiabetic drug from the biguanide class. It is the first-line drug for the treatment of type 2 diabetes, particularly in overweight and obese people and those with normal kidney function and evidence suggests it may be the best choice for people with heart failure. [6] It is also used in the treatment of polycystic ovary syndrome. Repaglinide (REPA) is the (Figure 1) Hypoglycaemic agents; Meglitinides, chemically it is (S)-2-Ethoxy-4-[2-[[methyl-1-[2-(1-piperidinyl)-phenyl] butyl] amino]-2-oxoethyl]-benzoic acid. For treatment of diabetes combinations with other hypoglycemic agents are commonly prescribed.In that 47.05% are two drug combination compares to single drug treatment (14.11%)[1]. There are various UV methods are available for estimation of this two drugs either individually or in combination with other drug and for both drug in combination two UV methods are available. Present work describes rapid, simple, sensitive,

accurate and reproducible spectrophotometric methods. [2] It improves control of glycemia primarily by inhibiting hepatic gluconeogenesis and glucogenolysis [1]Failure of monotherapy for treating type II diabetes mellitus leads to a switch to combination of various antidiabetic agents. Accordingly, the combined use of metformin andrepaglinide improved patient compliance through controlling the basal glycemia and post prandial levels.

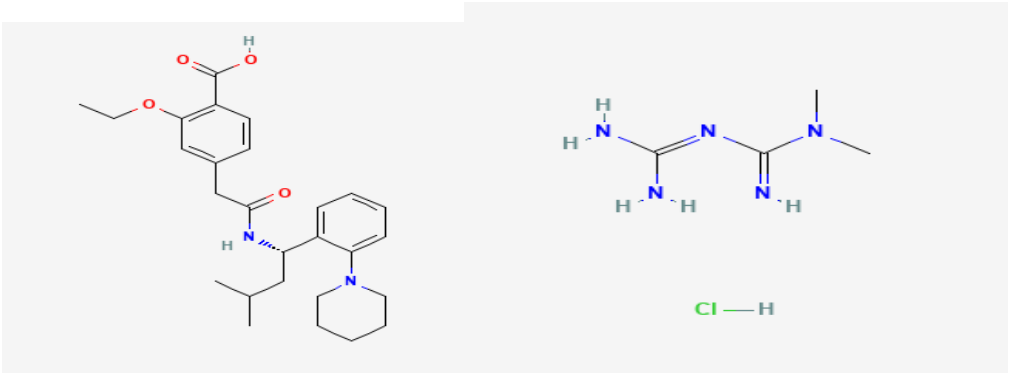

Chemical structure of repaglinide

chemical structure of metformin HCL

Materials and Methods

Instruments:

Shimadzu UV-1800 double beam spectrophotometer was used to record the spectra of sample and reference solutions using pair of quartz cells of 10 mm path length. All weighing was carried out on Sansui Vibra DJ-150S-S weighing balance. Sonicator of Fast Clean is used for the purpose of sonication , Filter papers of Sartorius Stedim Biotech of grade 292 are used for the filtration purpose.

Chemicals:

Repaglinide (1mg) and Metforminhcl (500mg) drugs were obtained as a gift sample fromAstrazeneca Pharmaceuticals India. The combined formulation EUREPA MF2 (2mg/500mg) ofthe two drugs purchased from Vikram Pharmacy Jalgaon. Analytical grade methanol purchased from Merck Chemicals Pvt. Ltd. Mumbai.

Preparation of stock solution and selection of wavelength:

Repaglinide stock solution

An accurately weighed quantity of repaglinide (1 mg) was taken in 10 mL volumetric flask and dissolved in methanol with the help of ultrasonication for about 10 min. Then the volume was made up to the mark using methanol to get repaglinide standard stock solution (100µg/mL).

Repaglinide working solution

Repaglinide standard stock solution (0.2 mL) was diluted to 10 mL using HPLC graded water to get working standard solution (2µg/mL)

Metformin HCL stock solution

An accurately weighed quantity ofMetformin HCL (10 mg) was taken in 10 mL volumetric flask and dissolved in methanol with the help of ultrasonication for about 10 min. Then the volume was made up to the mark using methanol to get Metformin HCL standard stock solution (1 mg/ mL).

Metformin HCL working solution

Metformin HCL standard stock solution (0.1 mL) was diluted to 10 mL using HPLC geated water to get working standard solution (10 µg /mL)

Determination of λ Max of Individual Component

An appropriate aliquot portion of Repaglinide (0.2 mL) and Metformin hcl (0.1 mL) were transferred to two separate 10 ml volumetric flasks, the volume was made up to the mark using HPLC graded waterto obtain Repaglinide (2 µg/mL) and Metformin hcl (10µg/mL) .Drug solutions were scanned separately between 200 nm to 400 nm Repaglinide shows the λmax at 281 nm while Metformin hcl shows λmax at 231 nm.

Overlay spectra ofRepaglinide and Metformin hcl

National Conference on «Modern Perspectives In Physical and Chemical Sciences » (MPPCS-2024) DOI: **10.13140/RG.2.2.13272.40962**

The overlay spectra of both drugs were recorded and two wavelengths 281 nm (λmax of Repaglinide) and 23nm(λmax of Metformin hcl) were selected for further study.

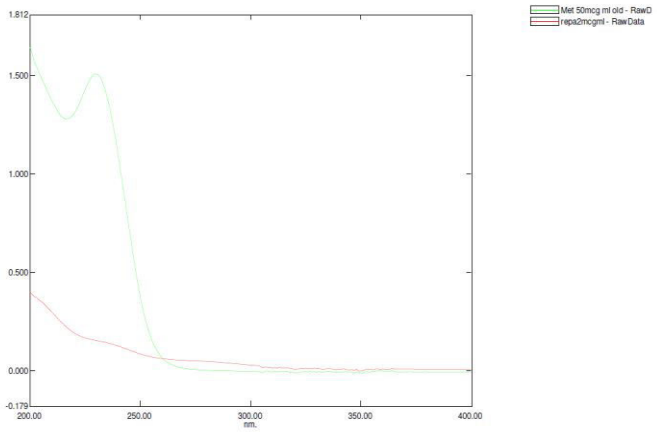

Graph No. 1 Overlay spectra of Repaglinide and Metformin hcl

Linearity study for Repaglinide

An accurately measured aliquot portion of working standard solution of Repaglinide was transferred to five separate 10 mL volumetric flasks. The volume was made up to the mark using HPLC graded waterto obtain concentrations of Repaglinide (2µg/ml, 4µg/ml, 6µg/ml ,8µg/ml,10µg/ml).Absorbance of these solutions was measured at 281 nm, Calibration curve was plotted, absorbanceVs concentration.

Linearity study for Metformin hcl

Accurately measured aliquot portions of working standard solution of Metformin hcl were transferred to five separate 10 mL volumetric flasks. The volume was made up to the mark using HPLC graded waterto obtain concentrations (10µg/ml, 20µg/ml, 30µg/ml, 40µg/ml, 50µg/ml) Absorbance of these solutions was measured at 231 nm. Calibration curve was plotted, absorbance Vs concentration. The results are shown in the Table No.1

Table No. 1 Regression and Optical characteristics of Repaglinide and Metformin HCL

Parameters	Value for repaglinide	Value for metformin
Beer's law limit (µg/ml)	2-10	10-50
Regression Coefficient(R2)	0.997	0.998
Regression equation	y = 0.0268x + -0.011	y = 0.035877x + 0.4827
Slope	0.0268	0.03587
Intercept	0.011	0.4827

The study of regression and optical characteristics of repaglinide and metformin are carried out in which Regression Coefficient (R2) of repaglinide is 0.997 and of metformin is 0.998.The slope of repaglinide 0.0268 and slope of metformin is 0.03587 with Intercept of repaglinide 0.011 and for metformin 0.4827.Therefore, Concentration vs Absorbance are fairly linear between both co-ordinates by statistical manner and obey ICH guidelines.

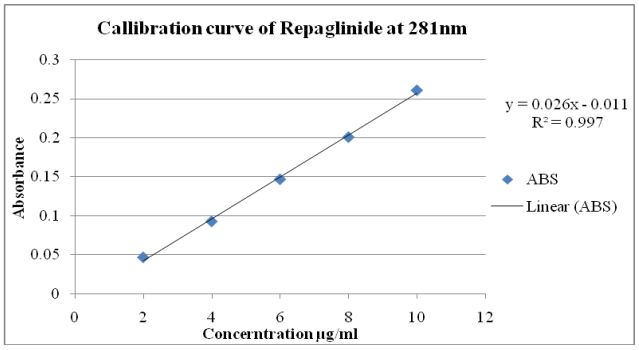

Graph No.2 Calibration curve of Repaglinide at 281nm

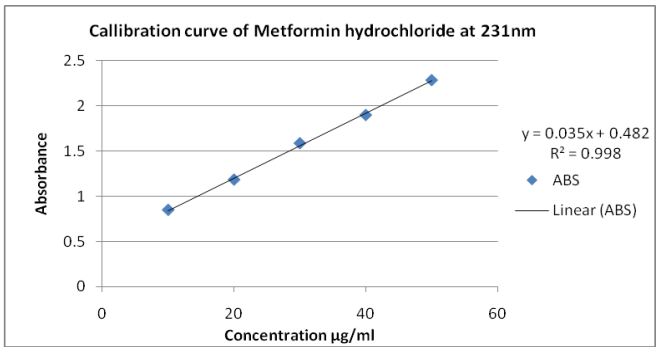

Graph No.2 Callibration curve of Metformin hydrochloride at 231nm

Estimation of Laboratory mixture by proposed method
Method: Simultaneous Estimation Method
If a drug sample contains two absorbing drugs (X and Y) each of which absorbs at the λmax of the other. Then, it may possible to estimate both drugs by this method. The scanning spectra of 2 µg/ml solution of repaglinide and 50µg/ml solution of Metformin hcl show clear peaks at 281 nm and 231nm respectively.
Amount of each drug was estimated using following equations

$$C_x = \frac{A_2 \times ay_1 - A_1 \times ay_2}{ax_2\, ay_1 - ax_1\, ay_2}$$

$$Cy = \frac{A_1 \times ax_2 - A2 \times ax_1}{ax_2\, ay_1 - ax_1\, ay_2}$$

Where;
A1 and A2 are the absorbance of diluted mixture at λ1 and λ2; Cx and Cy are the concentration of X and Y respectively ax1 and ax2 are absorptivities of X at λ1 and λ2 respectively; ay1 and ay2 are absorptivities of Y at λ1 and λ2 respectively.
The results are determined in the Table No. 2

Table No. 2. Results of Estimation of REPA and MET in standard laboratory mixture

Analyte	% Concentration estimated (Mean ± S.D)	% R.S.D
Repaglinide	99.5± 0.3055	0.3068
Metformin hcl	99.6 ± 0.2516	0.2525

The estimation of REPA and MET in Standard Laboratory Mixture are carried out in which % concentration of REPA and MET were found to be 99.5 and 99.6 respectively. Those values are fairly accurate by statistical manner and are as per ICH guidelines.

Application of proposed method for Estimation of drugs in tablets
EUREPA MF2 20 Tablets containing Repaglinide (2mg) and Metformin hcl(500 mg) were weighed and ground to fine powder. A quantity of sample equivalent to Repaglinide(2 mg) and Metformin (500 mg) was transferred into 100 mL volumetric flask containing methanol (60 mL), sonicated for 15 min and the volume was made up to the mark and filtered through Whatman filter paper (No. 45). This solution was (1 mL) transferred to 10 mL volumetric flaks, dissolved and volume was adjusted to the mark. The absorbances of the solutions were measured at 281 nm and 231 nm gainst blank. The concentrations of two drugs in sample were determined by using simultaneous equations. The results are shown in the Table No.3

Table No. 3 Results of Estimation of REPA and MET in tablets dosage form

Analyte	Label claim(mg/tab	% Label claim estimated(Mean±S.D)	% R.S.D
REPA	1	99.3 ± 0.264	0.2645
MET	500	99.6 ± 0.1527	0.1533

National Conference on «Modern Perspectives In Physical and Chemical Sciences » (MPPCS-2024) DOI: **10.13140/RG.2.2.13272.40962**

The results of Estimation of REPA and MET in tablets dosage shows the % purity 99.3 & 99.6 with SD and RSD bellow 2 which is fairly accurate by statistical manner and are as per ICH guidelines.

Validation of proposed method
The proposed method was validated as per ICH guidelines

Accuracy (Recovery study)
Accuracy of proposed method was ascertained on the basis of recovery study performed by standard addition method. A known amount of standard drug solutions were added to the tablet powder to make final concentrations in the range of 80%, 100% and 120% and re-analyzed it by the proposed method. The absorbance recorded and the % recoveries were calculated using formula

$$\% \text{ Recovery} = [A - B/ C] X 100$$

Where,
A = Total amount of drug estimated
B = Amount of drug found on preanalysed basis
C = Amount of Pure drug added

The results are shown in the Table No.4

Table No. 4 Recovery study

Drug in mixture solution (µg/ml)		% Recovery ± S.D.	
REPA	MET	REPA	MET
2	10	99.76 ± 0.1527	99.53 ±0.230
4	20	99.73 ± 0.208	99.53±0.251
6	30	99.71 ± 0.173	99.71 ± 0.154

The results of Recovery study of REPA and MET are found to be fairly accurate between 99.71% to 99.76 % for REPA 99.53% to 99.71 % for MET between various concentrations under observation by statistical way and are obey ICH guidelines.

Precision
Precision was determined as intra-day and inter-day variations. Intra-day precision was determined by analyzing Repaglinide (2,4 and 6 µg/mL) and Metformin hcl (10,20 and30 µg/mL) for three times on the same day. Inter-day precision was determined by analyzing the same concentration of solutions for three different days over a period of week. The results are shown in the Table No. 5.

Drug	Conc. [µg/mL]	Intra day Amount found		Inter day Amount found	
		Mean ± SD	% R.S.D.	Mean ± SD $[n = 5]$	% R.S.D.
REPA	2	1.97 ± 0.0208	1.0548	1.983 ± 0.0115	0.5822
	4	3.946 ±0.0351	0.889	3.95 ± 0.0529	1.339
	6	5.90±0.0503	0.852	5.946 ± 0.0585	0.985
MET	10	9.93 ± 0.015	0.153	9.93 ±0.025	0.253
	20	19.96 ±0.02	0.1002	19.93 ±0.037	0.189
	30	29.94 ± 0.045	0.153	29.91 ± 0.0152	0.0510

The Precision Study of REPA and MET were carried out and Results are found to be fairly accurate by statistical manner and obeys ICH guidelines.

Ruggedness
Ruggedness of the proposed method was determined by analysis of aliquots from homogenous slot by two different analyst using same operational and environmental conditions. The results are shown in Table No. 6.

National Conference on «Modern Perspectives In Physical and Chemical Sciences » (MPPCS-2024) DOI: **10.13140/RG.2.2.13272.40962**

Table No. 6 Ruggedness study

	Repaglinide 2 µg/ml		Metformin 50 µg/ml	
	Amount found in µg/ml Mean ± S.D. (n=3)	% R.S.D	Amount found in µg/ml Mean ± S.D. (n=3)	% R.S.D
Analyst I	1.95 ± 0.0529	2.713	49.94 ± 0.0378	0.0758
Analyst II	1.94 ± 0.0321	1.654	49.92 ± 0.0264	0.053
Day I	1.92 ± 0.404	2.097	49.94 ±0.0230	0.0462
Day II	1.96 ± 0.0264	1.349	49.93 ±0.0458	0.0917
Instrument I	1.91 ± 0.0416	2.175	49.96 ±0.0378	0.0757
Instrument II	1.94 ± 0.0378	1.944	49.93 ±0.0493	0.0987

The Ruggedness study of REPA and MET are carried out and results are found to be fairly accurate by statistical manner and obeys ICH guidelines

LOD: Limit of detection of Repaglinide and metformin hcl were found to be 0.54698 µg/ml and 1.87754 µg/ml respectively.

LOQ: Limit of Quantitation of Repaglinide and metformin hcl were found to be 1.65754 µg/ml and 6.25848 µg/ml respectively

Results and Discussion

A simultaneous UV Spectrophotometric Estimation method was developed for Repaglinide and metformin hcl .The method employs 281 nm as λ1 and 231 nm as λ2 for formation of equations. Repaglinide and metformin hcl obeys Beer's law in the concentration range 2-10 µg/ml (R2=0.997) and 10-50µg/ml (R2=0.998) respectively. The mean recovery for Repaglinide and metformin hcl was found to be 99.73% and 99.59 %respectively. The developed method were validated according to ICH guidelines and values of accuracy, precision and other statistical analysis were found to be in good accordance with the prescribed values

Conclusion

The proposed simultaneous UV Spectrophotometric Estimation method presented in this paper has advantages of simplicity, accuracy, precision and convenience for quantitation of Repaglinide and metformin hcl. The proposed method can be used for the quality control of Bilastine and Montelukast in typical laboratories.

Acknowledgement

Dr. Sachin S. Rane,Dr. Vijay R. Patil, Dr. Rajesh Y. Chaudhari,

Thank You for their valuable guidance providing the necessary resources and facilities to carried out this research and I am very Grateful to Everyone

References:

1. Neil J. O., The Merck index, 13th ed., pharmaceutical Press, London, UK; 2007 p. 5963,8220.
2. Hardman J.G., Limbard L.E., Goodman Gillman, "The pharmacological basis of therapeutics",11thed., Mc Graw Hill; 2005, pp.1704-1705.
3. M.D.Rockville, United States Pharmacopoeia; 25th (eds) United States Pharmacopoeial Convention Inc, 2002,2150
4. Serap Saglik Aslan et al. Derivative Spectrophotometric and Isocratic High Performance Liquid Chromatographic Methods for Simultaneous Determination of Repaglinide and Metformin Hydrochloride in Pharmaceutical Preparations. American Journal of Analytical Chemistry, 2017; 8:541-552
5. Manal M. Fouad et al. Development and Validation of Chromatographic and Spectroscopic Methods for Estimation of Repaglinide and Metformin HCl in Combined Dosage Form. Journal of Global Trends in Pharmaceutical Sciences, 2014; 5(3):844–1848
6. Boyles S., Popular Diabetes Drugs Tied to Heart Failure, Diabetes Health Center, WebMd Health News. December,2009 http://www.webmd.com/diabetes/news/20091204/metformin-vs-sulfonylureas-for
7. Nishith Patel et al. Development and Validation of UV Spectrophotometric Method for Simultaneous Estimation of Metformin HCL and Repaglinide in Bilayer Tablet. Journal of Pharmaceutical Science and Bioscientific Research, 2015; 5(1):104-109.
8. M. Dabrowski, P. Wahl, W. E. Holmes, and F. M. Ashcroft, *Diabetologia.*, **2001**, *44*, 747.
9. M. Salman S. J. Babu, P. C. Ray, S. Biswas, and N. Kumar, *Org. Proc. Res. Develop*., **2002**, *6(2)*, 184.
10. R. Landgraf, M. Frank, C. Bauer, and M. L. Dieken, *Int. J. Obesity*, **2000**, *24(suppl.3)*, S36.

11. Patel N et al. Development and Validation of UV Spectrophotometric Method for Simultaneous Estimation of Metformin HCL and Repaglinide in Bilayer Tablet. Journal of Pharmaceutical Science and Bioscientific Research, 2015; 5(1):104-109.
12. Sharma B. K, Instrumental Method of Chemical Analysis, 25th edition, Krishna Prakashan Media Ltd, Meerut, 2006. P. 183-184.
13. M. Niemi, P. J. Neuvonen, and K. T. Kivisto, *Clin. Pharmacol. Therapeutics*., **2001**, *70*, 58.
14. Domingues, D. S., Pinto, M. A., de Souza, I. D., Hallak, J.E., Crippa, J. A. and Queiroz, M. E. (2016). Determination of Drugs in Plasma Samples by High- Performance Liquid Chromatography-Tandem Mass Spectrometry for Therapeutic Drug Monitoring of Schizophrenic Patients. *J Anal Toxicol.*, *40*(1), 28-36.
15. Sharma, K., Pawar, G., Yadam, S., Giri S., Rajagopal S. and Mullangi R. (2013). LC-MS/MS-ESI method for simultaneous quantitation of metformin and repaglinidie in rat plasma and its application to pharmacokinetic study in rats. *Biomed Chromatogr*, *27*(3), 356-364.
16. Hiral, J., Varachhiya, Rohan, K. Barse, and Suresh, J. (2019). Development and Validation of Spectroscopic Simultaneous Equation Method for Simultaneous Estimation of Itopride Hydrochloride and Omeprazole in Synthetic Mixture. *Asian Journal of Pharmaceutical Research*, *9*(4), 238-242.
17. Mahrouse MA, Lamie NT. Experimental design methodology for optimization and robustness determination in ion pair RP-HPLC method development: Application for the simultaneous determination of metformin hydrochloride, alogliptin benzoate, and repaglinide in tablets. Microchem J. 2019;147:691-706
18. Shokouhi S, Sohrabi MR. Net analyte signal and radial basis function neural network for development spectrophotometry method for the simultaneous determination of metformin and sitagliptin in the anti-diabetic commercial tablet. Optik. 2021;243:167518
19. Godge RK, Shinde GS, Joshi S. Simultaneous estimation and validation of dapagliflozin and saxagliptin in bulk drug and dosage form by RP-HPLC. Res J Sci Technol. 2019;11(1):59-63.
20. Shah P, Pandya T, Gohel M, Thakkar V. Development and validation of HPLC method for simultaneous estimation of rifampicin and ofloxacin using experimental design. J Taibah Univ Sci. 2019;13(1):146-54.
21. A.H.Beckett, J.B.Stanlake Book of Pharmaceutical chemistry,Fourth edition.
22. .Mr.Gaikwad Utkarsh Ramesh,Miss.AkshadaNilkanthDombe, UV Theory , Principle, Instrumentation ,Application And Simultaneous Estimation Method Of Drug.©2023IJCRT | Volume 11, Issue 12 December 2023 | ISSN: 2320-2882.
23. Altinoz S. and Tekeli D. Analysis of Glimepiride by using derivative UV spectrophotometric method. J. Pharm .Biomed.Anal . 2001; 24 : 507-515.).

Book

1. H. Beckett, J. B. Sten Lake, Book of Practical Pharmaceutical Chemistry Fourth EditionPartTwo CBS Publication and Distributors, New Delhi 2005 ISBN: 8123905149 (284-286).

Content is available at: CRDEEP Journals
Journal homepage: http://www.crdeepjournal.org/category/journals/ijbas/

International Journal of Basic and Applied Sciences
(ISSN: 2277-1921) (Scientific Journal Impact Factor: 6.188)

UGC Approved-A Peer Reviewed Quarterly Journal

Developmentand Validation of Spectrophotometric Method for Simultaneous Estimation of Lobeglitazone Sulfate and Glimepiride in Bulk and Dosage Form

Patil Bhairav Girish, Ms. Jesika C. Rane, Dr. Sachin S. Rane
Honorable Lok sevak Madhukar Rao Chaudhari College of Pharmacy, Faizpur Dist.: Jalgaon.

Abstract
A simple, robust, precise, UV spectroscopic method has been developed for the simultaneous estimation of Lobeglitazone Sulfate and Glimepiride. In this paper the estimation of those drugs was carried out by simultaneous equation method. This method is based on measurement of absorption at 250 and 227 nm i.e., λ_{max} of Lobeglitazone Sulfate and Glimepiride respectively. The linearity observed for Lobeglitazone Sulfate is in the range of 10-50 µg/ml and for Glimepiride is in the range of 20-100 µg/ml. The mean recovery for Lobeglitazone Sulfate and Glimepiride was found to be 99.57 and 99.52 % respectively. The developed method validated with respect to linearity, accuracy (recovery), and precision and SD, %RSD was below two for all. The method can be employed for estimation of pharmaceutical formulations with no interference from any other excipients and diluents. The results were validated as per ICH guidelines.

Keywords: Lobeglitazone Sulfate, Glimepiride, ICH, Validation, UV etc.

Introduction

Lobeglitazone Sulphate (LBG) is a medication belonging to the thiazolidinedione class, serves as an antidiabetic agent[1-2]. Lobeglitazone Sulfate and Glimepiride combination the new drug combination used to cure diabetes.There are few methods published on HPLC[11-15] and UV[16-23] either in single or in combination with other drugs and no publications found on present combination, so it was thought worthwhile to research on same.

Itprimarily functions as an insulin sensitizer by binding and activating Peroxisome Proliferator-Activated Receptors (PPAR) gamma within fat cells[3]. By activating PPAR-gamma and promoting the binding of insulin at fat cells, Lobeglitazone thereby has been shown to reduce blood sugar levels, lower hemoglobin A1C (HbA1C) levels, and improve lipid and liver profiles. Unlike Pioglitazone, which is a dual PPAR agonist at PPAR-alpha and PPAR-gamma, Lobeglitazone is a pure PPAR-alpha agonist. Glimepiride is a member of the second-generation sulfonylurea (SU) drug class used for the management of type 2 diabetes mellitus (T2DM) to improve glycemic control. Type 2 diabetes is a metabolic disorder with increasing prevalences worldwide; it is characterized by insulin resistance in accordance with progressive β cell failure and long-term microvascular and macrovascular complications that lead to co-morbidities and mortalities.

Materials and Methods

Instruments

Shimadzu UV-1800 single beam spectrophotometer was used to record the spectra of sample and reference solutions using pair of quartz cells of 10 mm path length. All weighing was carried out on Sansui vibra DJ-150S-S weighing balance. Sonicator of fast clean is used for the purpose of sonication, Filter papers of Sartorius Stedim Biotech of grade 292 are used for the filtration purpose.

Chemicals

Lobeglitazone sulfate and Glimepiride pure drugs were obtained as a gift sample from Swiss Garnier Biotech Private Limited 21, Industrial area, Mehtapur Dist.: Una, Himachal Pradesh 174315.

Method

Preparation of stock solution and selection of wavelength

Lobeglitazone sulfate stock solution

National Conference on «Modern Perspectives In Physical and Chemical Sciences » (MPPCS-2024) DOI: **10.13140/RG.2.2.13272.40962**

An accurately weighed quantity of Lobeglitazone sulfate (10 mg) was taken in 10 mL volumetric flask and dissolved in methanol (8 mL) with the help of ultrasonication for about 10 min. Then the volume was made up to the mark using methanol to get Lobeglitazone Sulfate standard stock solution.

Lobeglitazone sulfate working solution
Lobeglitazone Sulfate standard stock solution was diluted to 10 mL using 70% v/v methanol to get working standard solution (100 µg / mL)

Glimepiride stock solution
An accurately weighed quantity of Glimepiride (10mg) was taken in 10 mL volumetric flask and dissolved in methanol (8 mL) with the help of ultrasonication for about 10 min. Then the volume was made up to the mark using methanol to get Glimepiride standard stock solution (1 mg / mL).

Glimepiride working solution
Glimepiride standard stock solution (5 mL) was diluted to 10 mL using 70% v/v methanol to get working standard solution (100 µg/mL)

Determination of λ Max of Individual Component
An appropriate aliquot portion of Lobeglitazone Sulfate and Glimepiride were transferred to two separate 10 mL volumetric flasks, the volume was made up to the mark using 70 %v/v methanol to obtain Lobeglitazone Sulfate and Glimepiride working standards. Drug solutions were scanned separately between 200 nm to 400 nm. Lobeglitazone Sulfate shows λ_{max} at 250 nm while Glimepiride shows λ_{max} at 227 nm.

Overlay spectra of Lobeglitazone Sulfate and Glimepiride
The overlay spectra of both drugs were recorded and two wavelengths (λ_{max} of Lobeglitazone Sulfate) and at 250 nm ($\lambda_{max}$of Glimepiride) were selected for further study and isobastic point at 227nm.

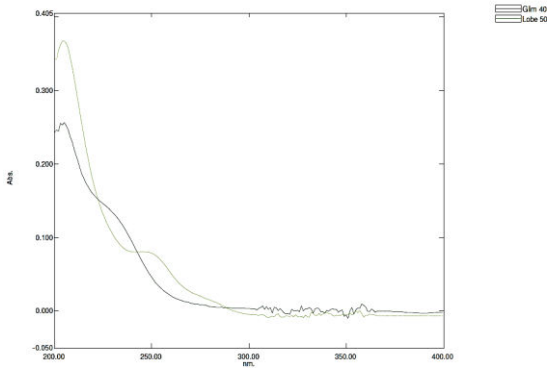

Graph No.1 Overlay Spectra of Lobeglitazone and Glimepiride

Linearity study for Lobeglitazone Sulfate
Accurately measured aliquot portions of working standard solution of Lobeglitazone were transferred to Four separate 10 mL volumetric flasks. The volume was made up to the mark using 70% v/v methanol to obtain concentrations (10µg/ml, 20µg/ml, 30µg/ml, 40µg/ml, 50µg/ml) absorbance of these solutions was measured at 250 nm. Calibration curve was plotted, absorbance vs concentration. The results are shown in the Table No.1

Linearity study for Glimepiride
An accurately measured aliquot portion of working standard solution of Glimepiride was transferred to Four separate 10 mL volumetric flasks. The volume was made up to the mark using 70% v/v methanol to obtain concentrations of Glimepiride (20µg/ml, 40µg/ml, 60µg/ml, 80µg/ml, 100 µg/ml). Absorbance of these solutions was measured at 227 nm, calibration curve was plotted, absorbance vs concentration.

Table No. 1 Regression and Optical characteristics of LOBE and GLIM

Parameters	Value for Lobeglitazone	Value for Glimepiride
Beer's law limit (µg/ml)	10-50 µg/ml	20-100 µg/ml
Regression Coefficient(R^2)	0.9992	0.9980
Regression equation	y= 0.0019x - 0.0158	y= 0.0047x - 0.0371
Slope	0.0019	0.0047
Intercept	0.0158	0.0371

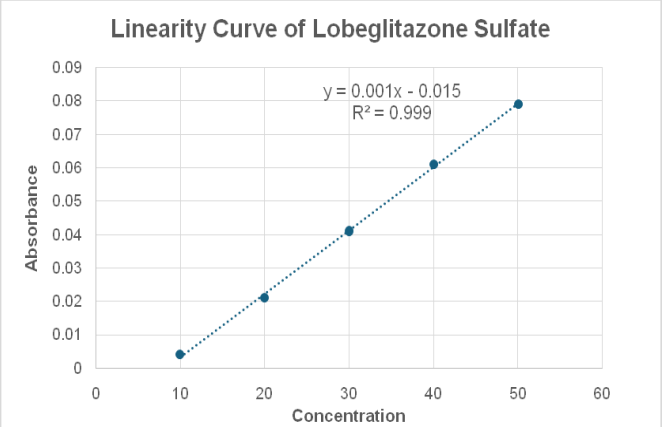

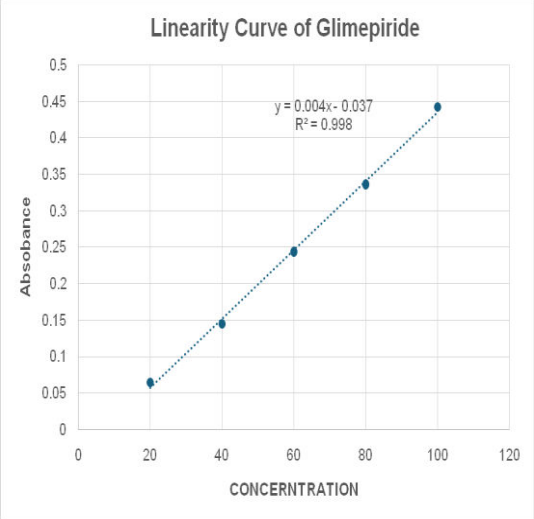

Simultaneous Estimation Method

If a drug sample contains two absorbing drugs (X and Y) each of which absorbs at the $\lambda_{max}$of the other. Then, it may possible to estimate both drugs by this method. The scanning spectra of 40µg/ml solution of Lobeglitazone Sulfate and 20µg/ml solution of Glimepiride show clear peaks at 250 nm and 227 nm respectively.

Amount of each drug was estimated using following equations,

$$C_{LOBE} = \frac{A_2 \times ay_1 - A_1 \times ay_2}{ax_2\, ay_1 - ax_1\, ay_2}$$

$$C_{GLIM} = \frac{A_1 \times ax_2 - A2 \times ax_1}{ax_2\, ay_1 - ax_1\, ay_2}$$

Where;

A1 and A2 are the absorbance of diluted mixture at λ_1 and λ_2

Cx and Cy are the concentration of X and Y respectively

ax1 and ax2 are absorptivity of X at λ_1 and λ_2 respectively

ay1 and ay2 are absorptivity of Y at λ_1 and λ_2 respectively.

The results are determined in the Table No. 2

Table No. 2. Results of Estimation of LOBE and GLIM in standard laboratory mixture

Analyte	% Concentration estimated (Mean ± S.D)	% R.S. D
Lobeglitazone Sulfate	99.93 ± 0.0642	0.0643
Glimepiride	99.91 ± 0.0305	0.0305

The estimation of LOBE and GLIM in Standard Laboratory Mixture are carried out in which % concentration of LOBE and GLIM were found to be 99.93 and 99.91 respectively. Those values are fairly accurate by statistical manner and are as per ICH[24] guidelines.

Application of proposed method for Estimation of drugs in tablets

National Conference on «Modern Perspectives In Physical and Chemical Sciences » (MPPCS-2024) DOI: **10.13140/RG.2.2.13272.40962**

Twenty 'LOBG G1' Tablets containing Lobeglitazone Sulfate (0.5mg) and Glimepiride (1mg) were weighed and ground to fine powder. A quantity of sample equivalent to Lobeglitazone Sulfate (0.5mg) and Glimepiride (10mg) was transferred into 100 mL volumetric flask containing methanol (70 mL), sonicated for 15 min and the volume was made up to the mark and filtered through Whatman filter paper (No. 45). This solution was (1 mL) transferred to 10 mL volumetric flaks, dissolved and volume was adjusted to the mark. The absorbances of the solutions were measured at 250 nm and 227 nm against blank. The concentrations of two drugs in sample were determined by using simultaneous equations. The results are shown in the Table No.3

Table No. 3 Results of Estimation of LOBE and GLIM in tablets dosage form.

Analyte	Label claim(mg/tab)	% Label claim estimated (Mean±S.D)	% R.S.D
Lobeglitazone Sulfate	0.5	99.66 ± 0.1106	0.1109
Glimepiride	1	99.57 ± 0.163	0.164

The results of Estimation of LOBE and GLIM in tablets dosage shows the % purity 99.66 & 99.57 with SD and RSD bellow 2 which is fairly accurate by statistical manner and are as per ICH guidelines.

Validation of proposed method

The proposed method was validated as per ICH guidelines Q2(R2)

Accuracy (Recovery study)

Accuracy of proposed method was ascertained on the basis of recovery study performed by standard addition method. A known amount of standard drug solutions was added to the tablet powder to make final concentrations in the range of 80%, 100% and 120% and re-analyzed it by the proposed method. The absorbance recorded and the % recoveries were calculated using formula.

% Recovery = [A - B/ C] X 100

Were,

A = Total amount of drug estimated
B = Amount of drug found on preanalyzed basis
C = Amount of Pure drug added

The results are shown in the Table No.4

Table No. 4 Recovery study

% Recovery ± S.D.	
Lobeglitazone Sulfate	Glimepiride
99.37 ± 0.586	99.75 ± 0.360
99.48± 0.466	99.90 ± 0.100
98.87 ± 0.383	98.91 ± 0.070

n=3

Precision

Precision was determined as intra-day and inter-day variations. Intra-day precision was determined by analyzing Lobeglitazone Sulfate (20, 30, and 40 µg/mL) and Glimepiride (40,60 and 80 µg/mL) for three times on the same day. Inter-day precision was determined by analyzing the same concentration of solutions for three different days over a period of week. The results are shown in the Table No. 5

Table No.5 Precision Study

Drug	**Conc. [µg/mL]**	**Intra-day Amount Found**		**Inter-day Amount Found**	
		Mean ± S.D [*n* = 3]	% R.S.D.	Mean ± S.D [*n* =3]	% R.S.D.
LOBE	20	19.78 ± 0.141	0.7131	19.82± 0.0208	0.1049
	30	29.57 ± 0.0173	0.0585	29.51 ± 0.0305	0.1035
	40	39.57 ± 0.0152	0.0386	39.46 ± 0.0528	0.0387
GLIM	40	39.59± 0.0153	0.0385	39.56 ± 0.0105	0.0265
	60	59.45± 0.030	0.0513	59.55 ± 0.0264	0.0444
	80	79.83 ± 0.0251	0.0315	79.80 ± 0.1135	0.1423

n=3

The Precision Study of LOBE and GLIM were carried out and Results are found to be fairly accurate by statistical manner and obeys ICH guidelines.

Ruggedness

Ruggedness of the proposed method was determined by analysis of aliquots from homogenous slot by two different analyst using same operational and environmental conditions. The results are shown in Table No. 6.

Table No.6 Ruggedness Study

	Lobeglitazone Sulfate 50 µg/ml		**Glimepiride 40 µg/ml**	
	Amount found in µg/ml Mean ± S.D. (n=3)	% R.S. D	Amount found in µg/ml Mean ± S.D. (n=3)	% R.S. D
Analyst I	49.93 ± 0.0252	0.0504	39.96 ± 0.0379	0.0947
Analyst II	49.85 ± 0.0351	0.0704	39.93 ± 0.0379	0.0948
Day I	49.90 ± 0.0208	0.0417	39.84 ± 0.0351	0.0881
Day II	49.84 ± 0.0603	0.1209	39.82 ± 0.0208	0.0522
Instrument I	49.82 ± 0.0503	0.1010	39.84 ± 0.0252	0.0631
Instrument II	49.85 ± 0.0361	0.0723	39.94 ± 0.0436	0.1091

n=3

LOD: Limit of detection of Lobeglitazone Sulfate and Glimepiride were found to be 0.2558µg/ml and 0.6899µg/ml respectively.

LOQ: Limit of Quantitation of Lobeglitazone Sulfate and Glimepiride were found to be 0.7751µg/ml and 2.0907µg/ml respectively.

Results and Discussion

A simultaneous UV Spectrophotometric Estimation method was developed for Lobeglitazone Sulfate and Glimepiride. The method employs 250 nm as λ1 and 227 nm as λ2 for formation of equations. Lobeglitazone Sulfate and Glimepiride obeys Beer's law in the concentration range 10-50 µg/ml (R^2=0.9992) and 20-100 µg/ml (R^2=0.9980) respectively. The mean recoveryforLobeglitazone Sulfate and Glimepiride was found to be 99.57 and 99.52 % respectively. The developed method was validated according to ICH guidelines and values of accuracy, precision and other statistical analysis were found to be in good accordance with the prescribed values.

Conclusion

The proposed simultaneous UV Spectrophotometric Estimation method presented in this paper has advantages of simplicity, accuracy, precision and convenience for quantitation of Lobeglitazone Sulfate and Glimepiride. The proposed method can be used for the quality control of Lobeglitazone Sulfate and Glimepiride in typical laboratories.

Acknowledgement

Dr. Vijay R. Patil, Dr. Rajesh Y. Chaudhari, Dr. Sachin S. Rane, Ms. Jesika. C. Rane.

Thank You for their valuable guidance providing the necessary resources and facilities to carried out this research and I am very Grateful to Everyone.

References

1. Dhara Patel, Jeel Dobariya, Prasanna Pradhan, Grishma Patel, Dhananjay Meshram, Development and Validation of UV Spectrophotometric methods for simultaneous estimation of Lobeglitazone Sulfate and Glimepiride in combined dosage form drug analytical research ISSN: 2527-2616.
2. Ashim Kumar Sen, Tantul Sarkar, Dhanya B. Sen, Rajesh A. Maheshwari, Aarti S. Zan war, Rajesh L. Dumpala. Quantitative determination of Lobeglitazone sulfate and glimepiride in combined tablet by robust high-performance thin layer chromatographic method. Analytical Science Journals. Published on May 2024. https://doi.org/10.1002/sscp.202400059.
3. https://pubchem.ncbi.nlm.nih.gov/compound/Lobeglitazone-sulfate#section=IUPAC-Name&fullscreen=trueGlimepiride: Uses, Interactions,Mechanismof Action//http://go drugbank.com/drugs/DB00222.
4. https://go.drugbank.com/drugs/DB09198
5. Ozadheoghene E. Afieroho Ogbonna Okorie Tochukwu J.N. Okonkwo. An Ultraviolet-Spectrophotometric Method for the Determination of Glimepiride in Solid Dosage Forms. Publication date: 2011-04-13.
6. Saradh Kumar Mudaliar, Sanjay Sharma. Quantification of Lobeglitazone Sulfate in Bulk and Tablet Dosage Form by a Validated UV Spectroscopy Method: A New Thiazolidinedione Anti-Diabetic Drug. Jul 8, 2024.
7. Khaldoon S, Alhadad HNK, and Salman AL, "Development of an RP-HPLC Method to estimation Glimepiride in Bulk and Solid Dosage Form." J Pop Ther Clin Pharmocol. 2023.
8. Kim MK. Cardiovascular safety of Lobeglitazone, a novel thiazolidinedione, in patients with type 2 diabetes mellitus.

9. Diabetes Metab J 2018; 45:363-72. Dr. Mukesh S. Patil, Liquid Chromatographic – Estimation of Lobeglitazone Sulphate in Bulk and Marketed Formulation, African Journal of Biological Science, Afr.J.Bio.Sc. 6(14) (2024).
10. Hanefeld M, Pfutzner A, Forst T, Lubben G. Glycemic control and treatment failure with pioglitazone versus glibenclamide in type 2 diabetes mellitus: a 42-month, open-label, observational, primary care study. Curr Med Res Opin 2006; 22:1211-5.
11. Kim KM, Jin HJ, Lee SY, Maeng HJ, Lee GY, Oh TJ, et al. Effects of Lobeglitazone, a new thiazolidinedione, on osteoblast genesis and bone mineral density in mice. Endocrinol Metab (Seoul) 2017; 32:389-95.
12. Kalepu Eswar Krishna Sai, Medidi Srinivas, Bula Udaya Kumari, Chepyala Sumalatha, Arram Madhavi, Development and Validation of an HPLC Method for the Determination of Lobeglitazone in Bulk and in Tablet Formulation. Int. J. Pharm. Investigation, 2024; 14(1):204-211. https://www.jpionline.org.
13. Kande T, Barge V, Bhosale A, and Khatal S, "Development and validation of analytical methods for simultaneous estimation of Pioglitazone and Glimepiride in bulk and pharmaceutical dosage form by using RP-HPLC method" Int. J. Curr. Adv. Res. 2019, 8, 20124-20129.
14. D. Jain, S. Jain, D. Jain, Simultaneous estimation of metformin hydrochloride, pioglitazone HCl, and glimepiride by RP-HPLC in tablet formulation, J. Chromatography. Sci. 46(2008)501–504.
15. D.C. Prem, Anand, K.L. Senthilkumar, B. Senthilkumar, Anew RP-HPLC method development and validation for simultaneous estimation of telmisartan and pioglitazone in pharmaceutical dosage form, Int. J. Chem. Tech Res. 3(2009)448–454.
16. Mehta RS, Patel DM, Bhatt KK, Shankar MB, et al., UV and Visible Spectrophotometric analysis of Pioglitazone Hydrochloride in Bulk and Tablets. Ind J Pharm Sci 2005; 67(4):487-489.
17. Anju Goyal, Singhvi I, Simultaneous spectrophotometric estimation of rosiglitazone maleate and glimepiride in tablet dosage form, Ind J Pharm Sci, 69, 2007, 780-83.
18. Madhusudhanareddy Induri, Development and Validation of a Spectrophotometric Method for Quantification and Dissolution Studies of Glimepiride in Tablets.First published: 20 September 2011 https://doi.org/10.1155/2012/856130.
19. A. H. Beckett, J. B. Stan Lake, Book of Pharmaceutical Chemistry Fourth Edition.
20. Mr. Gaikwad Utkarsh Ramesh, Miss. Akshada NilkanthDombe, UV Theory, Principle, Instrumentation, Application and Simultaneous Estimation Method of Drug. ©2023IJCRT | Volume 11, Issue 12 December 2023 | ISSN: 2320-2882.
21. Altinoz S. and Tekeli D. Analysis of Glimepiride by using derivative UV spectrophotometric method. J. Pharm. Biomed. Anal. 2001; 24: 507-515.
22. https://www.ema.europa.eu/en/ich-q2r2-validation-analytical-procedures-scientific-guideline.
23. Larisa Alagić-Džambić, UV VIS method of estimation for Glimepiride in Tablets Chemistry Research Journal, 2023, 8(6):1-4.
24. ICH Q2R1 and Q2R2. Validation of Analytical Procedures. Text and methodology.

Books

1.A. H. Beckett, J. B. Sten Lake, Book of Practical Pharmaceutical Chemistry Fourth EditionPartTwo CBS Publication and Distributors, New Delhi 2005 ISBN: 8123905149 (284-286).

National Conference on «Modern Perspectives In Physical and Chemical Sciences » (MPPCS-2024) DOI: **10.13140/RG.2.2.13272.40962**

Content is available at: CRDEEP Journals
Journal homepage: http://www.crdeepjournal.org/category/journals/ijbas/

International Journal of Basic and Applied Sciences
(ISSN: 2277-1921) (Scientific Journal Impact Factor: 6.188)

UGC Approved-A Peer Reviewed Quarterly Journal

Synthesis, Structural and Morphological Analysis of Co-doped ZnO Nanoparticles for Enhanced Functional Properties

M. R. Thokare[1], R. D. Khalapure[2], K. A. Takle[3], S. U. Shinde*[2]

1 JES College Jalna.
2 L. B. S. Sr College, Partur
3 JES College Jalna.
4 Pratishtan Mahavidhyalaya, Paithan

Abstract
This study presents the synthesis and characterization of ZnO and Co-doped ZnO nanoparticles prepared via the sol-gel method. X-ray diffraction (XRD) confirmed the hexagonal wurtzite structure of ZnO, with slight lattice distortions observed upon cobalt doping. Fourier-transform infrared (FTIR) spectroscopy revealed characteristic Zn-O vibrational modes and surface hydroxyl groups, with shifts indicating successful Co incorporation. Scanning electron microscopy (SEM) showed uniform spherical morphology, with a slight increase in particle size and agglomeration due to doping. The results highlight the structural and morphological changes introduced by cobalt doping and their potential impact on functional performance.

Keywords: ZnO, Co doping, XRD,FT-IR, SEM

Introduction

Zinc oxide (ZnO) is a versatile material belonging to the class of II-VI semiconductors, known for its wide bandgap (3.37 eV) and high exciton binding energy of 60 meV at room temperature. These properties make ZnO a popular choice for applications such as photocatalysis, gas sensing, UV detectors, transparent electrodes, and optoelectronic devices like light-emitting diodes and laser diodes [1, 2]. In addition to its optical and electrical characteristics, ZnO also exhibits excellent thermal and chemical stability, making it suitable for use in harsh environments [3].Despite its exceptional properties, ZnO has some limitations, such as a large bandgap and rapid recombination of photogenerated charge carriers, which restrict its efficiency in applications like photocatalysis and gas sensing. Transition metal doping has emerged as an effective way to address these limitations by introducing localized electronic states within the bandgap, altering the electronic structure, and improving charge carrier dynamics [4]. Among transition metals, cobalt (Co) is particularly effective as a dopant, as it modifies ZnO's structural and optical properties while also imparting magnetic behavior, which can expand its range of applications [5, 6].

Cobalt-doped ZnO (Co:ZnO) nanoparticles are of interest because of the changes Co ions introduce into the ZnO lattice. The substitution of Zn ions with Co ions creates localized energy states and alters the material's optical absorption and magnetic properties. These changes can improve photocatalytic performance by reducing the bandgap, enabling visible-light-driven photocatalysis [7]. Co doping can also enhance gas sensing performance by forming defect states that improve adsorption and reaction processes [8]. Additionally, Co doping can induce room-temperature ferromagnetism in ZnO, making it a potential candidate for spintronic devices [9].Various methods, including sol-gel, co-precipitation, hydrothermal, and chemical vapor deposition, have been used to synthesize Co-doped ZnO nanoparticles. Among these, the sol-gel method is widely preferred for its simplicity, cost-effectiveness, and ability to produce uniform and highly crystalline nanoparticles [10]. Characterization techniques such as X-ray diffraction (XRD), Fourier-transform infrared (FTIR) spectroscopy, scanning electron microscopy (SEM), and UV-Vis spectroscopy provide valuable insights into their structural, morphological, and optical properties. These studies are essential for understanding how synthesis parameters and doping affect material properties, enabling the optimization of their performance for specific applications.

In this study, Co-doped ZnO nanoparticles were synthesized using the sol-gel method. Structural properties were analyzed using XRD to confirm the crystalline phase and the effects of doping. FTIR spectroscopy was employed to investigate

chemical bonding and functional groups, while SEM provided insights into the surface morphology of the nanoparticles. The findings demonstrate the impact of Co doping on the structural, morphological, and optical behavior of ZnO nanoparticles, highlighting their potential for applications in photocatalysis, gas sensing, and spintronics.

Experimental

The synthesis of ZnO and Co-doped ZnO nanoparticles was carried out using the sol-gel method. For pure ZnO, zinc acetate dihydrate (Zn(CH3COO)2·2H2O was used as the precursor. It was dissolved in ethanol under constant stirring until a clear solution was obtained. Citric acid was added in a 1:3 molar ratio (metal ions to citric acid) as a stabilizing agent. The solution was stirred for 2 hours at room temperature and then heated to 80°C to form a viscous gel. This gel was dried in an oven at 120°C for 12 hours to obtain a dry precursor powder, which was finally calcined at 500°C for 4 hours to produce pure ZnO nanoparticles. For Co-doped ZnO, cobalt nitrate hexahydrate (Co(NO3)2·6H2O was used as the cobalt source along with zinc acetate. Both precursors were dissolved together in ethanol with the same process as ZnO synthesis. Citric acid was added in the same 1:3 molar ratio to stabilize the solution. The mixture was stirred, heated to form a gel, dried, and calcined under the same conditions as pure ZnO. The doping of Co into the ZnO lattice was achieved during this process, resulting in Co-doped ZnO nanoparticles.

Results and discussion

XRD Analysis

The X-ray diffraction (XRD) patterns of pure ZnO and Co-doped ZnO nanoparticles are presented in the figure. Both patterns exhibit well-defined peaks corresponding to the hexagonal wurtzite structure of ZnO (JCPDS Card No. 36-1451). The prominent diffraction peaks observed at 2θ values of approximately 31.8°, 34.4°, 36.3°, 47.6°, 56.7°, 62.9°, and 67.9° are indexed to the (100), (002), (101), (102), (110), (103), and (112) planes, respectively, confirming the crystalline nature of ZnO.

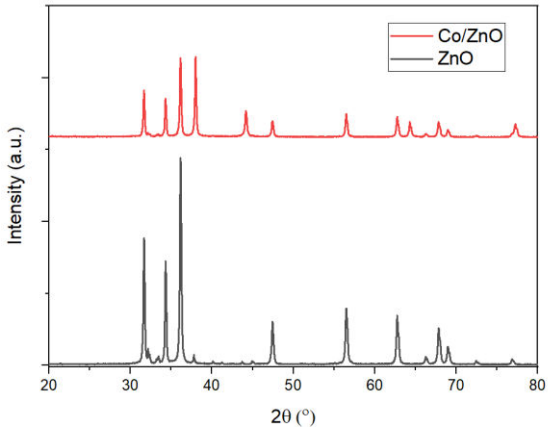

Fig. 1 . XRD pattern of ZnO &Co-doped ZnO

In the case of Co-doped ZnO, the XRD peaks remain sharp and match the wurtzite ZnO structure, indicating that the Co ions successfully substitute Zn ions in the lattice without altering the crystal structure. However, a slight shift in the peak positions can be observed, which is attributed to the incorporation of Co ions into the ZnO lattice. This shift arises due to the difference in ionic radii of Zn^{2+} (0.74 Å) and Co^{2+} (0.79 Å), causing lattice distortion.The crystallite size of the nanoparticles was calculated using the Debye-Scherrer formula:

$$D=K\lambda/\beta\cos\theta$$

where D is the crystallite size, K is the shape factor (taken as 0.9), λ is the X-ray wavelength (1.5406 Å), β is the full-width at half-maximum (FWHM) of the peak in radians, and θis the Bragg angle.The calculated crystallite size for pure ZnO is smaller than that of Co-doped ZnO, suggesting that Co doping leads to slight growth in crystallite size due to the incorporation of Co ions into the ZnO lattice. No secondary phases or impurity peaks related to cobalt oxides were observed, confirming the successful doping of Co into the ZnO matrix. The XRD analysis demonstrates that Co doping does not alter the wurtzite crystal structure of ZnO but induces slight lattice distortions, as evident from the peak shifts. This confirms the substitutional incorporation of Co ions into the ZnO lattice, which is crucial for tailoring the material's structural and functional properties.

FTIR Analysis

The FTIR spectra of pure ZnO and Co-doped ZnO nanoparticles provide insights into their structural and chemical properties. A broad band in the range of 3740–3850 cm^{-1} corresponds to the O-H stretching vibrations of surface hydroxyl groups and adsorbed water molecules. These bands are more intense in Co-doped ZnO, indicating higher surface activity or defect density due to cobalt incorporation. Peaks in the range of 2312–2388 cm^{-1} are attributed to the stretching vibrations of carbon-hydrogen (C-H) bonds, likely originating from residual organic compounds used during the synthesis process.

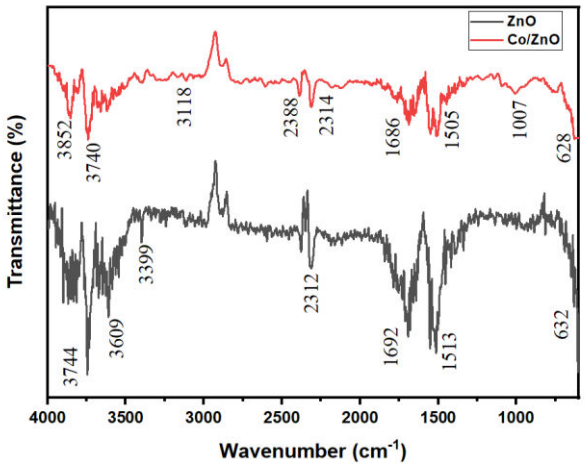

Figure 2. FTIR spectra for ZnO and Co/ZnO

A strong absorption band around 628–632 cm^{-1} is assigned to Zn-O stretching vibrations, confirming the formation of the ZnO crystal lattice. In the Co-doped ZnO sample, a slight shift in this peak indicates lattice distortions caused by the replacement of zinc ions with cobalt ions. Additionally, the peak near 1686 cm^{-1} is associated with the bending vibrations of water molecules, while peaks around 1505–1513 cm^{-1} are related to organic residues or adsorbed water.The observed shifts in peak positions and variations in intensities in the Co-doped ZnO spectrum confirm the successful doping of cobalt into the ZnO lattice. This doping introduces structural modifications, which are consistent with changes observed in other characterization techniques. The FTIR results validate the formation of ZnO and Co-doped ZnO nanoparticles with modified structural and surface properties.

SEM Analysis

The scanning electron microscopy (SEM) analysis of pure ZnO and Co-doped ZnO nanoparticles provides valuable insights into their surface morphology and particle distribution. The SEM images of pure ZnO nanoparticles reveal a uniform and nearly spherical morphology with slight agglomeration, which is typical for nanoparticles synthesized using the sol-gel method. The particles exhibit a smooth surface and are relatively well-dispersed, indicating efficient synthesis and minimal surface defects.

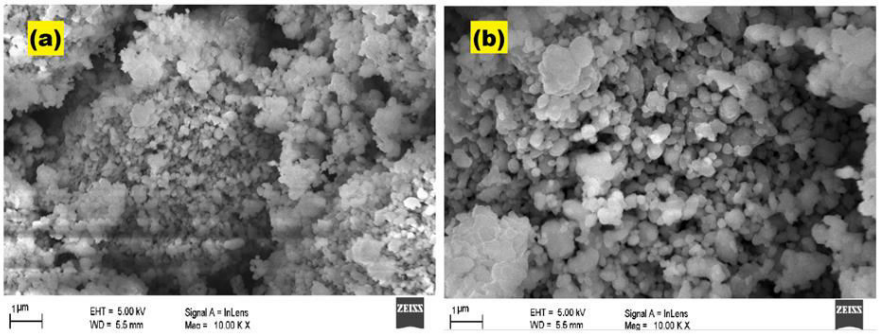

Figure 3: SEM Micrographs of (a)Pure ZnO and (b)Co-Doped ZnO Nanoparticles.

In the case of Co-doped ZnO, the morphology remains similar to that of pure ZnO, with spherical or near-spherical particles. However, slight changes in surface texture and particle size are observed, which can be attributed to the incorporation of Co ions into the ZnO lattice. The Co doping appears to induce a mild increase in particle size, which is consistent with the lattice distortions and structural modifications observed in XRD and FTIR analyses. Additionally, the Co-doped ZnO nanoparticles exhibit slightly higher agglomeration, possibly due to increased magnetic interactions or surface energy introduced by cobalt doping.

Overall, the SEM analysis confirms the successful formation of ZnO and Co-doped ZnO nanoparticles with a relatively uniform morphology. The slight changes in particle size and agglomeration in the Co-doped sample further validate the structural modifications introduced by cobalt doping. These morphological characteristics play a critical role in influencing the optical, magnetic, and photocatalytic properties of the synthesized nanoparticles.

Conclusion

The study successfully synthesized ZnO and Co-doped ZnO nanoparticles using the sol-gel method. XRD analysis confirmed the hexagonal wurtzite structure, with slight shifts in peak positions due to cobalt doping, indicating lattice distortions. FTIR spectroscopy validated the presence of Zn-O bonds and surface hydroxyl groups, while SEM revealed

uniform spherical morphology with a slight increase in particle size and agglomeration in the Co-doped samples. The structural and morphological modifications introduced by cobalt doping enhance the functional properties of ZnO nanoparticles, making them promising candidates for advanced technological applications.

References

[1] Etacheri, V., Roshan, R., & Kumar, V. "The effect of Mg-doping on the photocatalytic activities of ZnO under sunlight irradiation." *ACS Applied Materials & Interfaces*, 2012.
[2] Nair, M. G., Nirmala, M., Rekha, K., & Anukaliani, A. "Structural, optical, photocatalytic, and antibacterial activity of ZnO and Co-doped ZnO nanoparticles." *Materials Letters*, 2011.
[3] Singhal, S., Kaur, J., Namgyal, T., & Sharma, R. "Cu-doped ZnO nanoparticles: synthesis, structural and electrical properties." *Physica B: Condensed Matter*, 2012.
[4] Djerdj, I., Jagličić, Z., Arčon, D., & Niederberger, M. "Co-doped ZnO nanoparticles: minireview." *Nanoscale*, 2010.
[5] Bharat, T. C., Mondal, S., Gupta, H. S., Singh, P. K., & Others. "Synthesis of doped zinc oxide nanoparticles: a review." *Materials Today: Proceedings*, 2019.
[6] Guo, B. L., Han, P., Guo, L. C., Cao, Y. Q., & Li, A. D. "The antibacterial activity of Ta-doped ZnO nanoparticles." *Nanoscale Research Letters*, 2015.
[7] Singh, P., Kumar, R., & Singh, R. K. "Progress on transition metal-doped ZnO nanoparticles and its application." *Industrial & Engineering Chemistry Research*, 2019.
[8] Luo, J., Liang, J. K., Liu, Q. L., Liu, F. S., & Zhang, Y. "Structure and magnetic properties of Mn-doped ZnO nanoparticles." *Journal of Applied Physics*, 2005.
[9] Cimitan, S., Albonetti, S., Forni, L., & Peri, F. "Solvothermal synthesis and properties control of doped ZnO nanoparticles." *Journal of Colloid and Interface Science*, 2009.
[10] Kılınç, N., Arda, L., & Öztürk, S. "Structure and electrical properties of Mg-doped ZnO nanoparticles." *Crystal Research and Technology*, 2010.
[11] Djaja, N. F., & Saleh, R. "Characteristics and photocatalytic activities of Ce-doped ZnO nanoparticles." *Materials Sciences and Applications*, 2013.
[12] Dole, B. N., Mote, V. D., Huse, V. R., & Purushotham, Y. "Structural studies of Mn-doped ZnO nanoparticles." *Current Applied Physics*, 2011.
[13] Sathya, M., & Pushpanathan, K. "Synthesis and optical properties of Pb-doped ZnO nanoparticles." *Applied Surface Science*, 2018.
[14] Kumari, R., Sahai, A., & Goswami, N. "Effect of nitrogen doping on structural and optical properties of ZnO nanoparticles." *Progress in Natural Science: Materials International*, 2015.
[15] Abdollahi, Y., Abdullah, A. H., & Zainal, Z. "Synthesis and characterization of manganese-doped ZnO nanoparticles." *International Journal of Photochemistry and Photobiology*, 2011.
[16] Saleh, R., & Djaja, N. F. "Transition-metal-doped ZnO nanoparticles: synthesis, characterization and photocatalytic activity under UV light." *Spectrochimica Acta Part A: Molecular and Biomolecular Spectroscopy*, 2014.
[17] Rana, S. B., Singh, P., & Sharma, A. K. "Synthesis and characterization of pure and doped ZnO nanoparticles." *Journal of Materials Science and Engineering*, 2010.

Content is available at: CRDEEP Journals
Journal homepage: http://www.crdeepjournal.org/category/journals/ijbas/

International Journal of Basic and Applied Sciences
(ISSN: 2277-1921) (Scientific Journal Impact Factor: 6.188)

UGC Approved-A Peer Reviewed Quarterly Journal

Physicochemical Assessment of Drinking Water Quality at Malegaon, Dist. Nashik Maharashtra (India)

Ansari Gulam Rabbani Khaleel Ahmed(1) and Dr. Ansari Md Haroon Md Ramzan(2)
Research Scholar, K.R.T. Arts, B.H. Commerce and A.M. Science (KTHM) College Nashik, SPPU (India).
Department of Chemistry, K.R.T. Arts, B.H. Commerce and A.M. Science (KTHM) College Nashik, SPPU (India).

Abstract
Among all the resources available on earth, water is the most important resource. There are two types of usable water sources: surface water and groundwater. Surface water is stored in lakes and dams and is provided to the public through corporations or governments, which is referred to as tap water. However, if drinking water is contaminated, it can be detrimental to health. According to the World Health Organization, 80% of diseases in humans originate from contaminated water. The safety of drinking water is compromised by various pollutants, including chemical and microbiological agents. Such pollution leads to severe health issues. A study was performed on the physicochemical analyses of the drinking water quality in Malegaon (Including locations: Central Malegaon, Malegaon Camp, Dayane, Daregaon, Soygaon, Dabhadi), supplied by the Malegaon Corporation. Laboratory tests were conducted to analyze parameters such as pH, electrical conductance, total hardness, total dissolved solids, Cl^-, and alkalinity. These parameters are significant for assessing the quality of drinking water. The results were compared against the drinking water standards set by WHO and Indian guidelines. The quality of drinking water from the Malegaon Corporation is deemed appropriate for consumption based on physicochemical parameters.

Keywords: Physicochemical parameters, Drinking water, Values, Water quality, Malegaon Corporation.

Introduction:
The hydrosphere (total amount of water on a planet) covers more than 71% of the earth's surface in the forms of oceans, rivers, lakes, reservoirs, streams, polar ice caps and groundwater. Oceans or seas contain 97% of the water on the earth's surface, but they are not suitable for human beings due to their high salty contents. 2.8% of water trapped in the polar ice caps, glaciers, groundwater, ponds, lakes and rivers are called as fresh water. If fresh water is considered as 100% then quantity of ground water has become 20%.[Rajesh Kumar and Yadav S.S. 2011].This means that the remaining 80 percent of water is stored in ponds, rivers, and other forms.

Water a substance that contains the chemical elements H & O and it is present in 3 states [Gases, liquid, and solid]. It is the most important of the compounds. Tasteless and odourless liquid at room temperature. It has the important ability to dissolve many other substances. In fact, the ability of water as a solvent is essential for living things.According to WHO, about 80% disease in human beings are caused by water. [Neerja Kalra. 2012].The current study has investigated drinking water provided by the corporation. There is often a tendency among the public that the drinking water being provided is not of good quality. Water quality is primarily determined by its physical and chemical properties.[Singh, R.P., Chauhan...2000].Keeping these things in mind, a study has been conducted to assess the quality of drinking water supplied by the corporation and the results obtained will be compared with W.H.O. and the Indian Standard to determine the quality of water supplied by the corporation.The main objective of the study was to make various physicochemical parameters of drinking water to evaluate the water is suitable or not for drinking purpose. To assess the water quality some basic parameters are used in this study like pH, EC, TH, TDS, Chloride ion and Alkalinity.

Material and methods:
Water Samples Collections and Preservation:
Drinking water samples were collected on 10 November 2024 from different areas of Malegaon city. All collected samples were colorless and odorless. Water samples were taken in 1 L plastic bottles. Before taking water samples, the plastic bottles were already washed with 5% nitric acid solution to avoid any contamination. Extra care was taken during sampling. The bottles were rinsed several times with water. Electrical conductivity and pH was determined as a matter of

urgency after receiving the sample at the laboratory due to their unstable nature. Before storing, these samples were preserved with concentrated HNO_3 (2-3mL).

Apparatus and Chemicals:
Polyethylene bottle, glass bottles, oven, balance, desiccators, Measuring Cylinder, Filter paper, Conical flask, Burette, Pipette, Beaker, Measuring flask, pH meter, Conductivity Meter, Potentiometer, Glass electrode and Silver-silver electrode. 0.1M EDTA solution, Eriochrome Black Tea indicator, Basic buffer solution (NH4OH and NH_4Cl), Ethyl Alcohol, Magnesium bicarbonate, Sulphuric acid, Phenolphthalein, Mixed indicator, Silver nitrate, Distilled water, collected water samples.

Evaluation methods of Conclusion: Graphical method, Statistical methods and Multivariate analysis method.

Experimental evaluation:
pH and EC Analysis:
The water samples pH was determined with a pH meter, while electrical conductivity was assessed using a digital conductivity meter. All tests were conducted in a standardized lab that complies with international regulatory standards. The evaluation of water quality followed the applicable regulations. This methodology guarantees that the samples collected are analyzed per established criteria, suitable equipment and materials. All chemicals utilized in the physicochemical analysis were of analytical quality.

Total Hardness of Drinking Water Samples:
Filled the burette with EDTA solution up to the mark. Take a 9mL prepared water sample in a conical flask and add 5mL buffer solution and 40mL distilled water in it and also add the 4-5 drops of eriochrome black-T indicator. The solution turns into wine red color. Titrate it against standard EDTA solution. At the end the colour change from wine red to blue. Further add 1mL prepared water sample in it again colour turns into wine red then again titrate it with EDTA solution, Again addition of EDTA change the color of conical flasks solution into blue. One more time proceed the same procedure for equivalent value. Finally, using a calculation to find out the total hardness of water in ppm.($CaCO_3$)

Calculation of TH:
Total hardness of water in ppm ($CaCO_3$ Scale) = ml of EDTA used × 10^3/ml of sample

Total Dissolved Solids by using TDS Meter:
Dissolved solids are usually present in ions form in water. TDS Meter tip is dipped into water which measures the electricity getting conducted and electricity value is calibrated to TDS value in ppm or mg/L. This method is very quick and widely popular in researchers. Result of this tests are approximate because all the dissolved solids are not present in the form of ions.

Total Alkalinity:
Total alkalinity of water can be determined by titrating the water sample with the sulfuric acid. The collected water samples pH not more than 8.3 therefore the phenolphthalein alkalinity were not measure. Only the total alkalinity were measured with the help of mixed indicator. Add the mixed indicator in water samples, the presence of CO_3^{2-} and HCO_3^- ions turns the water samples in blue colour. While addition of sulfuric acid changes the colour blue to red. This colour change indicates the CO_3^{2-} and HCO_3^- ions neutralized, this is the end point.

Calculation of TA:
Total Alkalinity = Volume of H_2SO_4 × 0.02 × 50 × 1000 / 100 (Volume of Sample taken)
Volume of H_2SO_4 = Burette reading
Normality of H_2SO_4 = 0.02 N
3.5. Assessment of Cl^- : The potentiometric method were used to analyse chloride ion with silver nitrate solution by using glass electrode and silver-silver chloride electrode system. The end point of the titration is that instrument reading at which the greatest change in voltage has occurred for a small and constant increment of silver nitrate.

Calculation of Cl^-:
Chloride ion mg/L = (V_1 - V_2) × N × 35450 / V
V_1 = Volume of Silver nitrate titrant used in sample
V_2 = Volume of Silver nitrate used in blank
N = Normality of standard chloride solution
V = Volume in ml of the sample

Result and discussion :
The mean values of different selected Physicochemical parameters have been tabulated below;

National Conference on «Modern Perspectives In Physical and Chemical Sciences » (MPPCS-2024) DOI: **10.13140/RG.2.2.13272.40962**

Table: 1 Physicochemical parameters for water samples

Sr. No.	Parameters	DWS 1	DWS 2	DWS 3	DWS 4	DWS 5	DWS 6	DWS Avg. Values	WHO Standards	Indian Standards
1	pH	7.2	7.2	7.4	7.5	7.2	7.3	7.3	6.5-8.5	6.5-8.5
2	EC µS/cm	510	545	485	517	524	505	514.33	500-3000	2250
3	TH ppm	289	245	302	277	256	290	276.50	200-500	200-600
4	TDS ppm	684	705	668	652	679	605	665.50	500-1500	500-2000
5	TA ppm	294	257	288	275	263	295	278.66	200-500	200-600
6	Cl^- ppm	255	233	267	251	228	270	251	200-300	250

Hydrogen Ion Activity:
The pH of drinking water is very important basic parameter to determine whether the water is acidic or basic. The permissible limit for pH is specified between 6.5 to 8.5 according to both Indian Standard [IS 10500:2012] & the WHO guideline [2008]. Data were collected and compared against these permissible limits. The results indicated that all sample set the requirements for safe drinking water. The obtained results are 7.2, 7.2, 7.4, 7.5, 7.2 and 7.3 and their average result is 7.3.

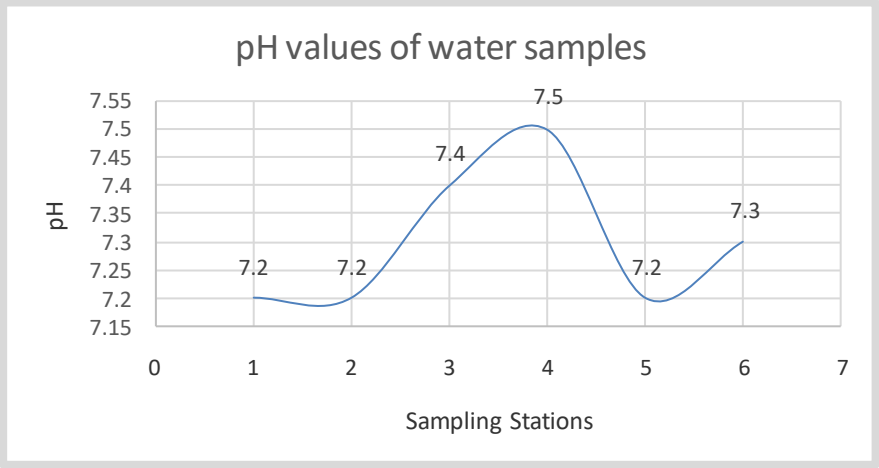

Fig: 1. pH Values of water samples

Electrical Conductance:
Electrical conductance is caused by the ions present in water. According to WHO [2008], The taste of water depends on electrical conductivity. The collected results are 510, 545, 485, 517, 524 and 505 and their average is 514.33. All results are within the permissible drinking water limit as per Indian Standard and WHO of electrical conductance.

Total Hardness of Water: As shown in below figure, the hardness of $CaCO_3$ was found to be 289, 245, 302, 277, 256 and 290 and their average value is 276.50. Hardness of drinking water is very important parameter to determine the toxicity of toxic elements. Above results were evaluated with Indian Standard and WHO values and found the all are remain in hardness level.

Total Dissolved Solids: Total dissolved solids (TDS) are also an important parameter in determining the drinking water quality. If total dissolved solids are exceed the permissible limit in water, they can cause health issues like diarrhea. Generally high TDS value are not significantly harmful for healthy humans, however, high dissolved solids can negatively affect the people, who suffering from kidney and heart diseases. The following figure indicates the result of all samples: 684, 705, 668, 652, 679 and 605 and their mean values is 665.50. Both the average result and all individual samples results fall within the permissible limit 500-1500 for TDS, which is prescribed by WHO and also IS limit 500-2000.

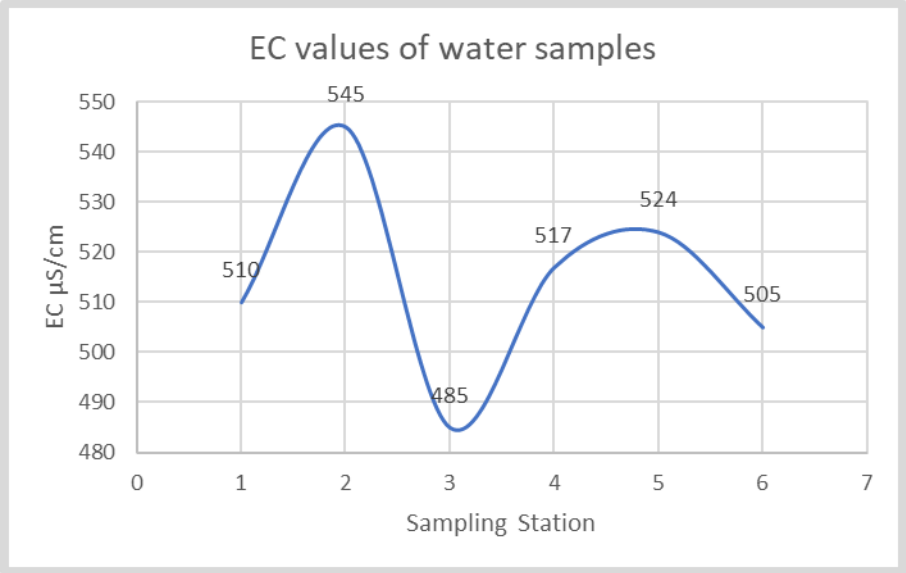

Fig: 2. EC Values of water samples

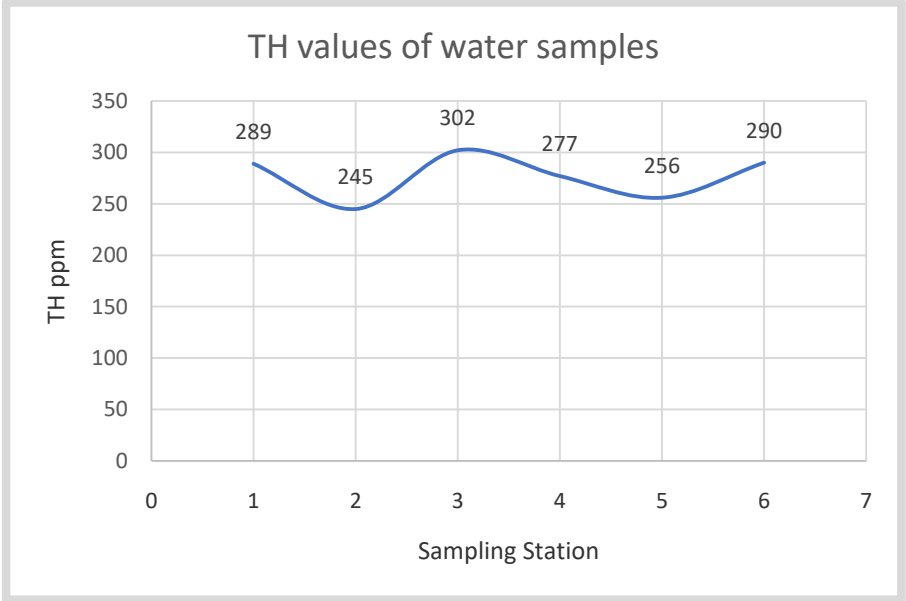

Fig: 3. TH Values of water samples

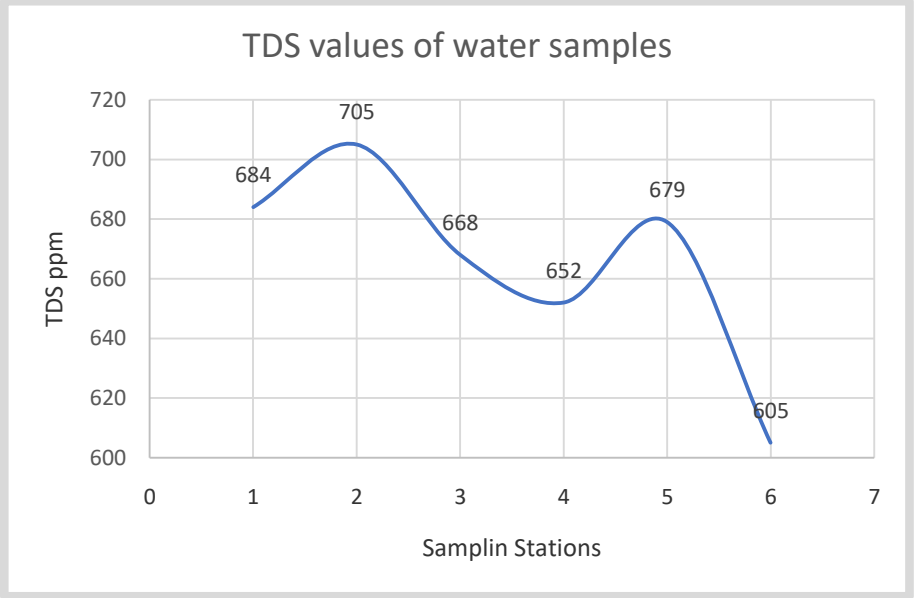

Fig: 4. TDS Values of water samples

National Conference on «Modern Perspectives In Physical and Chemical Sciences » (MPPCS-2024) DOI: **10.13140/RG.2.2.13272.40962**

Total Alkalinity of Water: Total alkalinity is a measurement of water strength to neutralize the acidity of water. It determines due to the presence of OH^- , CO_3^{2-} and HCO_3^-. Due to that parameter other parameters like pH of water is affected. The following results are shown in graph: 294, 257, 288, 275, 263 and 295 and the mean result of these 278.66. Allah results are fall within the permissible limits of WHO and Bureau of Indian Standard.

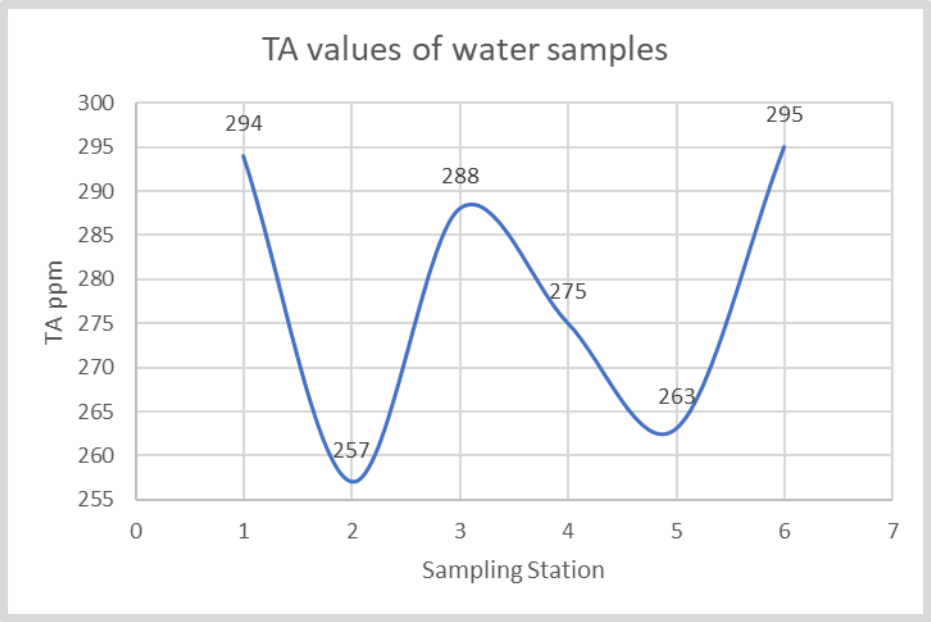

Fig: 5. TA Values of water samples

Chloride Ion concentration (Cl^-): The chloride ion concentration were analyzed by using potentiometric titration method and the result obtained from samples are 255, 233, 267, 251, 228 and 270 and the mean values is 251. According to WHO and IS the permissible limits are 200-300 and the obtained results are fall within the limits.

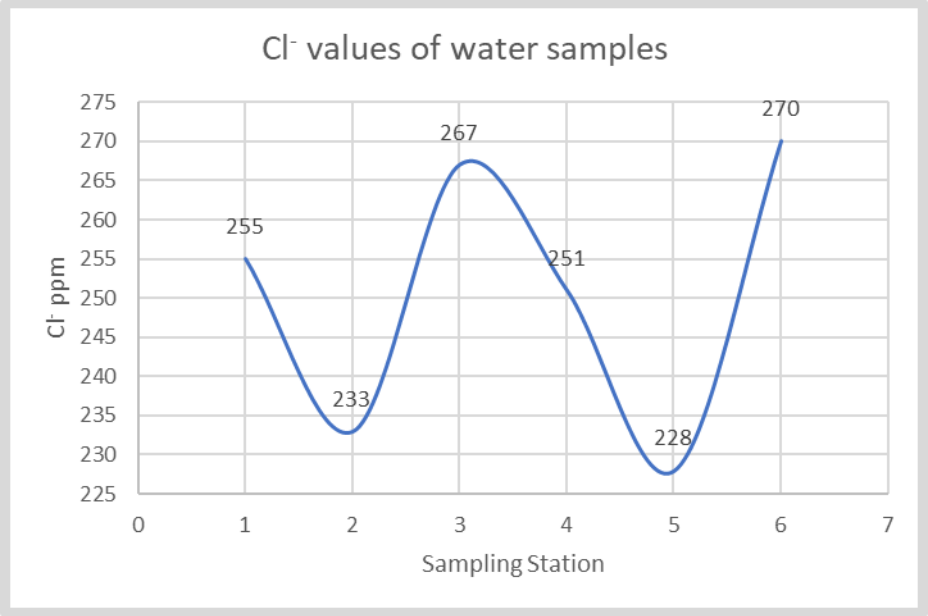

Fig: 6. Cl^- Values of water samples

Conclusion:

A comparative study of various water quality parameters was conducted on drinking water samples collected from 6 different sampling stations. All results fell within the permissible limits set by the World Health Organization (WHO) and Indian Standards. The results obtained during the study were compared to these established limits, and no water sample exceeded the permissible limits for any parameter. The results from all locations were very similar, likely attributed to the shared drinking water source. Sampling at multiple locations was crucial. Significant variations in results at any location would have indicated potential issues, such as construction work affecting the water supply or other unforeseen factors. Analysis of all water samples and their average values indicates that the drinking water supplied by the corporation is fit for human consumption. (The water is safe for people to drink).

National Conference on «Modern Perspectives In Physical and Chemical Sciences » (MPPCS-2024) DOI: **10.13140/RG.2.2.13272.40962**

References :

Rajesh Kumar and Yadav S.S, Correlation analysis of ground water quality in and around Shahzad nagar block of Rampur district, Uttar Pradesh, India, J.Chem. Sci, 9 (1), 2011, 440-447.
https://www.tsijournals.com/articles/correlation-analysis-of-ground-water-quality-in-and-around-shahzad-nagar-block-of-rampur-district-uttar-pradesh-india.pdf
Neerja Karla, Rajesh Kumar, Yadav S.S, Singh R.T, Water quality index assessment of ground water in Koilwar block of Bhojpur (Bihar) J.Chem. Pharm. Res, 4(3), 2012, 1782-1786.
https://www.jchps.com/issues/Volume%2010_Issue%201/77-0160916.pdf
Singh, R.P., Chauhan, B.S., Defender Swarop. and Yadav, Y.S. 2000. Seasonal variation in ground water quality of Agra City. Indian J. Environ. Hlth.42(2):59-69.
http://www.indiaenvironmentportal.org.in/files/Defluoridation%20of%20groundwater%20in%20Agra%20city.pdf
Das et. al., (2001). Chemistry of drinking water around Janakpur town of Nepal. Anantha krishnan, S., Loganathan, K and A. Jafar ahamed. 2012. Study on ground water quality and its suitability or drinking purpose in Alathur block - Perambalur district. Applied Science Research, 4 (3);1332-1338.
https://www.scholarsresearchlibrary.com/archive/aasr-volume-4-issue-3-year-2012.html
Zhang Q, Xu P, Qian H (2020) Groundwater quality assessment using improved water quality index (WQI) and human health risk (HHR) evaluation in a semi-arid region of northwest China. Expo Health 12:487–500.
Adhena Ayaliew Werkneh, Belay Zimbelachew Medhanit, Angaw Kelemework Abay, Jemal Yimer Damte: January 26, 2015 Physico-chemical water quality at Jigjiga City, Ethiopia. American Journal of Environmental Protection 2015; 4(1): 29-32. ISSN: 2328-5680 (Print); ISSN: 2328-5699 (Online)
Rahane Balasaheb and Bhalla Resham, Vol. 07, No.05, pp.2101-2105, May, (2018), ISSN:2319-9490
Mahananda, M.R., Mohanty, B.P. and Behera, N.R. 2010. Physico-chemical analysis of surface and ground water of Bargarh district, Orissa, India.I.J.R.R.A.S. 2(3):45-51. https://www.arpapress.com/Volumes/Vol2Issue3/IJRRAS_2_3_10.pdf
Indian standard drinking water specification. (second revision) IS 10500 : 2012.
WHO, (2008): Guidelines for drinking water quality. 3rd edn. World Health Organisation, Geneva.
WHO, (2011): WHO guidelines for drinking-water quality (Geneva: World Health Organization)
"Malegaon Taluka Population Nashik, Maharashtra, List of Villages & Towns in Malegaon Taluka"
Climatological Normals 1981–2010. India Meteorological Department. January 2015. pp. 467–468. Retrieved 21 September 2023.
https://imdpune.gov.in/library/public/19812010%20CLIM%20NORMALS%20%28STATWISE%29.pdf

Content is available at: CRDEEP Journals
Journal homepage: http://www.crdeepjournal.org/category/journals/ijbas/

International Journal of Basic and Applied Sciences
(ISSN: 2277-1921) (Scientific Journal Impact Factor: 6.188)

UGC Approved-A Peer Reviewed Quarterly Journal

Comparative Study of Dielectric Parameters: A Tool for Remote Sensing

Quadri F B
Associate Professor, Department Of Physics, Dr.RafiqZakaria College for Women, ChhatrapatiSambhajinagar, MS.

Abstract:
Interaction of electromagnetic waves with matter has always been a source to explore the new horizons and reveal many facts about the process. The present paper deals with the study of electrical parameters of dry soil and moist soil of a particular location of Maharashtra region. Microwaves of X band and S band are used for the experimental part. Soil of the location is treated well before experimentation and is filled up in the waveguide, after this it is exposed with the electromagnetic radiations. Reflected waves are analyzed to determine its electric parameters. Obtained results show various correlations between the electric parameters and the physical and chemical properties of the soil. This is a powerful tool for studying the matter that is physically out of reach.

Keywords: Electromagnetic waves, infinite sample method, dielectric constant, dielectric loss, electrical conductivity. Remote sensing.

Introduction

Background Study:

Interaction of electromagnetic waves with matter has always been the topic of curiosity for the researchers hence much work has been carried out in this regard. With the aim to explore the topic, different methods have been devised by different researchers to study the interaction of these two entities and determine the electrical parameter of the materials [1 – 4]. The aim of all these methods is to have easy observations and simple calculations. Microwave measurement of various materials has gained popularity due to its increased applications in different fields like agriculture, food processing companies, novel materials for electronic industries, etc [5, 6]. Determination of electrical parameter of the material helps in relating it with the physical and chemical properties of the matter. The experimental techniques that are used in dielectric studies are based on different principles in different frequency regions [6]. It involves the determination of complex permittivity, $\varepsilon^* = \varepsilon' - j\varepsilon''$, where ε' is the dielectric constant and ε'' is the dielectric loss and $j = \sqrt{-1}$.

Methodology:

The traditional methods of determining complex dielectric permittivity are focused around the measurements in the frequency domain. The material under test is taken in the sample holder and its dielectric constant is measured at various frequencies. The method used for determining the electrical parameters of the material depends on accuracy needed, its shape and convenience of measurement [7 – 9]. Some of the significant factors to consider are Frequency range, Expected values of ε_r, Required measurement accuracy, Material properties (i.e., homogeneous, isotropic), Form of material (i.e., liquid, solid, sheet), Sample size restrictions, Destructive or nondestructive, Cost and Temperature.

The soil samples were collected from the different landscapes of Maharashtra region, in the summer season from a depth of 10 – 15 cm. The landscapes include the fertile region, barren land, soil from hilly dry area, coastal region, etc. The geographical locations of each area, from where soil samples were collected, are noted. These soil samples were initially crushed or grated and sieved by a standard sieve to limit the size of the soil particles. The sample under test is then oven dried for few hours to remove any moisture present in it. This sample is taken as the basic one for our further studies. The soil samples that can fill the sample holder completely is taken and it is weighted. Moisture is then added to it in the gravimetric concentrations of 2% to 8%. The work was carried out at room temperature of 300K. Plain soil samples were analyzed for their physical properties and the available chemical constituents at Agricultural Office, Shah Noor Wadi, Aurangabad. To study the effect of moisture on different types of soil, infinite sample method was used with X and S band frequenciesand electrical parameters were determined.

National Conference on «Modern Perspectives In Physical and Chemical Sciences » (MPPCS-2024) DOI: **10.13140/RG.2.2.13272.40962**

The samples were analyzed for dielectric constant, dielectric loss, ac conductivity and relaxation time with different known concentration of moisture at 3GHz (S band) and 9.8GHz (X band). The results are tabulated as shown in the table below:

Table 1. showing the electrical parameters of two different soil at 3GHz and 9.8 GHz with different concentration of moistures.

Type of Soil	Conc of Moisture (%)	Dielectric constant		Dielectric loss		AC conductivity (mS/cm)		Relaxation time (psec)	
		3GHz	9.8 GHz	3GHz	9.8GHz	3GHz	9.8GHz	3GHz	9.8GHz
fertile soil	2	2.96	2.23	0.62	0.94	0.56	0.96	8.3	7.45
	4	3.12	2.64	0.78	1.24	0.69	1.42	9.25	7.96
	6	3.31	2.94	0.92	1.42	0.85	1.85	9.56	8.23
	8	3.56	3.14	1.08	1.96	0.97	2.13	9.85	8.56
	10	3.7	3.54	1.46	2.25	1.15	2.46	10.03	8.72
Barren Soil	2	1.33	1.10	0.54	0.68	0.35	0.45	6.24	4.54
	4	1.56	1.36	0.68	0.87	0.49	0.74	6.52	4.87
	6	1.82	1.62	0.81	1.23	0.64	0.86	6.86	5.19
	8	2.10	1.88	1.05	1.54	0.81	0.94	7.23	5.37
	10	2.34	2.10	1.25	1.70	0.96	1.25	7.54	5.78

Graphs showing the variation of electrical parameters of two different soil at 3GHz and 9.8 GHz with different concentration of moistures.

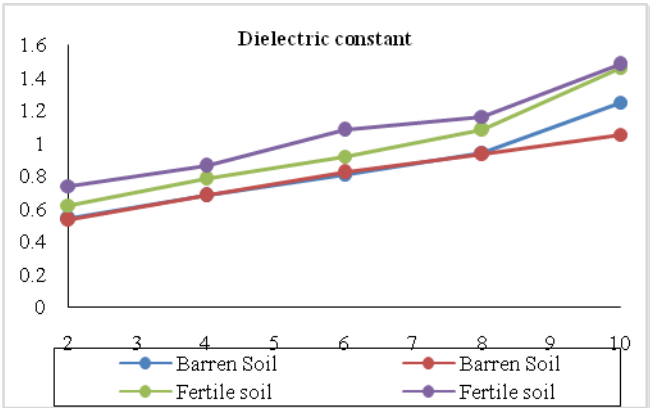

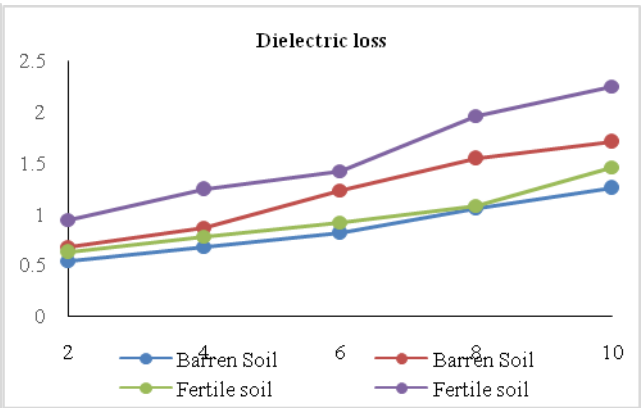

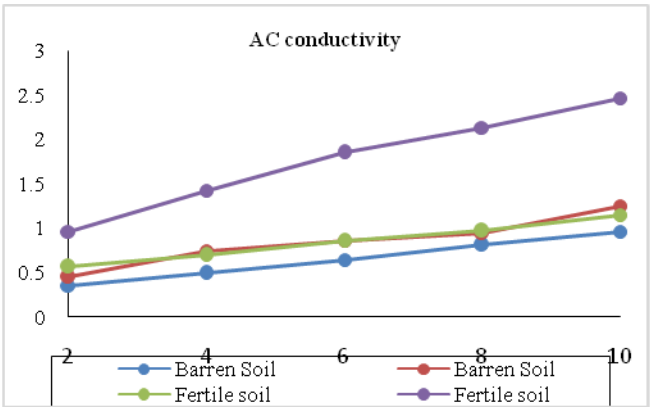

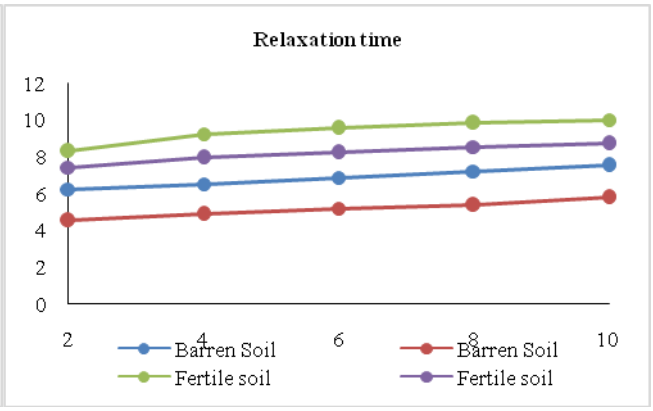

Results and Discussion

The dielectric parameters of the soil vary from region to region. No two soil samples have the same values. The electrical parameters depends on number of factors like the physical and chemical properties of the soil. It also depends on the amount of moisture present in it. The values are dependent on the frequency of measurement also.

Effect of frequency: With increase in the frequency of measurement, it was noted that the dielectrical parameter decreases. This is because, with the increase in frequency, the charges get less time to rearrange or align themselves hence the parameters have lesser values for higher frequency.

Effect of Moisture: As the concentration of moisture in the soil increases, the electrical parameters also increases as water is a polar molecule. The result shows that dielectric measurements are a tool for sensing the remote areas with the help of electromagnetic waves.

References:

[1] Rosaih Osman et al.(2017). Dielectric Properties of Ceramic Material Obtained from Rice Husk for Electronic Applications. *IEEE Regional Symposium on Micro and Nano Materials*.

[2] Telmos Santos, Anders J Johnsons and Fredrik Tufvesson. (2009). Dielectric Characterization of Soil Samples by Microwave Measurements.*Series of Technical Reports,* no.10.

[3] Hoekstra P and Delaney A. Dielectric Properties of Soils at UHF and Microwave Frequencies.(1974). *Journal of Geophysical Research*, 79/11 1699.

[4] RachidLahbibi, Hassan Ammor and HasanAlmajid. (2011). A New Engineering Approach to Evaluate the Dielectric Properties of Materials in K – band Frequency using Rectangular Waveguide Measurements.*ARPN Journal of Engineering and Applied Sciences*. 13(12).

[5] Salsman J B &Holderfield J P. (1994). A Technique for Measuring Dielectric Properties of Minerals at Microwave Heating Frequencies Using an Open Ended Line", *Report of Investigation,* 9519,Bureau of Mines, United States Department of the Interiors,

[6] Das R K. (). Measurement of Dielectric Properties at Microwave Frequencies.*International Journal of Scientific Research in Physics and Applied Sciences,* Vol.6, Issue.1, pp.15 – 17, E-ISSN: 2384 – 3423, February, 201

[7] Venkatesh M S and Raghavan G S V. (2005). An Overview of Dielectric Properties Measuring Techniques.*Canadian Bioengineering System*, Vol.47. pp. 7.15 – 7.30.

[8] Hewlett – Packard, "*Basics of Measuring the Dielectric Properties of* Materials", Model 4192A LF Impedance Analyzer, 1983

[9] Rohde & Schwarz. (2006). "Measurement of Dielectric Material Properties", Application Note, Application Center Asia/Pacific, RAC 0607 – 0019, CY Kuek 07, 2006.